A&A 479, 427–452 (2008)
DOI: 10.1051/0004-6361:20078723

Astronomy & Astrophysics

Full calculation of clumpiness boost factors for antimatter cosmic rays in the light of ΛCDM *N*-body simulation results

Abandoning hope in clumpiness enhancement?⋆

J. Lavalle[1], Q. Yuan[2], D. Maurin[3], and X.-J. Bi[2]

[1] Centre de Physique des Particules (CPPM), CNRS-IN2P3, Université de la Méditerranée, 163 avenue de Luminy, case 902, 13288 Marseille Cedex 09, France
e-mail: lavalle@in2p3.fr
[2] Key Laboratory of Particle Astrophysics, Institute of High Energy Physics, Chinese Academy of Sciences, PO Box 918-3, Beijing 100049, PR China
e-mail: [yuanq;bixj]@mail.ihep.ac.cn
[3] Laboratoire de Physique Nucléaire et Hautes Énergies (LPNHE), CNRS-IN2P3, Universités Paris VI et Paris VII, 4 place Jussieu, Tour 33, 75252 Paris Cedex 05, France
e-mail: dmaurin@lpnhe.in2p3.fr

Received 23 September 2007 / Accepted 27 November 2007

ABSTRACT

Context. Anti-proton and positron Galactic cosmic ray spectra are among the key targets for indirect detection of dark matter. The boost factors, corresponding to an enhancement of the signal, and linked to the clumpiness properties of the dark matter distribution, have been taken as high as thousands in the past. The dramatic impact of these boost factors for indirect detection of antiparticles, for instance with the PAMELA satellite or the coming AMS-02 experiment, asks for their detailed calculation.
Aims. We take into account the state-of-the-art results of high resolution *N*-body dark matter simulations to calculate the most likely energy dependent boost factors, which are linked to the cosmic ray propagation properties, for anti-protons and positrons. The results from extreme, but still possible, configurations of the clumpy dark matter component are also discussed.
Methods. Starting from the mass and space distributions of sub-halos, the anti-proton and positron propagators are used to calculate the mean value and the variance of the boost factor for the primary fluxes. We take advantage of the statistical method introduced in Lavalle et al. (2007) and cross-check the results with Monte Carlo computations.
Results. By spanning some extreme configurations of sub-halo and propagation properties, we find that the average contribution of the clumps is negligible compared to that of the smooth dark matter component. Dark matter clumps do not lead to enhancement of the signals, unless they are taken with some extreme (unexpected) properties. This result is independent of the nature of the self-annihilating dark matter candidate considered, and provides precise estimates of the theoretical and the statistical uncertainties of the antimatter flux from sub-halos.
Conclusions. Spectral distortions can still be expected in antimatter flux measurements, but scenarios invoking large and even mild clumpiness boost factors are strongly disfavoured by our analysis. Some very extreme configurations could still lead to large enhancements, e.g. (i) very small clumps with masses $\lesssim 10^{-6}\ M_\odot$ following a $M^{-\alpha}$ mass distribution with $\alpha \gtrsim 2$, highly concentrated with internal $r^{-\beta}$ profiles with $\beta \gtrsim 1.5$, and spatially distributed according to the smooth component; or (ii) a big sub-halo of mass $\gtrsim 0^7\ M_\odot$ within a distance of $\lesssim 1$ kpc from the Earth. However, they are very unlikely from either theoretical or statistical arguments.

Key words. cosmology: dark matter

1. Introduction

The existence of dark matter (DM) has been established by various astronomical observations, from galactic to cosmological scales. The evidence come from gravitational effects, such as the observation of the rotation curves in spiral galaxies and velocity dispersion in elliptical galaxies, the X-ray emission and peculiar velocity dispersion of galaxies in the clusters of galaxies and the weak lensing effects, all indicating much steeper gravitational potentials than those inferred from the luminous matter. Recently, there have been two strong smoking guns from the *Bullet* cluster system 1E0561 (Clowe et al. 2004, 2006; Bradač et al. 2006) and a DM ring discovered around the cluster CL0024+17 (Jee et al. 2007), which may indicate the existence of DM in the sense that it has first provided means to study the dynamics of DM itself. Note, however, that modified gravity models might still offer a viable alternative (Angus et al. 2006, 2007; Angus & McGaugh 2007; Famaey et al. 2007).

The nature of DM is still unknown, remains one of the most outstanding puzzles in astrophysics and cosmology, and is challenging from the particle physics view point. Nevertheless, the unprecedented precision reached in observational cosmology in the last decade, thanks to the combined use of different probes (CMB, type 1A supernovae, large scale structures, deep surveys, primordial abundances, etc.), yields a rather precise estimate of the total amount of non-relativistic matter in the Universe, encompassing the standard baryonic matter, of which density can be predicted and measured independently (for reviews, see e.g.

⋆ Appendices A and B are only available in electronic form at http://www.aanda.org

Tytler et al. 2000; Lesgourgues 2004; Yao & et al. 2006). The overall contribution of matter to the (critical) energy density of the Universe is ∼30%, while the baryonic component accounts for 4% only. Hence most of the matter should be dark and of non-baryonic origin, requiring physics beyond the standard model of particle physics. The most attractive scenario involves weakly interacting massive particles (WIMPs). An appealing idea is that WIMPs could be thermal relics of the early Universe, which naturally give rise to a cosmological abundance in the range of the observed value if both the interaction strength and the masses are taken at the weak scale. Indeed, because of their thermal origin, WIMPs should still (weakly) interact with ordinary matter, and even annihilate if they are preserved from matter-antimatter asymmetry. Such particles can originate naturally in the context of supersymmetric (SUSY) or extra-dimensional (ED) extensions of the standard model, independently developed to tackle the issues of the unification of interactions and energy scale hierarchical problems. Indeed, in such theories, the stability of the proton is very often ensured by the conservation of some new discrete symmetry that guaranties the lightest exotic particle to be stable. Such paradigms provide very good candidates for DM (for reviews, see e.g. Jungman et al. 1996; Bergström 2000; Bertone et al. 2005a). In particular, the minimal SUSY extension of the standard model (MSSM) can yield DM particles, the most famous being the neutralino, a Majorana fermion. The cosmological constraints on the SUSY parameter space have been extensively studied in the literature (Bélanger et al. 2006; Djouadi et al. 2006; Baer et al. 2005; Ellis et al. 2003): WIMPs could be detected on the present running or proposed experiments, either directly by measuring the recoil energy when they scatter off a detector nuclei (Muñoz 2004), or indirectly by observing their annihilation products, such as anti-protons, positrons, γ-rays or neutrinos (Bertone et al. 2005a; Carr et al. 2006). They may also be generated in the next generation colliders, which is the most direct way to probe the existence of new particles. The direct and indirect detection methods are viable and complementary to collider studies in order to further constrain the nature of DM.

For indirect detection in the Milky Way, since the annihilation rate is proportional to the square of the DM density, the Galactic Centre is believed to be a promising source of DM annihilation (Bergström et al. 1998). However, the existence of the central super-massive black hole and the supernova remnant Sgr A* are likely to heavily contaminate the DM signals with high-energy standard astrophysical processes (Aharonian et al. 2006). Alternative sites, such as the DM dominated dwarf spheroidal galaxies (dSph) orbiting close around the Milky Way, or even DM substructures inside the Milky Way, could be more favourable. Indeed, the existence of a myriad of sub-halos throughout galactic-scale host halos is a generic prediction of the cold dark matter (CDM) paradigm of structure formation in the Universe. High resolution simulations (e.g. Diemand et al. 2006, 2007a,b) show that for the ΛCDM scenario, the large scale structures form hierarchically by continuous merging of smaller halos. As remnants of the merging process, about 10% to 50% of the total mass of the halo could be in the form of sub-halos. Moreover, the centres of sub-halos, like their hosts, are found to have high mass densities and therefore, could be ideal targets for γ-rays searches of WIMP annihilation products (e.g. Koushiappas et al. 2004; Bi 2006; Bi et al. 2007, and references therein). A long-standing issue is the possible overall enhancement – *boost factor* – of the signals from the smooth component, due to the presence of such inhomogeneities (Silk & Stebbins 1993). The first studies dedicated to indirect detection of DM focused essentially on γ-rays, and more marginally on anti-protons, but suffered from the lack of information on DM substructures (see e.g. Bergström et al. 1999). More recently, Berezinsky et al. (2003) discussed in more details the γ-rays case, finding boost factors no larger than a few. Furthermore, a recent study by Diemand et al. (2005a) reheated the debate on clumpiness, because the authors, by means of a very high resolution N-body experiment (but stopping at $z = 26$), found that the Galaxy could be populated by a huge number density of sub-halos as light as the Earth. While the survival of such light clumps against tidal effects is still questionable, they could yield a significant contribution to the Galactic diffuse γ-ray flux by assuming a very cuspy sub-halo profile (Bi et al. 2006). Nevertheless, some recent works also indicate that the current parameter range for clumpiness may provide only marginal global effects (Diemand et al. 2007a; Pieri et al. 2007). The aim of the present paper is to provide a detailed study of the impact of cosmological sub-halos on the primary antimatter Galactic cosmic ray (GCR) flux, as elaborate as that already performed for γ-rays.

In Maurin & Taillet (2003), the authors noted that the difference in propagation properties for $\overline{\mathrm{p}}$ and e^+ was likely to translate into different boost factors for these species. More recently, Lavalle et al. (2007) provided a detailed formalism to tackle the calculation of antimatter CR fluxes, when boosted by DM clumpiness. They showed how the uncertainty on the spatial distribution of clumps transfers to an uncertainty to the predicted boosted cosmic ray positron flux, an effect that depends on energy. More generally, this effect depends on the clump number density in a volume bounded by the characteristic diffusion length of the involved species. For the sake of clarity, these authors have used a very simple model, in which all clumps have the same internal properties (masses and intrinsic luminosities), and mainly stressed the effects coming from their space distribution. Using this method, Brun et al. (2007) fully treated a particular class of DM inhomogeneities – the intermediate mass black holes (Bertone et al. 2005b) – finding large boosts with huge variances for the signals: such large variances tag unpredictive scenarios. This means that in the case of a positive detection, such scenarios can certainly be tuned to reproduce the data, but generally at the cost of a vanishingly small associated likelihood for this configuration.

In this paper, we study a more natural DM scenario (e.g. Diemand et al. 2005a), in which substructures fill the whole Galaxy down to a minimal mass $M_{\rm min} \gtrsim 10^{-6}\ M_\odot$, with a mass distribution $\mathrm{d}N/\mathrm{dlog}\,M \propto M^{-\alpha_{\rm m}}$ ($\alpha_{\rm m} \approx 0.9$), and a cored spatial distribution. We survey different DM configurations in great details by using different sub-halo inner profiles, different mass distributions or different concentration models (this has already been well studied in the context of gamma-rays, see e.g. Ullio et al. 2002). It is important to better quantify the boost and variance of antimatter signals since the satellite PAMELA (Picozza et al. 2006; Casolino et al. 2007), successfully launched in June 2006, will soon provide new results on antimatter fluxes. The DM description suffers uncertainties, and its impact on the calculated fluxes adds up to the existing uncertainties from the propagation parameters (Donato et al. 2001, 2004; Lionetto et al. 2005). Regarding this latter issue, PAMELA should also update our current knowledge of the particles transport in the Galaxy, thanks to secondary-to-primary ratio measurements (e.g. B/C). This is crucial for the background calculation (standard antimatter production) in order to confirm/support any claim of an *excess*. Besides, AMS-02 should be launched in the coming years,

and provide additional crucial information on GCR propagation by measuring the radioactive species (Battiston 2007).

Below, we take advantage of simplified formulations for the $\overline{\mathrm{p}}$ (e.g. Maurin et al. 2006a) and e^+ (e.g. Lavalle et al. 2007) propagators. Using the information of the mass and space distributions of sub-halos from N-body numerical simulations (see e.g. the recent Via Lactea simulation, Diemand et al. 2006, 2007a,b), we calculate the boost and the variance of the fluxes. We find that for all plausible choices of the clump properties and propagation parameters, boost factors for anti-protons and positrons are close to unity, with small systematic and statistical uncertainties.

The paper is organised as follows. All relevant aspects (for this study) of the DM distributions in the Galaxy, including N-body simulation results are discussed in Sect. 2. The configurations retained are given in Sect. 3, where the key parameters entering the calculation of the *clumpy flux* (and its variance) are underlined. The propagation aspects are treated in Sect. 4. The methodology to calculate the antimatter flux, its variance and the corresponding boost factors is given in Sect. 5, either by means of a semi-analytical approach (Sect. 5.2) or by Monte Carlo (MC) simulations (Sect. 5.3). The reader not interested in the technical details can directly jump to Sect. 6, where the results for positrons (Sect. 6.2) and anti-protons (Sect. 6.3) are presented, highlighting the physical effects coming from clump properties, space distribution, mass distribution and GCR propagation. Because of the complex origins and the mixing of the relevant physical quantities, such details really help to fully understand what kind of information *boost factors* actually encodes. We summarise and conclude in Sect. 7.

2. DM distribution

In the last few years, the advent of high resolution N-body simulations have increased the number of studies in this field, allowing for a better understanding and description of the DM dynamics. Even if many issues remain unclear, when comparing simulation results to the current observations, collisionless codes now agree at the 10% level over wide dynamic ranges, providing a robust framework for DM studies (Heitmann et al. 2007).

Throughout this paper, we will separate the WIMP annihilation contribution associated with *sub-halos* from that associated with a *smooth* component. The former will be related to *any DM inhomogeneity* in the Galactic halo, independently of its physical scale – resolved or not in N-body simulations – while the latter will refer to *the Galactic DM host halo itself*, which will be considered as a continuous fluid (again independently of the current resolution of N-body simulations). Although the Vlasov (or fluid) limit is likely to be reached when the number of particles involved in N-body experiments is huge, one should still be aware that such a statement is not trivial at all when dealing with the cosmological evolution of structures, and that discreteness might induce important biases (Joyce & Marcos 2007). Furthermore, one should also keep in mind that our DM modelling will rest on (or be extrapolated from) N-body experiment results, in the most precise of which the test particle mass is not lighter than $\sim 10^4\ M_\odot$ (cf. the *Via Lactea* simulation, Diemand et al. 2006), and for which the Vlasov limit is not reached at small scales. Nevertheless, we will assume throughout this study that the host halo profiles of Milky-Way-like galaxies provided by N-body simulations describe a smooth fluid (WIMP gas), on top of which some sub-halos may be wandering.

In the following subsections, we summarise the recent results concerning (i) generalities about DM distribution in halos of galaxies (Sect. 2.1) and (ii) some specific considerations about sub-halo description (Sects. 2.2 and 2.3).

Given the scope of this work, we will merely consider spherical profiles. For sub-halos, several cases will be chosen to encompass some extreme (but still plausible) scenarios. This aims at providing realistic estimates of the boost factor uncertainties related to the clumpy DM component.

2.1. Shape and profiles

2.1.1. Spherical profiles

A scale-invariant DM distribution based on N-body numerical simulation results can be written in a general form as (Zhao 1996)

$$\rho = \frac{\rho_\mathrm{s}}{(r/r_\mathrm{s})^\gamma [1 + (r/r_\mathrm{s})^\alpha]^{(\beta-\gamma)/\alpha}}, \quad (1)$$

where ρ_s and r_s are respectively a scale density and a scale radius, which can be determined by measuring the relation between the mass of the dark halo and the concentration parameter from simulations. Such an empiric law can be used for galaxy cluster halos, galaxy halos and for sub-halos. In the following, we focus on the central logarithmic slope α of the smooth halo component. We will discuss the Galactic scale radius r_s and density ρ_s in the section dealing with the concept of concentration (cf. Sect. 2.2.2).

Navarro, Frenk and White (Navarro et al. 1997) worked out the following set of parameters $(\alpha, \beta, \gamma) = (1, 3, 1)$, which define the NFW profile, with a cusp scaling like r^{-1} at radii smaller than r_s. Moore et al. (1998) found another set with $(\alpha, \beta, \gamma) = (1.5, 3, 1.5)$ to fit their simulation results, which is steeper than NFW at small radii, scaling like $r^{-1.5}$. More recent high resolution N-body simulations found that an NFW profile seems to underestimate the DM density in the central regions, while a Moore profile[1] probably overestimates it (Navarro et al. 2004; Diemand et al. 2004a, 2005b, and references therein). The mean slope of the cusp obtained from various codes is well fitted by a $(1, 3, \gamma)$ profile, with $\gamma = 1.16 \pm 0.14$ (Diemand et al. 2004a), still in agreement with ($\gamma = 1.3$) analytical similarity solutions (Ahn & Shapiro 2005). However, profiles may not have a universal shape (e.g. Navarro et al. 2004; Stoehr 2006). First, from the observational point of view, the relative scatter observed for the slope for four nearby low-mass spiral galaxies is 0.44 (Simon et al. 2005), three times larger than in simulations. Second, it was also recently stressed that asymptotic slopes may not be reached at all (Navarro et al. 2004; Stoehr 2006; Merritt et al. 2006; Graham et al. 2006; Ricotti et al. 2007): according to Graham et al. (2006), the Einasto function describes a simulated DM halo better than a NFW-like model.

Closer to the Galactic centre, the super-massive black hole dominates the mass ($r < r_\mathrm{BH} \approx 2$ pc). The adiabatic growth of the black hole, if taking place in the centre of the DM gravitational potential and without any merger, could lead to an enhanced DM density in this region (slope as steep as $\sim$2.3–2.4, dubbed *spike*). Nonetheless, recent works seem to prefer a final $r^{-1.5}$ behaviour for the DM density in the inner regions (see Merritt 2004; Gnedin & Primack 2004, and references therein).

Finally, the luminosity of cuspy or spiky halos is singular at the centre of the halo. However, a cut-off radius r_cut naturally appears, within which the DM density saturates due to the balance

[1] Though those authors have since improved their early time results and parametrisations, we will still use these generic profile names to deal with inner shapes of profiles, for the sake of simplicity.

between the annihilation rate $[\langle\sigma v\rangle\rho(r_{\rm cut})/m_\chi]^{-1}$ and the gravitational infalling rate of DM particles $(G\bar{\rho})^{-1/2}$ (Berezinsky et al. 1992). Taking $\bar{\rho}$ about 200 times the critical density, we get

$$\rho_{\rm sat} = 3\times10^{18}\left(\frac{m_\chi}{100\ {\rm GeV}}\right)\times\left(\frac{10^{-26}\ {\rm cm^3\ s^{-1}}}{\langle\sigma v\rangle}\right)M_\odot\ {\rm kpc^{-3}}. \quad (2)$$

2.1.2. Other open questions

During their history, structures undergo several mergers. The survival of the inner cusp of DM in these events has been investigated. The inner profile was found to be exceptionally robust, despite the relaxation that follows merging processes (Boylan-Kolchin & Ma 2004; Aceves & Velázquez 2006; Kazantzidis et al. 2006; McMillan et al. 2007; Valluri et al. 2007). The implications are deep: the characteristic *universal* shape of the DM density profile may be set early in the evolution of halos (Kazantzidis et al. 2006). However, it is still not clear whether the central cusp is steepened or flattened when the baryonic distribution is taken into account. Using N-body hydrodynamical simulations, Gnedin et al. (2004), Gustafsson et al. (2006) and Macciò et al. (2006) find that the effect of gas cooling steepens the inner density profile to 1.9 ± 0.2, while Mashchenko et al. (2006) claim that the random bulk motion of gas in small primordial galaxies (driven by supernovae explosions) removes the cusp, leaving only cored profiles for both small and large galaxies in the present Universe.

Several other controversial issues remain and we only briefly quote them. The first one is the question of the halo evolution in the presence of a rotating stellar bar, leading to either a destruction of the cusp (see Sellwood 2006; McMillan & Dehnen 2005, and references therein) or a steepening of the cusp (Gnedin et al. 2004; Colín et al. 2006). Some recent simulations including a stellar bar also hint at the emergence of a bar-like structure for the DM (DM bar) in the central region in the case of a strong stellar bar (Colín et al. 2006; Athanassoula 2007): this is the second issue, namely departure from sphericity. Direct observations either favour prolatness (Helmi 2004a,b; Libeskind et al. 2005) or oblateness (Johnston et al. 2005; Metz et al. 2007; Ružička et al. 2007), whereas for pure collisionless simulations, prolatness is generally preferred (see also Bett et al. 2007; Romano-Díaz et al. 2007; Kuhlen et al. 2007)[2]. Prolatness for sub-halos is likely to depend on the position in the galaxy, halos being more spherical in the outer regions (Hayashi et al. 2007). Then, more generally, there is some evidence that halos become more spherical when the baryonic cooling is taken into account (Kazantzidis et al. 2004a; Novak et al. 2006; Berentzen & Shlosman 2006; Macciò et al. 2007b; Debattista et al. 2007), or when a stellar bar is taken into account (Berentzen et al. 2006), or even during mergers (Novak et al. 2006).

2.1.3. Simplifying assumptions

It was shown that the choice of one or another DM profile for the smooth component (Maurin & Taillet 2003; Donato et al. 2004) is not crucial for the calculated flux of anti-protons and positrons. Indeed, charged particles diffuse on magnetic inhomogeneities and fluxes are heavily suppressed (escape from the Galaxy) when originating far away from us, i.e. those from the Galactic centre. For cuspy profiles, the maximal difference is obtained between cored isothermal and Moore profiles (a factor $\lesssim$2, see e.g. Fig. 2 of Barrau et al. 2005), the difference between isothermal and NFW profiles being even smaller ($\lesssim$20%, see Table II in Donato et al. 2004). Due to the lack of a definitive answer for the DM profile in the Galaxy (see the above-discussion), we will restrict ourselves in this paper to a spherically symmetric NFW profile $(\alpha,\beta,\gamma) = (1,3,1)$ for the galactic smooth distributions. Using triaxial halos or different profiles (e.g. $\gamma = 1.2$ or any other profile) is expected to leave the main conclusions of the paper concerning the effects of clump granularity in the Galactic halo unchanged. Sphericity is also assumed for the substructures[3]. Departure from spherical symmetry is left to a forthcoming study.

Finally, we stress that although the existence of a DM spike in the Galactic centre is crucial in the context of γ-ray/neutrino indirect detection (Bertone & Merritt 2005), its effect is merely not relevant in this study. This is due to the depletion of the signal through the diffusive transport of antiparticles, and also to the fact that GCRs originating from annihilations in the very tiny extent of this region are only a small fraction of the total yield that can reach the Earth (the DM annihilation contribution to the GCR flux is integrated over a diffusion volume instead of a line of sight for γ-rays).

2.2. Concentration parameter and sub-halo description

The concentration parameter is a crucial quantity for computing the annihilation rates in (sub)structures. In this section, we actually present all relevant parameters that define a sub-halo. We will come back to the concentration (and the scale radius) associated with the host smooth halo just at the end (Sect. 2.2.2).

In the ΛCDM cosmology, the structures form hierarchically bottom-up via gravitational amplification of initial density fluctuations. The properties of the emerging structures and their subsequent evolution may be described by using the virial quantities. Following the approach and definitions of Bullock et al. (2001), the two parameters $\rho_{\rm s}$ and $r_{\rm s}$, defined in Eq. (1), of a structure of mass $M_{\rm vir}$ are expressed in terms of the concentration $c_{\rm vir}$ and the virial radius $R_{\rm vir}$. This outer radius is defined as the radius within which the mean density is $\Delta_{\rm vir}(z)$ times the matter density $\Omega_{\rm m}\rho_{\rm c}$ at redshift z. At $z = 0$,

$$R_{\rm vir} = \left(\frac{M_{\rm vir}}{(4\pi/3)\Delta_{\rm vir}(0)\Omega_{\rm m}\rho_{\rm c}}\right)^{1/3}. \quad (3)$$

In the following, we use the standard ΛCDM values ($\Omega_{\rm m} = 0.24$, $\rho_{\rm c} = 148\ M_\odot\ {\rm kpc^{-3}}$) and $\Delta_{\rm vir}(0) \approx 340$ (Bullock et al. 2001; Colafrancesco et al. 2006).

The concentration parameter is defined as (Bullock et al. 2001)

$$c_{\rm vir} \equiv \frac{R_{\rm vir}}{r_{-2}}, \quad (4)$$

where r_{-2} is the radius at which $\mathrm{d}/\mathrm{d}r\left(r^2\rho(r)\right)|_{r=r_{-2}} = 0$. It was found (Navarro et al. 1997; Bullock et al. 2001; Eke et al. 2001) that $c_{\rm vir}$ strongly correlates with $M_{\rm vir}$, with larger concentrations observed in the first structures, i.e. in the lighter halos, which

[2] For further developments on the topic of triaxiality, asymmetries, as well as on the spin of halos, see e.g. Moore et al. (2004); Zentner et al. (2005); Lee & Kang (2006); Gao & White (2006); Capuzzo-Dolcetta et al. (2006); Gustafsson et al. (2006); Bett et al. (2007). For the dependence of halo parameters on the environment, see Maulbetsch et al. (2007); Hahn et al. (2007a,b); Ragone-Figueroa & Plionis (2007).

[3] Small structures, which formed earlier, are expected to be more spherical (Moore et al. 2004; Allgood et al. 2006).

have formed in a denser Universe. This relation allows to express ρ_s and r_s in terms of the sole quantity M_{vir}. Note that the $c_{vir} - M_{vir}$ is generally given for a NFW profile, for which $r_s^{nfw} = r_{-2}$, so that:

$$r_s^{nfw}(M_{vir}) = \frac{R_{vir}(M_{vir})}{c_{vir}(M_{vir})} . \quad (5)$$

This is easily transposed to other profiles. For example, for a Moore profile, $r_s^{moore} = 4^{1/3} r_{-2}$, and the corresponding scale radius for the sub-halo is obtained from rescaling the NFW one, i.e. $r_s^{moore} = r_s^{nfw}/0.63$.

The last relation links ρ_s to M_{vir}. Rewriting the profile $\rho(r) = \rho_s \times f(r)$, we get

$$\rho_s = \frac{M_{vir}}{4\pi \int_0^{R_{vir}} r^2 f(r) dr} . \quad (6)$$

When sub-halos are embedded in a larger host halo, the virial radius does not describe the physical radius anymore, and the integration should be performed up to the actual gravitational boundary of the object. For the isothermal case, for instance, the bound radius r_b would be defined such as $\rho(r_b) = 2\rho_{host}(r)$, where r is the sub-halo location. Nevertheless, such a change is negligible for small clumps, apart from the very central regions of the host halo, of which all details are erased by GCR propagation. We will therefore neglect this further, as we have checked that it does not affect our results. For a NFW profile, the integration leads to (see e.g. Fig. 2)

$$\rho_s^{nfw} = M_{vir}/[4\pi r_s^3 A(c_{vir})], \quad (7)$$

where $A(c_{vir}) \equiv \ln(1 + c_{vir}) - c_{vir}/(1 + c_{vir})$.

Hence, in these models, once the $c_{vir} - M_{vir}$ relation is specified, the profile of a clump is fully determined by its virial mass M_{vir}. The behaviour of $r_s^{nfw}(M_{vir})$, ρ_s^{nfw}, as well as c_{vir} and other related quantities, are illustrated in Fig. 2.

2.2.1. $c_{vir} - M_{vir}$ relation: B01 and ENS01 models

We will use the two toy models B01 (Bullock et al. 2001) and ENS01 (Eke et al. 2001), which are based on N-body simulations; we refer the reader to these two papers for a detailed description.

These models predict that the halo concentration decreases with the halo mass (see also Navarro et al. 1997). Note that this behaviour has been observationally confirmed recently at the cluster scale (Buote et al. 2007; Comerford & Natarajan 2007), albeit with a slightly higher $c_{vir} - M_{vir}$ normalisation than predicted (Comerford & Natarajan 2007). In subsequent N-body simulations (Wechsler et al. 2002; Kuhlen et al. 2005; Wechsler et al. 2006; Macciò et al. 2007a), a good agreement was found with the B01 model, adjusted to a slightly lower normalisation ~15–20%[4]. On the other hand, the ENS01 model is excluded in Macciò et al. (2007a) (because of a too shallow slope), but preferred from the analysis of analytic lens models in Fedeli et al. (2007). The state-of-the-art results for halo concentrations come from the recent *Millennium Simulation* (Neto et al. 2007). The analysis at $z = 0$ shows a clear disagreement with B01 for high halo masses $M_{vir} \gtrsim 10^{13}\ M_\odot$ with a better match with ENS01. Still, no conclusion can be drawn to favour one model or another at the low mass end (Neto et al. 2007).

In any case, both toy models are likely to be not realistic enough. For example, Romano-Díaz et al. (2007) showed that, to some extent, the evolution of c_{vir} could forget the initial conditions depending on the degree of violence in its merger events. The dependence of dark halo clustering on the concentration parameter also affects the relation (Sheth & Tormen 2004; Wechsler et al. 2006; Gao & White 2007; Jing et al. 2007; Diemand et al. 2007b), but this is sub-dominant compared to the observed dispersion of c_{vir} (Ragone-Figueroa & Plionis 2007; Macciò et al. 2007a, and references therein).

However, as our goal is to bracket the uncertainties due to the clumpy contribution, we will stick to the simple descriptions of B01 and ENS01, which give respectively an *upper limit* and a *lower limit* on the concentration for the lower masses (see also Fig. 1 in Colafrancesco et al. 2006)[5]. For our purpose, it is sufficient (and convenient) to use a fitted polynomial form at $z = 0$, to encompass the two extreme cases (see Fig. 2 for an illustration of the B01 relation):

$$\ln(c_{vir}) = \sum_{i=0}^{4} C_i \times \left[\ln\left(\frac{M_{cl}}{M_\odot}\right)\right]^i \quad (8)$$

with

$$C_i^{B01} = \{4.34,\ -0.0384,\ -3.91 \times 10^{-4},\ -2.2 \times 10^{-6},\ -5.5 \times 10^{-7}\} \quad (9)$$

and

$$C_i^{ENS01} = \{3.14,\ -0.018,\ -4.06 \times 10^{-4},\ 0,\ 0\}. \quad (10)$$

2.2.2. Scale radius and local DM density in the Milky Way

The DM smooth halo of the Galaxy also follows the previous relation, but a more precise description of the halo properties is in principle possible from in-situ observations. However, the determination of the mass distributions in the Galaxy remains challenging, especially if no assumption is made on the DM profile.

In Dehnen & Binney (1998), the authors fitted a multi-parameter mass model to the available kinematic data for the Galaxy. They found a wide variety of models surviving the fitting process, showing that the mass distribution within the Milky Way is still ill-defined. The case of the NFW profile, which performs as good as any other profile (see Model 2c in their Table 4), was best fitted with a scale radius $r_s = 21.8$ kpc and $\rho_\odot \approx 0.27$ GeV cm^{-3}. A more recent analysis (Battaglia et al. 2005) using a new sample of 240 halo objects (including globular clusters, satellite galaxies and stars) found that the isothermal profile was ruled out for a constant velocity anisotropy of DM. This conclusion is disputed by Dehnen et al. (2006). Nevertheless, both analyses come to similar conclusions concerning the best fit profiles. For example, for the NFW profile, Battaglia et al. (2006) find $r_s = 17.3$ kpc, $\rho_\odot \sim 0.4$ GeV cm^{-3} (corresponding to $M_{vir} = 1.5 \times 10^{12}\ M_\odot$ for $R_{vir} = 312$ kpc). These values are in agreement with those found for simulated halos with similar mass ranges (see e.g. Navarro et al. 2004; Diemand et al. 2007a): in the *Via Lactea* run, $r_s \approx 25$ kpc, $\rho_\odot \sim 0.2$ GeV cm^{-3} (corresponding to $M_{vir} = 1.77 \times 10^{12}\ M_\odot$ for $R_{vir} = 389$ kpc). Finally note that a recent analysis (Cowsik et al. 2007) based on the dynamics of dwarf-spheroidals derives $\rho_\odot \approx [0.25–0.4]$ GeV cm^{-3}.

[4] The concentration is modified when considering dark energy with various values of ω (Dolag et al. 2004), the constant equation of state, but still remains consistent with B01 model (Wechsler et al. 2006).

[5] Their figure corresponds to slightly modified B01 and ENS01, which are not retained here.

We shall fix the parameters of the Milky Way smooth DM distribution. In agreement with the previous values, we define our reference model with $r_s = 20$ kpc and normalise it to the local density $\rho_\odot = 0.3$ GeV cm^{-3} at $R_\odot = 8.0$ kpc. This allows the calculation of the mass within any radius r, which gives the virial halo radius $R_{\rm vir}^{\rm h}$ when combined with Eq. (3): $R_{\rm vir}^{\rm h} = 280$ kpc (so that $c_{\rm vir} = 14$), $M_{\rm vir}^{\rm h} = 1.1 \times 10^{12}\ M_\odot$. Varying $\rho_\odot$ only changes the overall normalisation of all fluxes, whereas modifying r_s would slightly change the spatial distribution, which does not affect the conclusions of this paper.

2.3. Number density of clumps $n_{cl}(M_{cl},r)$

High resolution simulations have revealed that a large number of self-bound substructures survived in the Galactic halo (Tormen et al. 1998; Klypin et al. 1999; Moore et al. 1999; Springel et al. 2001; Zentner & Bullock 2003; De Lucia et al. 2004; Kravtsov et al. 2004; Weinberg et al. 2006; Macciò et al. 2007a; Diemand et al. 2007a).

The mass and spatial distribution of sub-halos shown by these simulations can be approximated as (e.g. Diemand et al. 2004b)

$$\frac{{\rm d}N_{\rm cl}(r,M_{\rm cl})}{{\rm d}V{\rm d}M_{\rm cl}} \equiv \frac{{\rm d}n_{\rm cl}(r,M_{\rm cl})}{{\rm d}M_{\rm cl}} = N_{\rm cl} \times \frac{{\rm d}\mathcal{P}_M(M_{\rm cl})}{{\rm d}M_{\rm cl}} \times \frac{{\rm d}\mathcal{P}_V(r)}{{\rm d}V}, \quad (11)$$

where the last two quantities are probability functions:

$$\int_{M_{\rm min}}^{M_{\rm max}} \frac{{\rm d}\mathcal{P}_M(M_{\rm cl})}{{\rm d}M_{\rm cl}} {\rm d}M_{\rm cl} \equiv 1 \quad (12)$$

$$\int_0^{R_{\rm vir}^{\rm h}} \frac{{\rm d}\mathcal{P}_V(r)}{{\rm d}V} {\rm d}V \equiv 1. \quad (13)$$

The parameter $N_{\rm cl}$ is the total number of clumps within the virial radius $R_{\rm vir}^{\rm h}$ of the Galaxy (see Sect. 2.3.3). This means that the mass distribution of sub-halos does not depend of their locations in the host halo (tidal effects modify this picture, but only in the very central regions of the host halo).

2.3.1. Mass distribution and cut-off

For the mass distribution, the following power-law dependence is observed:

$$\frac{{\rm d}\mathcal{P}_M(M_{\rm cl})}{{\rm d}M_{\rm cl}} = K_M \times \left(\frac{M_{\rm cl}}{M_\odot}\right)^{-\alpha_{\rm m}}. \quad (14)$$

The factor K_M is such that the previous distribution is normalised to 1 for $M_{\rm cl} \in [M_{\rm min}, M_{\rm max}]$:

$$K_M = \frac{1}{M_\odot} \times \frac{(\alpha_{\rm m}-1)}{\left(\frac{M_{\rm min}}{M_\odot}\right)^{1-\alpha_{\rm m}} - \left(\frac{M_{\rm max}}{M_\odot}\right)^{1-\alpha_{\rm m}}}. \quad (15)$$

In the limit $M_{\rm max} \gg M_{\rm min}$, we have $K_M \simeq (\alpha_{\rm m}-1){M_{\rm min}}^{\alpha_{\rm m}-1}$. The logarithmic slope $\alpha_{\rm m} \approx 2.0$ (e.g. Moore et al. 1999; Gao et al. 2004; Reed et al. 2005; Diemand et al. 2006), but the range of $\alpha_{\rm m}$ values obtained in published studies spreads between 1.7 and 2.1 (Shaw et al. 2007, and references therein). For their Milky Way simulation, Diemand et al. (2007a) find ∼1.9. Note that this is in agreement with the value $\alpha_{\rm m} = 1.91 \pm 0.03$ found in Shaw et al. (2007). However, when using an improved identification method of sub-halos on the same simulations, the latter authors conclude to a shallower dependence $\alpha_{\rm m} = 1.79 \pm 0.04$.

The mass distribution covers a wide range, from the heaviest sub-halo mass in the Galaxy, $M_{\rm max} \sim 10^{10}\ M_\odot$ (e.g. Moore et al. 1999; Diemand et al. 2005a), down to a mass $M_{\rm min}$, of which the value is still debated. At an early stage of structure formation, a cut-offs on the lower masses appears due to (i) the diffusion of the DM particles (collisional damping) out of a fluctuation and (ii) free streaming (Hofmann et al. 2001; Berezinsky et al. 2003; Bringmann & Hofmann 2007, and references therein). The first process occurs after freeze-out of the DM particles, when it is still in kinetic equilibrium for some time with the thermal bath (leptons, quarks, gauge bosons). Elastic and inelastic scattering on fast particles results in momentum exchange such that DM particles diffuse in space, leading to a cut-off mass $M_{\rm D}$ for the structures. After kinetic decoupling, the particles move freely in the expanding Universe background and the temperature of this decoupling sets the free streaming cut-off $M_{\rm fs}$ of the mass spectrum. Both cut-off depend on the DM candidate properties. For neutralinos, Berezinsky et al. (2003); Green et al. (2004, 2005) find $M_{\rm D} \approx 10^{-12}$–$10^{-10}\ M_\odot$ and $M_{\rm fs} \approx 10^{-8}$–$10^{-6}\ M_\odot$. This lower mass is slightly increased when taking into account acoustic oscillations owing to the initial coupling between the CDM and the radiation field (Loeb & Zaldarriaga 2005; Bertschinger 2006). A more careful analysis of the temperature of kinetic decoupling taking into account a more realistic range of variations of the particle-physics models consistent with cosmological data was recently done in Profumo et al. (2006). Considering SUSY models (MSSM and mSUGRA) as well as models with universal extra dimensions (UED), these authors found the range $M_{\rm fs} \in [10^{-12}$–$10^{-4}]\ M_\odot$.

To follow the history of these tiny substructures, Diemand et al. (2005a) performed a high resolution N-body simulation. The authors were able, for the first time, to resolve a Milky-Way size dark halo down to the free-streaming stage. They report survival from the smallest structures (injected down to $M_{\rm min} \sim 10^{-6}\ M_\odot$, size ∼0.01 pc) at $z = 26$. However, tidal destruction of the lightest clumps and encounters with stars are still possible at late stages. In an analytical model, Berezinsky et al. (2006) compared the strength of tidal stripping (i) during the hierarchical clustering, (ii) by stars from the stellar bulge, (iii) by stars from the halo and (iv) by the Galactic disk. They found that the last of these processes was the most effective, predicting that only 17% of the Earth-mass clumps survived the tidal destruction. Note that the efficiency of tidal disruption depends on the mass of the clump but also on its environment (position in the Galaxy) so that, in principle, Eq. (11) cannot be used. Indeed, tidal stripping is more efficient towards the Galactic centre: for example, Berezinsky et al. (2006) predict no *light* clumps at the radial distance $r \lesssim 3$ kpc. However, the fraction of surviving clumps is still controversial. Several recent studies have focused on the fate of these Earth-mass clumps. Although some of them conclude to near-complete destruction (Zhao et al. 2007; Angus & Zhao 2007), some others underlined their resilience (Hayashi et al. 2003; Green & Goodwin 2007; Goerdt et al. 2007) in the Galactic potential. In the latter case, it is likely that the inner density slope of cuspy satellite halos remains unchanged, even if the halo loses a lot of its mass (Kazantzidis et al. 2004b).

In any case, as we have already emphasised, the contribution of the central regions of the Galaxy is suppressed by the diffusive transport (for charged particles), therefore it is expected to be unimportant. This assumption is reinforced by the fact that, compared to the smooth distribution that is cuspy, the clump distribution might be cored (see Sect. 2.3.2 below). We checked that taking or not taking into account a significant destruction of low mass clumps – as modelled and described, in e.g. Bi (2006) – left

the results unchanged. Thus, for our purpose, Eq. (16) is a good enough description of the clump distribution. The mass distribution is then fully characterised by its slope α_m and its minimal mass cut-off M_{min}.

2.3.2. Spatial distribution of clumps

In most N-body experiments, the spatial distribution of clumps is found to be anti-biased with respect to the DM density, at least down to the smallest clumps resolved ($\sim 10^6\ M_\odot$) at the moment (Ghigna et al. 2000; De Lucia et al. 2004; Gill et al. 2004; Gao et al. 2004; Diemand et al. 2004b, and references therein). It is parametrised as (spherical symmetry is assumed)

$$\frac{\mathrm{d}\mathcal{P}_V(r)}{4\pi r^2 \mathrm{d}r} = K_V \times \left[1 + \left(\frac{r}{r_H}\right)^2\right]^{-1} \quad (16)$$

where r_H, the core radius, is a fraction of the virial halo radius R^h_{vir}. The constant K_V is chosen here to ensure normalisation to unity when integrating over R^h_{vir}:

$$K_V \equiv \left\{4\pi r_H^3 \times \left[\frac{R^h_{vir}}{r_H} - \tan^{-1}\left(\frac{R^h_{vir}}{r_H}\right)\right]\right\}^{-1}.$$

Diemand et al. (2004b) found $r_H \approx 0.14\ R^h_{vir}$ for galactic-like sub-halos. This bias could be due to the fact that, on average, tidal mass loss experienced by sub-halos is larger in the inner regions than near and beyond the virial radius. This result seems to be largely unaffected by the baryon dissipation (Nagai & Kravtsov 2005; but see Weinberg et al. 2006, for a slightly different conclusion from a SPH simulation).

However, some recent studies argue that this cored distribution could be a selection bias (Kuhlen et al. 2007) or a limitation of collisionless simulations (Macciò et al. 2006; Shaw et al. 2007). For example, Kuhlen et al. (2007) find in their Via Lactea run a spatial distribution that matches the prolate shape of the host halo. The same trend is observed in Macciò et al. (2006), where the dissipation of the baryons greatly enhances the survival of the sub-halos. These authors (see also Nagai & Kravtsov 2005) find that the clumps profile is well fitted by a NFW, even if the latter is still less concentrated ($c_{vir} \approx 6.5$) than their simulated overall mass distribution ($c_{vir} = 9.6$). Indeed, the smallest clumps are likely to follow the smooth DM spatial distribution, and such an assumption has very often been used in analytical studies of DM clumpiness effects on gamma-ray production (e.g. Berezinsky et al. 2003). For the sake of completeness, such a configuration will also be used later for the calculations, and to be conservative, the space distribution of clumps will be taken to be exactly that of the smooth component (same global concentration relation).

2.3.3. Clump number normalisation N_{cl}

The parameter N_{cl} is often determined by adopting the number of sub-halos within a mass range. For example, Moore et al. (1999) found 500 sub-halos with bound masses $\gtrsim 10^8\ M_\odot$. The recent *Via Lactea* simulation of Diemand et al. (2006) gives $N_{cl}(>M_{ref}) = 6.4 \times 10^{-3}\ (M_{ref}/1.8 \times 10^{12}\ M_\odot)^{-1}$, which corresponds to $N_{cl}(>10^8\ M_\odot) \approx 115$.

In a more general context of various masses of host halos, several simulations (van den Bosch et al. 2005, and references therein) are compatible with the value $N_{cl}(>M_{ref}) = 0.017 \times (M_{ref}/M_{host})^{-0.91}$. Taking a mass $M_{host} = 1.1 \times 10^{12}\ M_\odot$ for the Galaxy leads to $N_{cl}(>10^8\ M_{cl}) \approx 81$.

For definitiveness, we choose to set the normalisation N_{cl} such as $N_{cl}(M_{cl} > 10^8\ M_\odot \equiv M_{ref}) = 100 \equiv N_{ref}$. Taking an upper bound of $M_{max} = 10^{10}\ M_\odot$, we get for $\alpha_m \neq 1$:

$$N_{cl} = \frac{N_{ref}}{K_M} \times \frac{(\alpha_m - 1)}{M_{ref}^{1-\alpha_m} - M_{max}^{1-\alpha_m}} \quad (17)$$

$$\simeq (N_{ref} M_{ref}^{\alpha_m - 1}) \times {M_{min}}^{1-\alpha_m} \ (\text{if } M_{min} \ll M_{max}) \quad (18)$$

where K_M is the normalisation given in Eq. (15). For instance, taking $\{M_{min}, M_{ref}, M_{max}\} = \{10^{-6}, 10^8, 10^{10}\}\ M_\odot$ and $\alpha_m = 1.9$, we find $N_{cl} \simeq 4 \times 10^{14}$ clumps, consistent with values obtained by Diemand et al. (2005a).

3. DM modelling choices and salient features

Having discussed in detail the values, uncertainties and relevance of various parameters entering the DM distributions (both smooth and clumpy), we now summarise the reference configurations used as inputs of this paper (Sect. 3.1). Two main consequences are observed: the index of the mass distribution strongly affects the mass fraction of DM in clumps (Sect. 3.2), whereas the $c_{vir} - M_{vir}$ relation impacts on the luminosity profile (Sect. 3.3).

3.1. Reference configurations

The distance of the Sun to the Galactic centre is fixed to $R_\odot = 8.0$ kpc. Whatever the clump configuration, the virial radius of the dark halo in the Galaxy is set to $R^h_{vir} = 280$ kpc, and the local DM density (smooth and clump altogether) to $\rho_\odot = 0.3$ GeV cm^{-3} (Sect. 2.2.2).

3.1.1. The smooth component

It is chosen as a NFW (see discussion in Sect. 2.1.3) with an inner radius $r_s = 20$ kpc ($c_{vir} = 14$). In the absence of any clump – we denote $\rho^0_{sm}(r)$ the corresponding smooth distribution – and with the above values for $\rho_\odot$, R^h_{vir} and r_s, we recover $M^h_{vir} \equiv M^0_{sm} = 1.1 \times 10^{12}\ M_\odot$. The fraction f is usually defined as the fraction of DM taken from the smooth profile and redistributed into the clumps. The smooth contribution in this configuration is then $\rho_{sm}(r) = (1-f)\rho^0_{sm}(r)$, such that $M_{sm} = (1-f)M^h_{vir}$.

3.1.2. The sub-halo component

If the spatial density of clumps is $\propto \rho_{sm}(r)$, the redistribution of the fraction f of the DM into clumps is straightforwardly written as $\rho_{cl} = f\rho^0_{sm}(r)$. Note that in this case, we have a local density of clumps $f\rho_\odot$ and $M^{tot}_{cl} = fM^h_{vir}$ (such that $M^{tot}_{cl} + M_{sm} = M^h_{vir}$). We elaborate on the important case when the two distributions are different in the next Sect. 3.1.3. Otherwise, the clumps parameters are as follows:

1. the inner profile of the clumps $\rho_{cl}(r)$ is taken as a NFW or a Moore. The saturation density is taken from Eq. (2), with $\rho_{sat} \sim 10^{19}\ M_\odot$ kpc^{-3} for typical WIMP parameters[6]. The scale parameters r_s and ρ_s depend solely on c_{vir} and M_{vir}

[6] See discussion in Sect. 3.3 for the consequences of varying ρ_{sat} and considering different inner profiles (e.g. a Moore inner profile).

Table 1. Useful parameters and reference configuration of the DM modelling (see text for further details).

Cosmology	DM (Milky Way)	Clumps	Smooth DM halo
$\Omega_m = 0.24$	$R_{vir} = 280$ kpc	Global†: cored, $\alpha_m = 1.9$, $M_{min} = 10^{-6}\ M_\odot$	NFW (1,3,1)
$\rho_c = 148\ M_\odot\ \mathrm{kpc}^{-3}$	$M_{vir} = 1.1 \times 10^{12}\ M_\odot$	Inner profile: NFW, B01‡	$r_s = 20$ kpc ($c_{vir} = 14$)
$\Delta_{vir}(0) = 340$	$\rho_\odot(R_\odot)^\S = 0.3$ GeV cm^{-3}	$N_{cl}(>10^8\ M_\odot) = 100$	$\rho_{sat}{}^\star \sim 10^{19}\ M_\odot\ \mathrm{kpc}^{-3}$

† Number density of clumps as defined in Eq. (11). ‡ $c_{vir} - M_{vir}$ relation, see Eq. (8). § The distance of the sun to the galactic centre is set to $R_\odot = 8.0$ kpc. * Full expression for the saturation density is given by Eq. (2). It also applies to the clumps inner profile.

Table 2. Description of the various configurations used in the paper for the sub-halo parameters.

Clump description	Values
$d\mathcal{P}_V(r)/dV$	Cored‡ or NFW
Inner profile	NFW‡ or Moore
α_m	[1.8–1.9‡ – 2.0]
M_{min}	[10^{-6} ‡ – 1–10^6] $M_\odot$
$c_{vir} - M_{vir}$	B01‡ or ENS01

‡ Reference configuration.

through Eqs. (5) and (6). The concentration c_{vir} depends on the virial mass M_{vir}, as provided by the B01 and ENS01 models (see Sect. 2.2.1, Eqs. (9) and (10));

2. the clump numerical density $n_{cl}(M_{cl}, r)$ is given by Eq. (14) with $r_H = 0.1 \times R^h_{vir} = 28$ kpc. N_{cl} is set from the condition $N_{cl}(>10^8\ M_\odot) = 100$, with a clump mass upper boundary of $10^{10}\ M_\odot$. The logarithmic slope of the mass distribution is $\alpha_m \in [1.8–2.0]$, and we will survey minimal clump masses starting from $M_{min} = 10^{-6}\ M_\odot$. These last two parameters completely set the mass fraction f_M of the virial mass in clumps (see Sect. 3.2 below), defined as $M^{tot}_{cl} = f_M M^h_{vir}$ (note that f_M does not necessarily coincide with f, see below).

A synthetic view of the relevant parameters retained in this study are proposed in Tables 1 and 2. Note that all varying parameters come from the clumpy distribution (spatial distribution, M_{Min}, α_m, inner profile and the $c_{vir} - M_{vir}$ relation). The configurations, for which we will calculate the boost factors, are listed in Table 2.

3.1.3. Defining the local fraction of DM $f_\odot$ in clumps

If the smooth (e.g. NFW) and the sub-halos (e.g. cored) spatial distributions are different, the mass fraction of DM in sub-halos within $r < R^h_{vir}$ is not constant, but depends on the galactocentric radius r. The point is that in order to compute boost factors, one would naively want to subtract any fraction of DM added in the form of clumps to the smooth component, and compare this new setup to the case in which DM is only smooth. A clear definition of that fraction is crucial before going further. Indeed, we show hereafter that if not treated carefully, there is a source of ambiguity in the interpretation of the resulting boost factor.

Let us first introduce the total mass carried by the clumps within R^h_{vir}, defined as

$$M^{tot}_{cl} \equiv N_{cl} \int_{M_{min}}^{M_{max}} dM_{cl}\, M_{cl}\, \frac{d\mathcal{P}_M(M_{cl})}{dM_{cl}} = N_{cl}\langle M_{cl}\rangle. \quad (19)$$

The quantity $\langle M_{cl}\rangle$ is the mean clump mass associated with the mass range $[M_{min} - M_{max}]$, the mass probability distribution (Eq. (14)), and N_{cl} is the total number of clumps (Eq. (17)).

Without loss of generality, the total density profile of DM may be expressed as

$$\rho_{tot}(r) = (1-f)\rho_{sm}(r) + M^{tot}_{cl}\frac{d\mathcal{P}_V(r)}{dV}, \quad (20)$$

where f is a DM fraction subtracted to the smooth component, which we discuss later on. The quantity $M^{tot}_{cl} d\mathcal{P}_V(r)/dV$ is merely the averaged mass density profile of the whole sub-halo population, obtained from integrating Eq. (11) over the whole mass range of clumps.

Two observational constraints can help to define what kind of fraction f is needed for consistency: the total mass of the Galaxy M^h_{vir}, and the local density $\rho_\odot$. If one wants to ensure that the total mass is left unchanged when adding clumps, then f is the *mass fraction* f_M given by:

$$f = f_M \equiv \frac{M^{tot}_{cl}}{M^h_{vir}}\cdot \quad (21)$$

Otherwise, if one prefers to have a constant local matter density, then f is defined as a *local density fraction* $f_\odot$ as follows:

$$f = f_\odot \equiv \frac{M^{tot}_{cl}}{\rho_\odot} \times \frac{d\mathcal{P}_V(R_\odot)}{dV}\cdot \quad (22)$$

First, if the spatial distribution of clumps tracks the smooth profile, then we have by definition $d\mathcal{P}_V(r)/dV = \rho_{sm}(r)/M^h_{vir}$, and $f_M = f_\odot$. Using either one of these fraction concepts is therefore equivalent: in other words, the halo mass and the mass density (at any r) are conserved when sub-halos are added.

Now, if the two distributions spatially differ, it is no longer possible to fulfil both constraints. We have no choice but to abandon either the halo mass to be constant, or the local density to be constant. Let us see what happens when one of the two above conditions, Eqs. (21) or (22), is plugged in Eq. (20).

First option – ensuring M^h_{vir} is constant: this choice sets that the fraction to be used is the *mass fraction* defined in Eq. (21). An immediate consequence is that the total local DM density is now slightly modified. Plugging this condition (Eq. (21)) in Eq. (20) for $r = R_\odot$ leads to

$$\rho_{tot}(R_\odot) = \left[1 - f_M\left(1 - \frac{M^h_{vir}}{\rho_\odot}\frac{d\mathcal{P}_V(R_\odot)}{dV}\right)\right] \times \rho_\odot. \quad (23)$$

Taking our reference configuration, i.e. the NFW profile for the smooth component (Sect. 3.1.1) and a cored profile for the clump component (Sect. 3.1.2), gives

$$\rho_{tot}(R_\odot) = \left[1 - f_M\left(1 - 5.5\times 10^{-2}\right)\right] \times \rho_\odot \simeq (1-f_M)\rho_\odot. \quad (24)$$

Such a modification of the local DM density translates the fact that the clumpy contribution is locally almost negligible, in that

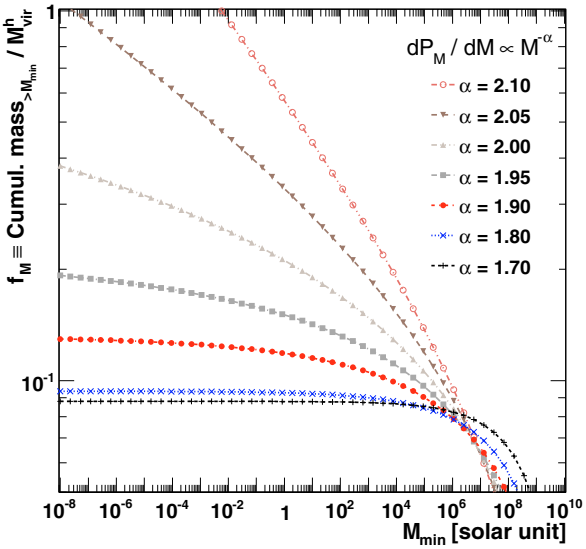

Fig. 1. Mass fraction f_M as a function of $M_{\rm min}$, for different logarithmic slopes $\alpha_{\rm m}$ of the mass distribution (from 2.1 down to 1.7 – top to bottom curves).

case. This will occur every time the clump distribution is flatter than the parent one. As the local density may certainly vary within a factor of two (Sect. 2.2.2), even putting up to 50% of the DM mass in clumps is acceptable. Such a hypothesis is very often made in the literature dealing with γ-rays, but the previous consequence is almost never mentioned.

However, this choice is not judicious in our study. Doing so would even bring additional confusion to the issue of boost factors. Indeed, unlike γ-rays, we remind that for primary cosmic antimatter, the flux is very sensitive to the local density (see Appendix A). Assuming for a while that the smooth component locally dominates the clumpy one (it will actually be shown later to be the case, see e.g. Fig. 5), the calculated mean boost factor would be $B_{\rm eff} \sim (1 - f_M)^2$ (see Eqs. (67) and (68)), which would result in a number significantly less than unity. This would consequently lead to a *damping* factor instead of a an enhancement, which would bring about misleading interpretations.

Second option – ensuring $\rho(Rsol)$ to be constant: to avoid the above situation, we may use the concept of *local density faction* instead, defined by Eq. (22). It comes to demanding $\rho_{\rm tot}(R_\odot) = \rho_\odot$. The boost factor now asymptotically goes to $(1 - f_\odot)^2 \sim 1$ if the clump contribution is negligible. However, this normalisation has to face again an unavoidable issue: the total halo mass will be modified by the adjunction of clumps to the smooth component. Plugging back $f_\odot$ in Eq. (20), integrating over the virial volume and using again f_M (see Eq. (21)), we get

$$M^{\rm tot} = (1 - f_\odot + f_M) \times M^{\rm h}_{\rm vir} \simeq (1 + f_M) \times M^{\rm h}_{\rm vir}. \quad (25)$$

With the different clump configurations used throughout the paper, the total halo mass within the virial radius can be increased up to $f_M \lesssim 50\%$ level (see curves $\alpha_{\rm m} \lesssim 2.0$ in Fig. 1). Such values remain within current estimates of the total mass of the dark halo, as recalled in Sect. 2.2.2.

Closing the case: we conclude by reminding that neither of these choices is better than the other. Both are, somehow, equally artificial. Indeed, there is only, if so, one *true* distribution of smooth and clump DM in the Galaxy. The ambiguity appears because we wish to compare the calculated fluxes to a hypothetical configuration with no clumps. In the context of antimatter fluxes, as explained, the second option (ensuring the same local DM density whatever the configurations) makes more sense, as it leads to boost factor values *asymptotically* reaching 1. This second option is retained throughout the paper[7].

Finally, before closing the DM section, let us discuss how the various configurations gathered in Table 2 impact on some generic properties for the clumps (mass fraction f_M and luminosities).

3.2. Mass fraction f_M in sub-halos

The minimal mass $M_{\rm min}$ of the clumps able to form – and to survive tidal disruption – is a crucial parameter (see also next subsection). Along with the slope $\alpha_{\rm m}$ appearing in the mass distribution Eq. (14), it sets the fraction of DM in clumps, $f_M \equiv M^{\rm cl}_{\rm tot}/M^{\rm h}_{\rm vir}$.

The evolution of f_M with $\alpha_{\rm m}$ and $M_{\rm min}$ is shown in Fig. 1. The behaviours are in agreement with the figures discussed in several simulations. For example, taking a resolved mass $M_{\rm min} \gtrsim 10^{-6}\ M_\odot$, Shaw et al. (2007, and references therein) found $f \sim 5$–10% for $\alpha_{\rm m} = 1.8$. As argued in Diemand et al. (2007a), where a larger value of $\alpha_{\rm m} \sim 2.0$ is preferred, 10% might be only a lower limit and this fraction could reach $f_M \sim 50\%$. In the extreme case of a slope $\alpha_{\rm m} = 2.1$, all the DM could be distributed in clumps, even forbidding the existence of clumps of mass smaller than $\lesssim 10^{-2}\ M_\odot$. This latter configuration is probably not realistic, so we choose to limit the study to the range $\alpha_{\rm m} \in [1.8$–$2.0]$. Consequently, as observed from Fig. 1, the fraction of mass in clumps $M^{\rm cl}_{\rm tot}$, corresponding also to the additional mass added to $M^{\rm h}_{\rm vir}$ (see Eq. (25)), will lie in the range ∼10–40%.

3.3. Luminosity: a closer look on the astrophysical term

Before plugging the propagation, it is interesting to have a look at the luminosity of the source terms in the various configurations. The total luminosity of DM sources can be separated into a particle physics term times an astrophysical term:

$$L_{\rm source}(E, r) \equiv ({\rm d}N/{\rm d}E) \times \mathcal{L}_{\rm astro}(r).$$

The particle physics term is factored out by normalising to the local luminosity $L_\odot \equiv L_{\rm source}(R_\odot) \propto {\rho_\odot}^2$. The relative astrophysical luminosity is then defined as

$$\mathcal{L}(r) \equiv L_{\rm source}(r)/L_\odot = \mathcal{L}_{\rm astro}(r)/\mathcal{L}_{\rm astro}(R_\odot).$$

For short, below, we will continue to call this quantity the luminosity, and use M instead of $M_{\rm cl}$ for the mass clump.

Smooth component: it is straightforwardly written as

$$\mathcal{L}_{\rm sm}(r) \equiv \frac{\rho^2_{\rm sm}(r)}{{\rho_\odot}^2}\,. \quad (26)$$

Substructures: it is convenient to separate the total clump contribution as the sum of the contributions of each decade of mass (throughout the paper, the logarithm bins of mass are denoted $M_i \equiv [10^i$–$10^{i+1}]\ M_\odot$ with i an integer). Taking into account

[7] Let us say it again: should the first option have been retained, we would have ended up with boost factors smaller than one!

the space and mass distributions of the clumps, the total and per logarithmic mass bins luminosities are defined as:

$$\mathcal{L}_{\rm cl}^{\rm tot} \equiv \sum_i \mathcal{L}_{\rm cl}^i, \tag{27}$$

$$\mathcal{L}_{\rm cl}^i(r) \equiv \frac{{\rm d}\mathcal{P}_V}{{\rm d}V}(r) \times \int_{M_i} \frac{{\rm d}\mathcal{L}_{\rm cl}}{{\rm d}\ln M}(M)\ {\rm d}(\ln M), \tag{28}$$

with

$$\frac{{\rm d}\mathcal{L}_{\rm cl}}{{\rm d}\ln M}(M) \equiv N_{\rm cl} \times M \times \frac{{\rm d}\mathcal{P}_M}{{\rm d}M}(M) \times \xi(M), \tag{29}$$

$$\xi(M) \equiv \int_{V_{\rm cl}} \left[\frac{\rho_{\rm cl}(r, M)}{\rho_\odot}\right]^2 {\rm d}^3\boldsymbol{x}\,. \tag{30}$$

The above Eq. (29) defines the luminosity mass profile while Eq. (30) defines an intrinsic effective annihilation volume for a clump of mass M. Note that introducing the mean value $\langle\xi^i\rangle_M$ of ξ over the ith mass bin, allows the luminosity per logarithmic mass Eq. (28) to be recast under a form where the dimensions appear more explicitly:

$$\mathcal{L}_{\rm cl}^i(r) = N_{\rm cl} \times \langle\xi^i\rangle_M \times \frac{{\rm d}\mathcal{P}_V}{{\rm d}V}(r), \tag{31}$$

$$\langle\xi^i\rangle_M \equiv \int_{10^i\ M_\odot}^{10^{i+1}\ M_\odot} {\rm d}M \xi(M) \frac{{\rm d}\mathcal{P}_M(M)}{{\rm d}M}\,. \tag{32}$$

Last, it is useful to introduce a dimensionless intrinsic boost factor $B_{\rm cl}(M)$ for a clump (not to be mistaken with the global boost factor defined in Eq. (67)). The latter compares the annihilation rate of the clump, to the rate that would be obtained for a clump that had the same volume, but with a constant DM density $\rho_\odot$. The *local* intrinsic boost factor can be expressed as

$$B_{\rm cl}(M) \equiv \xi(M) \times \frac{\rho_\odot}{M}\,. \tag{33}$$

We emphasise that such a quantity is meaningful since i) antimatter fluxes mostly depend on the local DM density and ii) unlike γ-rays, we do not look in one specific direction, but rather integrate on the whole clump signal.

Before concluding on resulting luminosities $\mathcal{L}_{\rm sm}(r)$ and $\mathcal{L}_{\rm cl}^i$, let us further detail the various terms appearing in the clump luminosity term.

3.3.1. Annihilation volume $\xi(M)$

This quantity is a function of the mass clump M, and it depends on the inner profile (NFW or Moore), the $c_{\rm vir} - M_{\rm vir}$ relation (B01 or ENS01) and the saturation density $\rho_{\rm sat}$.

Reference configuration (NFW inner profile): for an NFW profile, the annihilation volume has a simple analytical expression

$$\xi^{\rm nfw}(M) = \frac{4\pi}{3}(r_{\rm s}^{\rm nfw})^3 \left(\frac{\rho_{\rm s}^{\rm nfw}}{\rho_\odot}\right)^2 \times \left[\eta^{\rm nfw}(r_{\rm sat}^{\rm nfw}) - \eta^{\rm nfw}(R_{\rm vir})\right], \tag{34}$$

where the scale radius $r_{\rm s}^{\rm nfw}$ and the density at scale radius $\rho_{\rm s}^{\rm nfw}$ depend on the clump mass M, as given in Eqs. (5) and (7). The function $\eta^{\rm nfw}(r)$ is defined as

$$\eta^{\rm nfw}(r) \equiv \left[1 + \frac{r}{r_{\rm s}^{\rm nfw}(M)}\right]^{-3}, \tag{35}$$

Table 3. Sub-halo parameters (reference configuration, i.e. inner NFW and B01 for $c_{\rm vir} - M_{\rm vir}$) for different masses: virial radius $R_{\rm vir}$ (Eq. (3)), scale radius $r_{\rm s}^{\rm nfw}$ (Eq. (5)), scale density $\rho_{\rm s}^{\rm nfw}$ (Eq. (7)), concentration parameter $c_{\rm vir}^{\rm B01}$ (Eq. (9)), effective volume $\xi^{\rm nfw,B01}$ (Eq. (34)), intrinsic local boost $B_{\rm cl}^{\rm nfw,B01}$ (Eq. (33)). See text for details.

$M_{\rm cl}$ ($M_\odot$)	$R_{\rm vir}$ (kpc)	$r_{\rm s}^{\rm nfw}$ (kpc)	$\rho_{\rm s}^{\rm nfw}$ ($M_\odot$ kpc^{-3})	$c_{\rm vir}^{\rm B01}$	$\xi^{\rm nfw,B01}$ (kpc^3)	$B_{\rm cl}^{\rm nfw,B01}$
10^{-6}	2.7×10^{-4}	2.3×10^{-6}	1.8×10^{9}	119	2.5×10^{-12}	20
10^{-3}	2.7×10^{-3}	2.8×10^{-5}	1×10^{9}	98	1.6×10^{-9}	12
1	2.7×10^{-2}	3.5×10^{-4}	5.4×10^{9}	77	8.6×10^{-7}	6.8
10^3	0.27	4.7×10^{-3}	2.5×10^{8}	58	4.3×10^{-4}	3.4
10^6	2.7	6.6×10^{-2}	9.9×10^{7}	41	0.19	1.5
10^9	27	1	3×10^{7}	26	69	0.5

where the saturation density for a NFW is given by

$$r_{\rm sat}^{\rm nfw}(M) = r_{\rm s}^{\rm nfw}(M) \times \frac{\rho_{\rm s}^{\rm nfw}(M)}{\rho_{\rm sat}}\,. \tag{36}$$

It is easily checked that $\xi^{\rm nfw}(M)$ is largely insensitive to the exact value of $\rho_{\rm sat}$ ($\sim 10^{19}\ M_\odot$ kpc^{-3}).

The local intrinsic boost factor $B_{\rm cl}^{\rm nfw}(M)$ can also be analytically expressed in terms of the virial parameters:

$$B_{\rm cl}^{\rm nfw}(M) = \frac{M}{12\pi\rho_\odot {R_{\rm vir}}^3} \times \frac{{c_{\rm vir}}^4\,(3 + c_{\rm vir}(3 + c_{\rm vir}))}{(1 + c_{\rm vir})[c_{\rm vir} - (1 + c_{\rm vir})\ln(1 + c_{\rm vir})]^2}. \tag{37}$$

As $c_{\rm vir}$ is only very slightly mass dependent and $R_{\rm vir} \propto M^{1/3}$, the intrinsic boost factor, $B_{\rm cl}$, is almost constant over a wide range of sub-halo masses. More precisely, for the NFW case in the B01 model, we find it to scale with the concentration parameter like

$$B_{\rm cl}^{\rm nfw,B01}(M) \simeq 1.29\times10^{-4} \left({c_{\rm vir}}^{\rm B01}\right)^{5/2}. \tag{38}$$

For illustration purpose, typical values for all above quantities (for various masses of clumps) are gathered in Table 3. After applying a suitable renormalisation, the same quantities – some of which having power law dependencies with M – are also displayed in Fig. 2. We check that $\xi^{\rm nfw}$ roughly scales like M, a very common feature already emphasised in the literature that focuses on gamma-rays (see the consequences in the next subsection). For the intrinsic local boost factor, we read off the last column in Table 3 that only clumps below $M \lesssim 10^6\ M_\odot$ may significantly overcome the local annihilation signal. The first conclusion that can be drawn is that massive clumps, unless close to the solar neighbourhood (which is very unlikely), will not be able to *boost* the antimatter signals. More importantly, the very same parameter allows an upper limit to the total boost expected to be set, $B_{\rm cl}^{\rm nfw,B01} < 20$.

Moore vs. NFW inner profile – ENS01 vs. B01: these conclusions are very easily extended to other configurations. We actually find a very simple rescaling factor linking the annihilation volume $\xi^{\rm moore}(M)$ to the above $\xi^{\rm nfw}(M)$, when $\rho_{\rm sat}^{\rm ref} = 10^{19}\ M_\odot$ kpc^{-3}:

$$\xi^{\rm moore}(M, \rho_{\rm sat}) \simeq 8 \times \xi^{\rm nfw}(M). \tag{39}$$

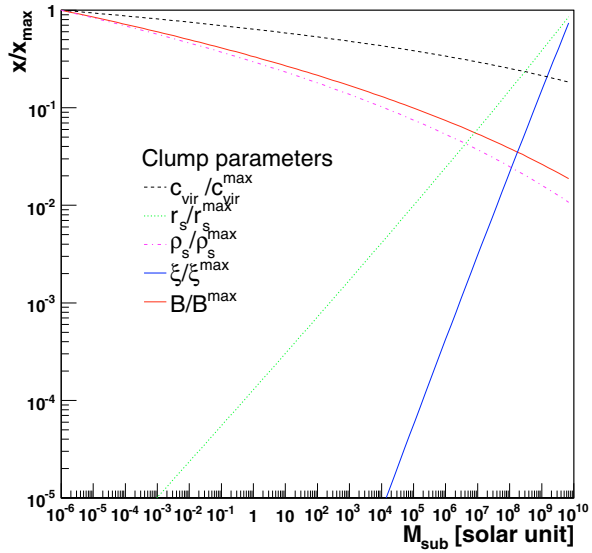

Fig. 2. Same as in Table 3. Each parameter is normalised with respect to its maximum value (in the mass range displayed).

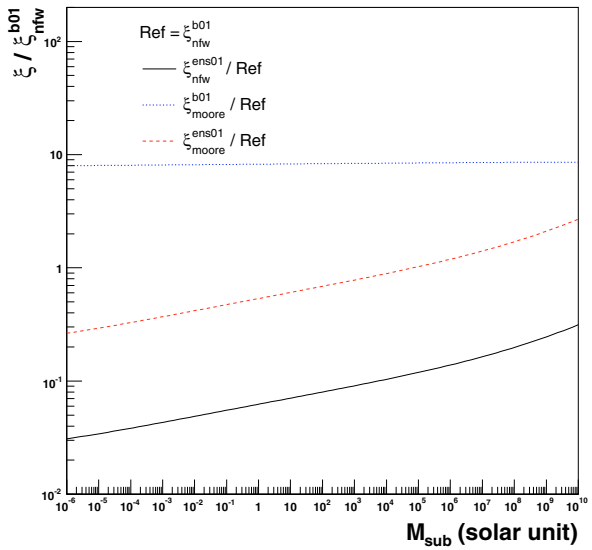

Fig. 3. Ratio of the annihilation volume for three benchmark sub-halo models to the reference one, defined as $\xi_r^{\rm X} \equiv \xi^{\rm x}/\xi^{\rm ref} = B^{\rm x}/B_{\rm cl}^{\rm ref}$. The reference configuration is an inner NFW profile with B01 concentration. The three benchmark configurations are X = (Moore, B01) (upper curve), X = (Moore, ENS01) (middle curve) and X = (NFW, ENS01) (lower curve).

This does not depend on the $c_{\rm vir} - M_{\rm vir}$ relation, and to a good extent, neither on the WIMP mass and annihilation cross section, nor on the clump mass, as illustrated in Fig. 3 Note that, as expected, the ENS01 configuration is lower than B01, implying, for the intrinsic boost factor, the hierarchy $B_{\rm cl}^{\rm nfw,ENS01} < B_{\rm cl}^{\rm nfw,B01} \simeq B_{\rm cl}^{\rm moore,ENS01} < B_{\rm cl}^{\rm moore,B01}$ (roughly corresponding to 0.1:1:10). Hence the former configuration will provide the minimal boost, the reference configuration the median boost and the last configuration the maximal boost.

3.3.2. $\mathrm{d}\mathcal{L}_{\rm cl}/\mathrm{dln}\,M$

The differential luminosity Eq. (29) is evaluated taking into account the mass distribution of clumps Eq. (14). The result is shown in Fig. 4 for different values of the slope $\alpha_{\rm m}$. We recover

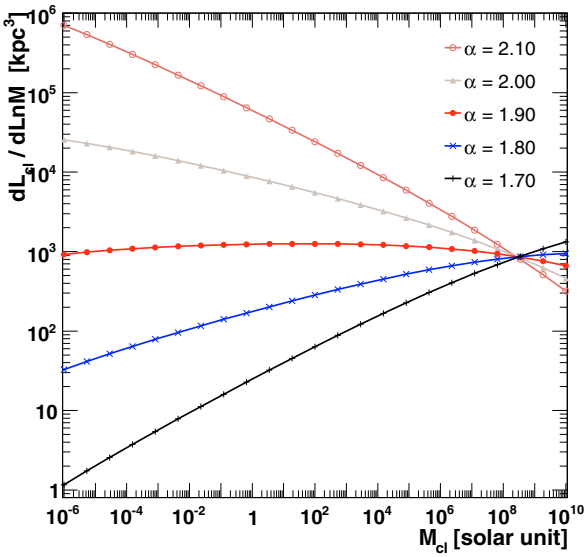

Fig. 4. Differential luminosity (true units in kpc^3) of the population of clumps $\mathrm{d}\mathcal{L}_{\rm cl}/\mathrm{dln}\,M$ as defined in Eq. (29). The curves correspond to the NFW-B01 reference configuration, for various values of $\alpha_{\rm m}$. The curves for any other configuration may be obtained by multiplying these curves to the ratios shown in Fig. 3.

the various trends seen in the literature (see, e.g. Fig. 8 of Diemand et al. 2007a; Berezinsky et al. 2003). In particular, the value $\alpha_{\rm m} = 1.9$, favoured in simulations, shows a roughly constant luminosity per decade. For smaller (respectively greater) value of $\alpha_{\rm m}$, the luminosity will be dominated by the heaviest (lightest) clumps. In that case, based upon the understanding gained from the previous discussions, the boost is expected to be small (close to unity, from the intrinsic boost factor). At the same time, the variance of the clumpy signal is expected to be large (light clumps add no contribution and heavy clumps are scarce). For larger $\alpha_{\rm m}$, the mass $M_{\rm min}$ of the lightest clump is crucial, because the latter drives the total luminosity. These large $\alpha_{\rm m}$ configurations are expected to give the largest boost factors. The last step is to put together the smooth and clumpy luminosities.

3.3.3. Luminosity profiles $\mathcal{L}_{\rm sm}(r)$ and $\mathcal{L}_{\rm cl}^i(r)$ in the Galaxy

The last hint at small boost factors for the case of antimatter DM is given when comparing the smooth and clump luminosities. This is first shown for the reference configuration in Fig. 5 (top left panel). As already emphasised (see also Diemand et al. 2007a), for the reference configuration $\alpha_{\rm m} = 1.9$, the contributions to the average annihilation fluxes of any decade mass range will be almost the same on the whole range of mass clumps (see also Fig. 1 of Yuan & Bi 2007). Around $r = R_\odot$, the luminosity is completely dominated by the smooth contribution (~100 times more than the total clump luminosity), so that for this configuration, we may predict beforehand (i) no boost factor and (ii) a small variance on this boost factor.

The logarithmic slope of the mass distribution $\alpha_{\rm m}$ reverses hierarchy in the mass contribution: for $\alpha_{\rm m} = 1.8$ (see Fig. 5, top right), the more massive the population of clump the more luminous it is, whereas for $\alpha_{\rm m} = 2$ (see Fig. 5, bottom left), the less massive, the more luminous. The trade off is reached close to $\alpha_{\rm m} = 1.9$. However, the total clump luminosity never reaches the level of the smooth one! In the best case ($\alpha_{\rm m} = 2$), it is 10 times smaller. Nevertheless, taking larger $\alpha_{\rm m}$ values naturally leads to larger boost, in a more general context.

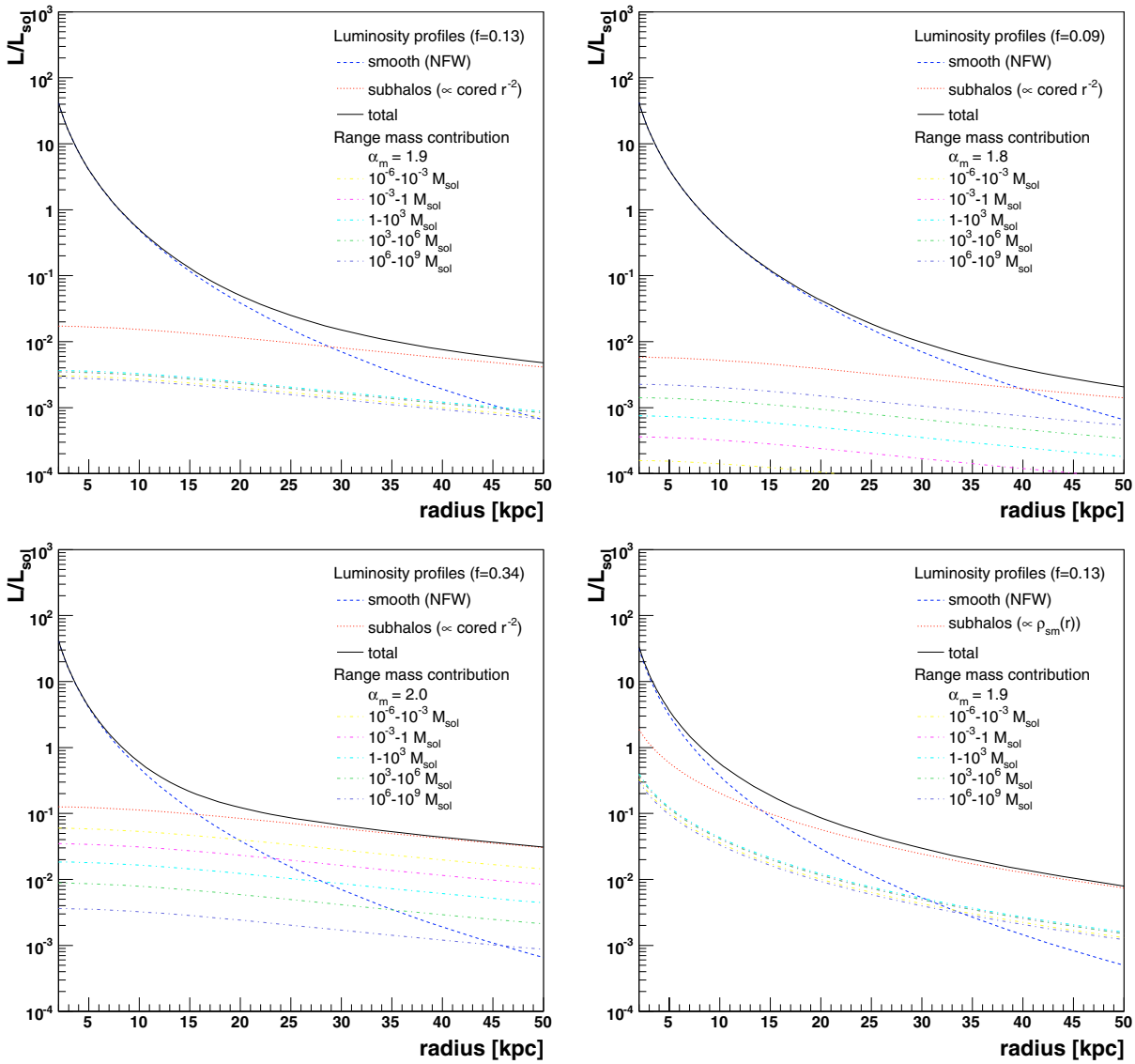

Fig. 5. Relative luminosity profiles as functions of the galactocentric radius r, in units of local luminosity $L_\odot$. Luminosities are plotted for the smooth DM contribution and for clumps in logarithmic mass bins of 3-decade width. *Top left*: reference configuration (ref). *Top right*: as ref but $\alpha_\mathrm{m} = 1.8$. *Bottom left*: as ref but $\alpha_\mathrm{m} = 2.0$. *Bottom right*: as ref but for a spatial distribution of clumps $\propto \rho_\mathrm{sm}(r)$.

Now, if we now assume that, instead of having a cored profile, the spatial distribution follows the parent one (NFW), we see in Fig. 5 (bottom right) that the situation is more favourable for the boost factors. Keep in mind that this is an upper limit since the the averaged radial mass density profile of clumps is believed to be a flatter distribution than the smooth one (see Sect. 2.3.2).

Anticipating the results of using ENS01 instead of B01, or using a Moore inner profile instead of a NFW, especially from Fig. 3, we already know that ENS01 will only further decrease the total clump luminosity (roughly by a factor of 10 compared to B01), whereas Moore will increase the total clump luminosity (roughly by a factor of 10 compared to NFW).

To summarise, from the general study of the luminosity, we might already conclude that no configuration of DM will lead to huge boost factors. Pushing all the parameters for the maximum effect, i.e. Moore inner profile, NFW spatial distribution, B01 and $\alpha_\mathrm{m} = 2.0$, would possibly lead to a boost factor of a few, but certainly not a hundred. We can expect all other configurations to end up with a boost factor close to unity. The rest of the paper is devoted to the full calculations to confirm these expectations.

4. Propagation model

In the Galaxy, a charged particle travelling from its source to the solar neighbourhood is affected by several processes. The scattering off random magnetic fields leads to spatial and energy diffusion (reacceleration) and particles may also be spatially convected away by the galactic wind (which induces adiabatic losses).

In this paper, the framework used is the following (e.g. Berezinskii et al. 1990): for the transport processes we take a spatial independent diffusion coefficient $K(E) = \beta K_0 \mathcal{R}^\delta$ (where $\mathcal{R} = pc/Ze$ is the rigidity) and a constant wind V_c directed outwards along z. Cosmic rays are confined within a diffusive halo L, such as the differential density, $\mathrm{d}N/\mathrm{d}E \equiv N$, is bound by $N(z = L, r) = 0$. The free parameters of the model are the halo size L of the Galaxy, the normalisation of the diffusion coefficient K_0 and its slope δ, and the constant galactic wind V_c (see Sect. 4.3). Other processes (such as continuous and catastrophic gain/losses) are more species-dependent. Hence, although all charged particles are propagated in the same framework, due

to this dependence, the phenomenology of propagation is completely different for $\overline{\mathrm{p}}$ and positrons.

The reader is referred to Maurin et al. (2001) for a more detailed presentation and motivation of the framework. Note that this model has been repeatedly and consistently used in several studies to constrain the propagation parameters (Maurin et al. 2001, 2002; Donato et al. 2002) and examine the consequences (Taillet & Maurin 2003; Maurin & Taillet 2003) for the standard $\overline{\mathrm{p}}$ flux (Donato et al. 2001), the exotic $\overline{\mathrm{p}}$ and $\overline{d}$ fluxes (Maurin et al. 2004, 2006a; Donato et al. 2004; Barrau et al. 2002, 2005; Bringmann & Salati 2007), but also for positrons (Lavalle et al. 2007; Brun et al. 2007).

4.1. Propagator and flux for anti-protons

It was shown in Maurin et al. (2006a) that neglecting all energy redistribution terms (energy losses, reacceleration and tertiary source term) provides a correct description at sufficiently high energy, while remaining good enough down to ~GeV IS energies (better than 50% depending on the propagation parameters considered). This approximation is retained here. The only catastrophic losses for anti-protons are spallations – the particle does not survive the interaction.

Denoting $\Gamma_{\rm tot} = \sum_{\rm ISM} n_{\rm ISM}.v.\sigma^{\bar{\rm p}}_{\rm ISM}$ the destruction rate of $\overline{\mathrm{p}}$ in the thin gaseous disk ($n_{\rm ISM}$ = H, He), the transport equation for a point source, defining the propagator, reads (Maurin et al. 2006a):

$$\left\{-K\triangle + V_{\rm c}\frac{\partial}{\partial z} + 2h\Gamma_{\rm tot}\delta(z)\right\}\mathcal{G}^{\,\bar{\rm p}} = \delta(\boldsymbol{r}-\boldsymbol{r}'). \tag{40}$$

For simplicity, we only consider a flux detected at solar position $\boldsymbol{r}_\odot = (x_\odot = R_\odot, y_\odot = 0, z_\odot = 0)$. For a point source S at $\boldsymbol{r}_S$, the corresponding flux only depends, in cylindrical coordinates, on the relative distances $r = |\boldsymbol{r}_\odot - \boldsymbol{r}_S|$ and $z = z_S$. The propagator $\mathcal{G}^{\bar{p}}_\odot(r,z)$ is given by

$$\mathcal{G}^{\bar{p}}_\odot(r,z) = \frac{\exp^{-k_v z}}{2\pi KL} \times \sum_{n=0}^{\infty} c_n^{-1} K_0\left(r\sqrt{k_n^2+k_v^2}\right)\sin\left[k_n L\right]\,\sin\left[k_n(L-z)\right] \tag{41}$$

where K_0 is the modified Bessel function of the second kind. The quantity k_n is the solution of

$$2k_n\cos k_n L = -k_d \sin k_n L,$$

and

$$c_n = 1 - \frac{\sin k_n L\cos k_n L}{k_n L}\,. \tag{42}$$

We also have

$$k_v \equiv V_{\rm c}/(2K) \quad \text{and} \quad k_d \equiv 2h\,\Gamma_{\rm tot}/K + 2k_v.$$

For a source term $q_\odot(r,z,\theta)Q(E)$ (origin is taken to coincide with solar location) the equilibrium spectrum at solar position is finally given by

$$\Phi^{\bar{p}}_\odot(E) = \frac{vQ(E)}{4\pi}\times 2\int_0^L {\rm d}z\int_0^\infty r{\rm d}r\;\mathcal{G}^{\bar{p}}_\odot(r,z)\int_0^{2\pi}{\rm d}\theta\, q_\odot(r,z,\theta). \tag{43}$$

4.2. Positrons

Contrarily to nuclear species, there are no catastrophic losses for positrons. A more crucial point is that propagation of positrons is dominated by energy losses (e.g. Moskalenko & Strong 1998). In that case, a monochromatic line at the source leads to a spectrum once propagated. This is at variance to $\overline{\mathrm{p}}$ whose propagator for exotic sources is at constant energy.

The diffusion equation that characterises the evolution of the positron number density N per unit energy, with a source term $q(\boldsymbol{r})Q(E)$, reads

$$-K_0\left(\frac{E}{E_0}\right)^\delta \triangle N + \frac{\partial}{\partial E}\left\{\frac{{\rm d}E}{{\rm d}t}\,N\right\} = q(\boldsymbol{r})Q(E). \tag{44}$$

The first term is simply the diffusion coefficient written as $K(\mathcal{R}) \approx K_0(E/E_0)^\delta$. For simplicity, we have also neglected the effect of the Galactic wind (see next section for a discussion).

We proceed as in Lavalle et al. (2007, and see references therein). The synchrotron and inverse Compton losses can be written as ${\rm d}E/{\rm d}t(E) = -E^2/(E_0\tau_E)$, with $E_0 = 1$ GeV and $\tau_E \approx 10^{16}$ s. Defining a pseudo-time

$$\hat{t} \equiv \tau_E\,\frac{(E/E_0)^{\delta-1}}{1-\delta}$$

and applying the following rescaling,

$$\hat{N} \equiv (E/E_0)^2 N \quad \text{and} \quad \hat{Q}(E) \equiv (E/E_0)^{2-\delta}Q(E),$$

the diffusion equation can be rewritten as

$$\frac{\partial}{\partial\hat{t}}\hat{N} - K_0\triangle\hat{N} = q(\boldsymbol{r})\hat{Q}(E). \tag{45}$$

Thus, instead of finding the solution of Eq. (44), we are left to solve the well-known time-dependant diffusion equation Eq. (45).

It proves convenient to separate diffusion along the radial and vertical direction. Considering a source located at $(x,y,z,\hat{t})$ detected at $(R_\odot,0,0,\hat{t}_{\rm O})$, the corresponding flux depends only on the radial relative distance $r = |\boldsymbol{r}_S - \boldsymbol{r}_{\rm O}|$, the distance of the source from the plane $z = z_S$ and the relative pseudo-time $\hat{\tau} = \hat{t}_{E_{\rm O}} - \hat{t}_{E_S}$. The Green function $\hat{\mathcal{G}}_\odot(r,z,\hat{\tau})$ of Eq. (45) is then given by:

$$\hat{\mathcal{G}}_\odot(r,z,\hat{\tau}) = \frac{\theta(\hat{\tau})}{4\pi K_0\hat{\tau}}\;\exp\left(-\frac{r^2}{4K_0\hat{\tau}}\right)\times\mathcal{G}^{1D}(z,\hat{\tau}). \tag{46}$$

The effect of boundaries along $z = \pm L$ appears in $\mathcal{G}^{1D}(z,\hat{\tau})$ only. For convergence properties, two distinct regimes are worth considering (Lavalle et al. 2007):

1. for sources close to us, it is best to use the so-called electrical image formula (e.g. Baltz & Edsjö 1999):

$$\mathcal{G}^{1D}(z,\hat{\tau}) = \sum_{n=-\infty}^{+\infty}(-1)^n\,\frac{\theta(\hat{\tau})}{\sqrt{4\pi K_0\hat{\tau}}}\;\exp\left\{-\frac{(z_n-z)^2}{4K_0\hat{\tau}}\right\}, \tag{47}$$

   where $z_n = 2Ln + (-1)^n z$;
2. for far away sources, a more suitable expression is

$$\mathcal{G}^{1D}(z,\hat{\tau}) = \frac{1}{L}\sum_{n=1}^{+\infty}{\rm e}^{-K_0k_n^2\hat{\tau}}\phi_n(0)\phi_n(z) + {\rm e}^{-K_0k'^2_n\hat{\tau}}\phi'_n(0)\phi'_n(z) \tag{48}$$

Table 4. Propagation parameters giving the maximal, median and minimal antiparticle DM fluxes compatible with B/C analysis.

	δ	K_0 (kpc^2 Myr^{-1})	L (kpc)	V_c (km s^{-1})
max	0.46	0.0765	15	5.0
med	0.70	0.0112	4	12.0
min	0.85	0.0016	1	13.5

where

$$\phi_n(z) = \sin\left[k_n(L-|z|)\right];\ k_n = \left(n-\frac{1}{2}\right)\frac{\pi}{L}\ \text{(even)}$$
$$\phi'_n(z) = \sin\left[k'_n(L-z)\right];\ k'_n = n\frac{\pi}{L}\ \text{(odd)}.$$

Coming back to the non-hat quantities, the propagator for a monochromatic point source is related to Eq. (46) by

$$\mathcal{G}_\odot^{e^+}(r,z,E\leftarrow E_S) = \frac{\tau_E E_0}{E^2}\times\hat{\mathcal{G}}_\odot(r,z,\hat{\tau}=\hat{t}_E-\hat{t}_{E_S}). \quad (49)$$

It follows that for a spatial and spectral distribution of sources $q_\odot(\boldsymbol{r})Q(E)$ (origin of coordinates at solar neighbourhood), the equilibrium spectrum at solar position and energy E is given by

$$\Phi_\odot^{e^+}(E) = \frac{v}{4\pi}\times 2\int_0^L \mathrm{d}z\int_0^\infty r\mathrm{d}r \quad (50)$$
$$\times\int_E^\infty \mathrm{d}E_S\left\{Q(E_S)\mathcal{G}_\odot^{e^+}(r,z,E\leftarrow E_S)\right\}\int_0^{2\pi}\mathrm{d}\theta q(r,z,\theta).$$

4.3. Propagation parameters

A few important points are reminded concerning the role of the various transport parameters on the propagated spectra of the antiparticles created in the DM halo. More details can be found in Donato et al. (2004); Barrau et al. (2005).

The halo height L determines the total number of sources inside the diffusive region and the typical distance a GCR can travel before escaping from the Galaxy (see also Appendix A). The galactic wind wipes the particles away from the disk, and a similar effect occurs if V_c is large enough. The parameters L, V_c and K_0 are correlated. In the subset of parameters giving the observed B/C ratio (Maurin et al. 2001, 2002), low values of K_0 generally correspond to low L and V_c, so that the DM signal is expected to decrease with decreasing K_0. On that basis, extreme and median parameters can be extracted, in the sense that these parameters lead to the minimal and maximum expected flux, while the median parameters (best fit to B/C data) provide the most likely flux. These parameters are recalled in Table 4.

Having in mind the connection between the propagation parameters and the fluxes, we can now justify discarding, for our calculations, the effects of the wind and reacceleration for the positrons. For example, for configurations with small δ, as the effect of the wind is always negligible for anti-protons, it is also the case for positrons (their travel time in the Galaxy is less or at most that of the anti-protons). For the sets of parameters with larger δ, the effect of the wind becomes dominant below $\lesssim$1 GeV. However, we are mainly interested in the high energy regime for positrons. Furthermore, if the low-energy behaviour is strongly dominated by convection (as is the case for anti-protons when $\delta = 0.85$), then it superseeds energy loss effects for positrons: in that case, all the conclusion about $\bar{\mathrm{p}}$ would also hold for e^+.

5. Methods

The smooth contribution is straightforwardly calculated, contrarily to the clumpy contribution that is plagued by *statistical* uncertainties (in the sense that the position of clumps is a random variable, see Sect. 5.2). The latter issue is the primary concern of this section.

Two complementary approaches are followed to calculate the *Galactic variance* of the clumpy contribution. The first one (Lavalle et al. 2007) is a semi-analytical calculation of the mean and variance from the generic statistical properties of the clumps (spatial and mass distributions), using the particle propagators that we recalled. The second one uses the same ingredients, but quantities under scrutiny (mean and variance) are obtained by accumulating realisations of a clumpy galactic halo. Due to the lack of any clue about the precise location and intrinsic properties of each individual DM clump, working with statistical tools is well motivated. The numerous clumps can be treated as random objects, which average properties are taken here from N-body simulations.

Note that both methods rest on the assumption that clumps are considered as point-like sources. This is correct while the distance of a clump to the Earth is greater than its spatial extension, and if the GCR propagation properties do not change within the spatial extension of a clump (see Table 3). As the flux, on average, is not dominated by nearby substructures, and since for those far away clumps the spatial dependence of the propagator is smooth enough (diffusive process), the point-like source assumption holds. Would a nearby clump dominate the positron or anti-proton flux – which is very unlikely according to our calculation – a single source computation would be enough to deal with the clumpiness issue. Nevertheless, such a case, while easier to calculate, would make the clumpiness itself an absolutely unpredictive scenario for the indirect search for DM using antimatter GCRs, and is beyond the scope of this paper.

5.1. Generalities

Before exposing the methods, it is convenient to define a pseudo-Green function, denoted $\tilde{\mathcal{G}}$, by absorbing the energy dependence of the GCR propagators. To this aim, we define the quantity $\mathrm{d}N/\mathrm{d}E_S(E_S)$ to be the antimatter species spectrum at the source, which is defined here as the number of antimatter particles injected per annihilation and per energy unit.

For anti-protons, the pseudo-Green function reads:

$$\tilde{\mathcal{G}}^{\bar{\mathrm{p}}}(E) \equiv \frac{\mathrm{d}N}{\mathrm{d}E}(E)\times\mathcal{G}_\odot^{\bar{\mathrm{p}}}(r,z,E). \quad (51)$$

The propagation term and the source term can be factorised (no energy mixing during propagation, a $\bar{\mathrm{p}}$ emitted at E_S is detected at the same energy E_S). It means that the results for the relative uncertainties on the fluxes and for boost factors are independent of the particle physics model. Unfortunately, this is not the case for positrons:

$$\tilde{\mathcal{G}}^{e^+}(E) \equiv \int_E^\infty \mathrm{d}E_S\left\{\frac{\mathrm{d}N}{\mathrm{d}E_S}(E_S)\times\mathcal{G}_\odot^{e^+}(r,z,E\leftarrow E_S)\right\}. \quad (52)$$

The integral characterises energy losses and the source spectrum cannot be factored out of the integrand. Nevertheless, in the following, in order to keep the discussion at the most general possible level, we will mainly focus on a monochromatic line of positrons at E_S, i.e. $\mathrm{d}N/\mathrm{d}E_S(E_S) = \delta(E-E_S)$. The results for positrons are thus forced to be independent of any particle

physics model. As we will see in Sect. 6, as the boost factor is close to unity for all energies, convolving the propagator with a realistic DM source spectrum would yield a similar boost factor as obtained from the monochromatic line.

In the following, we will make use of $\tilde{\mathcal{G}}$, where the energy dependence is implicit for any species.

The total GCR flux $\phi_{\rm tot}$ originating from DM annihilations may be separated into two contributions, for the smooth component and for clumps:

$$\phi_{\rm tot} = \phi_{\rm sm} + \phi_{\rm cl}. \tag{53}$$

Smooth contribution: The *smooth* contribution to the flux $\phi_{\rm sm}$ is calculated using the smooth density profile $\rho_{\rm sm}$:

$$\phi_{\rm sm} = \frac{v}{4\pi} S \int {\rm d}^3\boldsymbol{x} \left(\frac{\rho_{\rm sm}}{\rho_\odot}\right)^2 (\boldsymbol{x})\, \tilde{\mathcal{G}}(\boldsymbol{x}_\odot \leftarrow \boldsymbol{x}), \tag{54}$$

where v is the cosmic ray velocity, $\tilde{\mathcal{G}}$ is the pseudo-Green function, defined above for $\bar{\rm p}$ and $\rm e^+$, and S is a particle physics coefficient[8] depending on the WIMP model[9]:

$$S \equiv \delta \frac{\langle\sigma v\rangle}{2} \left(\frac{\rho_\odot}{m_{\rm wimp}}\right)^2 \cdot \tag{55}$$

The normalisation is thus chosen with respect to the local DM density $\rho_\odot = 0.3$ GeV cm^{-3} and $\delta = 1$ (1/2) if the WIMP of mass $m_{\rm wimp}$ is a Majorana (respectively Dirac) particle. S is actually counting the number of annihilations occurring in an infinitely small volume, in which the DM density is set to $\rho_\odot$.

Sub-halo contribution: The Galactic halo is populated by a constellation of many clumps, whose positions and masses are actually unknown. Nevertheless, if $N_{\rm cl}$ is the number of clumps in a certain diffusive volume in the Galaxy, then their total contribution to the flux reads:

$$\phi_{\rm cl}^{\rm tot} = \sum_{i=1}^{N_{\rm cl}} \phi_i. \tag{56}$$

The spatial dependence of the propagator is smooth enough (diffusive process) so that $\tilde{\mathcal{G}}$ may be considered constant over the clump scale: each clump behaves as a point-like source. The cosmic ray flux measured at the Earth from the ith clump is therefore given by:

$$\phi_i(\boldsymbol{x}_\odot) = \frac{v}{4\pi} \times S \times \xi_i \times \tilde{\mathcal{G}}(\boldsymbol{x}_\odot \leftarrow \boldsymbol{x}_i), \tag{57}$$

where ξ_i is the effective annihilation volume defined by Eq. (30).

5.2. Semi-analytical calculation of the flux and the boost factor, and associated variances, due to sub-halos

In this section, we apply the formalism developed in Lavalle et al. (2007) in order to predict how boosted the antimatter cosmic ray fluxes should be when adding sub-halos.

[8] So that ${\rm d}N/{\rm d}E \times S \equiv Q(E)$, as used in Sect. 4.

[9] This differs from the convention used in Lavalle et al. (2007) for which $(v/4\pi)$ is included in S.

5.2.1. Whole sub-halo flux $\langle\phi_{\rm cl}^{\rm tot}\rangle$

The propagator describes the probability for a cosmic ray injected at position $\boldsymbol{x}_S$ with energy E_S to be detected at the Earth ($\boldsymbol{x}_\odot$) with energy E (recalling that for anti-protons, $E_S = E$, as they do not loose energy).

As the intrinsic luminosity of a clump is entirely set once its mass is known, the effective volume ξ_i can be expressed as $\xi_i(M_{{\rm cl},i})$. Thus, given Eq. (57), the flux associated with a single clump is a stochastic variable that depends on two probability distributions: the space and the mass distributions (Sect. 2.3). This is summarised in the following equation:

$$\frac{{\rm d}P_\phi}{{\rm d}\phi_{\rm cl}} = \frac{{\rm d}P(\boldsymbol{x}_{\rm cl}, M_{\rm cl})}{{\rm d}^3\boldsymbol{x}_{\rm cl}{\rm d}M_{\rm cl}} = \frac{1}{4\pi r^2}\frac{{\rm d}\mathcal{P}_V(r)}{{\rm d}r} \times \frac{{\rm d}\mathcal{P}_M(M_{\rm cl})}{{\rm d}M_{\rm cl}}, \tag{58}$$

where both distributions, given by Eqs. (16) and (14), respectively, are considered uncorrelated[10].

The halo is populated by a constellation of many clumps whose total contribution to the GCR flux is given by

$$\phi_{\rm cl}^{\rm tot}(\boldsymbol{x}_\odot) = \sum_{i=1}^{N_{\rm c}} \phi_i = \frac{v}{4\pi} S \sum_{i=1}^{N_{\rm c}} \xi_i \times \tilde{\mathcal{G}}(\boldsymbol{x}_\odot \leftarrow \boldsymbol{x}_i). \tag{59}$$

Though the previous expression would be the actual expected flux for our Galaxy, we do not neither know the number nor the precise locations and the masses of clumps in the halo. Nevertheless, the knowledge of their phase space distribution can be used to determine the mean value of that flux:

$$\langle\phi_{\rm cl}^{\rm tot}\rangle = N_{\rm cl} \times \frac{v}{4\pi} \times S \times \langle\xi\rangle_M \times \langle\tilde{\mathcal{G}}\rangle_V, \tag{60}$$

where $N_{\rm cl}$ is the number of sub-halos hovering in the DM volume V of interest, and

$$\langle\tilde{\mathcal{G}}\rangle_V = \langle\tilde{\mathcal{G}}\rangle \equiv \int_V {\rm d}^3\boldsymbol{x}\, \tilde{\mathcal{G}}(\boldsymbol{x}_\odot \leftarrow \boldsymbol{x}) \times \frac{{\rm d}\mathcal{P}_V(\boldsymbol{x})}{{\rm d}V}; \tag{61}$$

$$\langle\xi\rangle_M = \langle\xi\rangle \equiv \int_{M_{\rm min}}^{M_{\rm max}} {\rm d}M\, \xi(M) \frac{{\rm d}\mathcal{P}_M(M)}{{\rm d}M} \cdot \tag{62}$$

Equation (60) is the mean value of the flux, in the statistical sense, due to all clumps in the Galaxy for a given model (space and mass distributions)[11]. Anticipating the next section, we stress that any MC approach should converge to these values when taking a very large number of halo realisations.

5.2.2. Variance $\sigma_{\rm cl}^{\rm tot}$ of the whole sub-halo flux

The fact that we do not know how clumps are actually distributed, in the phase space defined by their locations and masses, can be expressed in terms of a variance $\sigma_{\rm cl}^{\rm tot}$ associated with their total mean flux $\langle\phi_{\rm cl}^{\rm tot}\rangle$. For a single clump, the relative flux variance is given by:

$$\frac{\sigma_{\rm cl}^2}{\langle\phi_{\rm cl}\rangle^2} = \frac{\sigma_{\tilde{\mathcal{G}}}^2}{\langle\tilde{\mathcal{G}}\rangle^2} + \frac{\sigma_\xi^2}{\langle\xi\rangle^2} + \frac{\sigma_{\tilde{\mathcal{G}}}^2}{\langle\tilde{\mathcal{G}}\rangle^2} \times \frac{\sigma_\xi^2}{\langle\xi\rangle^2}, \tag{63}$$

[10] We remind that tidal disruption of a clump in the Galactic centre depends either on its mass and on its location, which induces a small correlation between the mass and the space distributions. Nevertheless, we have checked that it could be neglected for this purpose.

[11] The integration volume V is the DM halo volume, but in practical calculations, we reduce it to the diffusion volume.

where the individual variances affecting $\tilde{\mathcal{G}}$ and ξ are respectively

$$\sigma^2_{\tilde{\mathcal{G}}} = \int_{\rm halo} {\rm d}^3\boldsymbol{x}\, \tilde{\mathcal{G}}^2(\boldsymbol{x}_\odot \leftarrow \boldsymbol{x}) \times \frac{{\rm d}\mathcal{P}_V}{{\rm d}V} - \langle\tilde{\mathcal{G}}\rangle^2; \tag{64}$$

and

$$\sigma^2_{\xi} = \int_{M_{\rm min}}^{M_{\rm max}} {\rm d}M\, \xi^2(M) \times \frac{{\rm d}\mathcal{P}_M}{{\rm d}M} - \langle\xi\rangle^2. \tag{65}$$

Quantities related to ξ and $\tilde{\mathcal{G}}$ will be quoted as mass- and space-related, respectively (see Sect. 6). We will further show that mass-related effects dominate among the relative variances, in spite of sizable space-related ones. The (third) crossing term of the right hand side of Eq. (63) will consequently set the full variance of the clump flux.

The resulting relative flux variance for the whole population of sub-halos is then merely:

$$\frac{\sigma^{\rm tot}_{\rm cl}}{\phi^{\rm tot}_{\rm cl}} = \frac{1}{\sqrt{N_{\rm cl}}} \frac{\sigma_{\rm cl}}{\phi_{\rm cl}}\,. \tag{66}$$

5.2.3. Boost factor $B_{\rm eff}$ and its variance $\sigma_{\rm B}$

Once the contribution of sub-halos to the flux is fully determined, the *boost factor* is easily computed for any species. As cosmic ray propagation has an explicit energy dependence, the boost factor is also energy-dependent (Lavalle et al. 2007), and, of course, also depends on the cosmic ray species (Maurin & Taillet 2003).

The energy-dependent mean effective boost factor is given by the sum of the clumpy and the smooth contribution divided by the flux that would provide the only smooth reference halo $\rho^0_{\rm sm}(r)$ (see Sect. 3.1.1):

$$B_{\rm eff} = (1-f_\odot)^2 + \frac{\phi^{\rm tot}_{\rm cl}}{\phi_{\rm sm}}, \tag{67}$$

where the local density fraction $f_\odot$ has been defined in Eq. (22), in order to keep the local DM density constant (see Sect. 3.1).

It may be useful to determine the limit for which only an infinitely small volume around the Earth $\delta(\boldsymbol{x}-\boldsymbol{x}_\odot)$ is taken into account. Actually, this will give a rough estimate of the asymptotic (maximum) value of the boost factor for both positrons (at detected energies very close to injected energies) and antiprotons (at low energies), because we are blind to contributions from regions close to the Galactic centre – where the smooth DM density dominates – in this case. This *local* asymptotic value is given by:

$$B_\odot = (1-f_\odot)^2 + N_{\rm cl} \times \langle\xi\rangle_M \times \frac{{\rm d}\mathcal{P}}{{\rm d}V}(R_\odot)\,. \tag{68}$$

This expression neither depends on the WIMP model, nor on the species. We see that, as ${\rm d}\mathcal{P}/{\rm d}V(R_\odot) = 3.9\times10^{-7}$ kpc^{-3} in our reference model, only configurations with $N_{\rm cl}\times\langle\xi\rangle_M \gtrsim 2.6\times10^6$ kpc^3 will yield a relevant averaged contribution of clumps compared to the smooth component. From Table 3, one can already see that the corresponding probability is likely to be very small. We can therefore provide a very simple criterion to check whether a boost is likely to appear in any (many-object) configuration:

$$n_{\rm cl}(R_\odot)\times\langle\xi\rangle = N_{\rm cl}\frac{{\rm d}\mathcal{P}}{{\rm d}V}(R_\odot)\times\langle\xi\rangle \gtrsim 1, \quad \Rightarrow B_{\rm eff} \gtrsim 1. \tag{69}$$

Should the sub-halos spatially track the smooth component, then one would get:

$$B^{\rm sm}_\odot = (1-f_M)^2 + f_M \times \frac{\rho_\odot \times \langle\xi\rangle_M}{\langle M_{\rm cl}\rangle} \tag{70}$$

where f_M is the mass fraction of DM in clumps, and $\langle M_{\rm cl}\rangle$ is the mean mass of clumps. The previous criterion to get a relevant boost factor then becomes merely $\langle\xi\rangle \gtrsim \langle M_{\rm cl}\rangle/(f_M\rho_\odot)$.

The above value of the boost factor fluctuates up to a variance σ_B, which reads

$$\sigma_B = \frac{\sigma^{\rm tot}_{\rm cl}}{\phi_{\rm sm}}, \tag{71}$$

leading to

$$\frac{\sigma_B}{B} = \frac{\sigma^{\rm tot}_{\rm cl}}{(1-f_\odot)^2\phi_{\rm sm} + \phi^{\rm tot}_{\rm cl}}\,. \tag{72}$$

If the sub-halo contribution dominates over the smooth component, then the relative variance of the effective boost factor is roughly equal to that of the sub-halo flux. Nevertheless, as soon as sub-halos become irrelevant in the flux estimate, the variance of the boost factor is strongly diluted by the smooth term. In this case, we obviously find a very small variance associated with the boost factor, even when the relative statistical uncertainty on the sub-halo flux itself is large.

5.3. MC approach

A complementary approach is to calculate and add explicitly the contribution of each clump by MC drawing. Simulating many realisations of the DM sub-halos is another way to extract the mean flux as well as the variance of the clump contribution. The ensuing calculation of boost factors is as before, but in addition, MC provides the law of probability for the stochastic variable $\phi_{\rm cl}$ that describes the single clump flux, which is hardly inferred from the clump phase space distribution itself due to the needed convolution with propagation.

From a technical point of view, it is very inefficient to calculate contributions from so many sub-halos (e.g. $\gtrsim 10^{15}$ for the lightest ones) one at a time. Indeed, for the clumps in a given mass range, two types of contributions exist. For low mass clumps, which are numerous, the variance associated with the flux is expected to be small (i.e. $\sigma_{\rm cl}/\phi_{\rm cl} \ll 1$). In this case, we can spare the effort of averaging many configurations and directly compute the flux from a single realisation. Conversely, as the mass of the sub-halos increases, the associated number of clumps decreases, so that the variance finally become sizable. A threshold mass $M_{\rm th}$ needs to be specified, below which the contribution to the total variance $\sigma^{\rm tot}_{\rm cl}$ can be neglected: only sub-halos that have masses $M_{\rm cl} > M_{\rm th}$ need to be calculated for all samplings. The value of $M_{\rm th}$ is discussed in Appendix A.

For one sample, the total annihilation flux observed in the solar neighbourhood may be rewritten as

$$\phi^{\rm tot}_{\rm cl} = \phi_{\rm low} + \phi_{\rm high},$$

where the quantities

$$\phi_{\rm low} = \frac{v}{4\pi} S \int {\rm d}^3\boldsymbol{x} \int_{M_{\rm min}}^{M_{\rm th}} {\rm d}M_{\rm cl}\, \tilde{\mathcal{G}}(\boldsymbol{x}\rightarrow\boldsymbol{x}_\odot) n(M_{\rm cl}, r) \times \int_{\rm sub} \left(\frac{\rho_{\rm sub}}{\rho_0}\right)^2 (\boldsymbol{x}') {\rm d}^3\boldsymbol{x}' \tag{73}$$

$$\phi_{\rm high} = \sum_{M_{\rm i}>M_{\rm th}} \phi_{\rm i}, \tag{74}$$

are the contributions from the low-mass sub-halos component and the high-mass sub-halos component, respectively. The number density of clumps was defined in Eq. (11), and the flux from a single clump ϕ_i is given by Eq. (57).

When taking into account all realisations:

$$\langle \phi_{\rm high} \rangle = \left\langle \sum_{M_i > M_{\rm th}} \phi_i \right\rangle_n$$

where $\langle . \rangle_n$ denotes the average over $n \gg 1$ realisations of the spatial distribution. This leads to:

$$\langle \phi_{\rm cl}^{\rm tot} \rangle \equiv \phi_{\rm low} + \langle \phi_{\rm high} \rangle \tag{75}$$

and

$$\frac{\sigma_{\rm cl}^{\rm tot}}{\langle \phi_{\rm cl}^{\rm tot} \rangle} \simeq \frac{\sigma_{\rm high}}{\langle \phi_{\rm cl}^{\rm tot} \rangle}, \tag{76}$$

where $\sigma_{\rm high}$ is the variance associated to high-mass clumps ($\sigma_{\rm low}$ is neglected as underlined above).

The total flux and variance are now given by

$$\langle \phi_{\rm tot} \rangle \equiv \phi_{\rm sm} + \phi_{\rm low} + \langle \phi_{\rm high} \rangle \tag{77}$$

and

$$\frac{\sigma_{\rm tot}}{\langle \phi_{\rm tot} \rangle} \simeq \frac{\sigma_{\rm high}}{\langle \phi_{\rm tot} \rangle} . \tag{78}$$

Thanks to this reasoning, a simple picture emerges, and a qualitative behaviour of the expected variance nicely complements the discussion from the previous method. The highest-mass sub-halos, which are rare, carry all the variance of the total flux. In Appendix A.3, they are found to be in the mass range $M_{\rm cl} \gtrsim 10^7\ M_\odot$. Thus, as soon as the integrated luminosity of lower-mass clumps (that depends on $\alpha_{\rm m}$) is much larger than that of the high-mass ones, the variance of the total clump contribution is expected to vanish. According to Fig. 4, such a situation will occur for $\alpha_{\rm m} \gtrsim 1.9$. Actually, even for $\alpha_{\rm m} < 1.9$, the variance will still be significantly decreased, because, as we already underlined, the local smooth contribution dominates over the clump one (see Fig. 5).

6. Results and discussion

Fluxes, boost factors and associated variances have been calculated for both positrons and anti-protons using a semi-analytical approach (Sect. 5.2) and, for the sake of comparison, MC simulations (Sect. 5.3).

The coming results are based on a fiducial model for the injection of antimatter in the Galaxy, which allows a WIMP-model-independent analysis. In practise, for positrons, a monochromatic line of 200 GeV is injected at a rate assumed to be proportional to the squared density of DM in sources. In order to recover realistic orders of magnitude, especially for fluxes, we will also suppose that those positrons originate from, e.g. not-s-wave-suppressed annihilations of WIMPs at rest, with masses of 200 GeV and annihilation cross-section $\langle \sigma v \rangle / 2 = 3 \times 10^{-26}$ cm^3 s^{-1} (for instance, Dirac fermions/anti-fermions with only trilinear couplings to $e^- \phi^+ / e^+ \phi^-$, where $\phi^{+/-}$ would be some exotic – conjugate – charged scalar fields). Besides, because anti-protons do not loose energy, we took their injection spectrum to be constant $dN/dT = 1$ GeV^{-1} between kinetic energies 0.1–200 GeV (any spectrum could have been taken, as it can be factorised out). One can easily guess what the results for any injection spectrum would be (originating from hadronisation or fragmentation processes for instance) by a mere rescaling. In this case, the WIMP properties can be almost the same as for positrons: fluxes have been computed using a Majorana WIMP with a mass of 200 GeV, and an annihilation cross-section of $\langle \sigma v \rangle = 3 \times 10^{-26}$ cm^3/s.

Before going into the details of the studied configurations, we show in Fig. 6 the extreme cases that we obtained for both species (with the medium set of propagation parameters). The first line panels are plots of the smooth and sub-halo fluxes and the resulting effective boosts, with associated $1-\sigma$ statistical contours. The second line panels are the same plots, but for anti-protons. The *maximal* configuration is given by: largest $\alpha_{\rm m}$ (2), cuspiest sub-halo inner profile (Moore), smallest $M_{\rm min}$ ($10^{-6}\ M_\odot$), spatial distribution according to the smooth NFW profile, and the B01 concentration model. The *minimal* configuration is the reverse: smallest $\alpha_{\rm m}$ (1.8), flattest inner profile (NFW), greatest $M_{\rm min}$ ($10^6\ M_\odot$), and smallest local number density (cored isothermal profile). The *intermediate* is close to the reference configuration, given in Sect. 3.1.2, and takes the most likely values of parameters according to N-body simulations (except for $M_{\rm min}$, of which the used reference value is $10^{-6}\ M_\odot$; and for the spatial distribution of sub-halos which tracks the smooth NFW profile).

From this figure, we see that the boost factors obtained are functions of the energy and lie between 1 and 20, with small statistical uncertainties. Such a range has to be taken as that of theoretical uncertainties affecting the DM distribution in the Galaxy. From the approximate Eq. (68), the asymptotic values obtained are also 1 and 20 (neglecting the density fraction $f_\odot$), which are in excellent agreement with our full results. Before going into deeper details, it is worth emphasising that the maximal value of ~20 is as large as unlikely, as already discussed in Sect. 2. For completeness, we have checked our results with MC simulations (see Sect. 5.3). In Fig. 7, we show that the agreement between the MC and the semi-analytic calculation is excellent for anti-protons, up to a few percents. It is the same for positrons, as already demonstrated in Lavalle et al. (2007); Brun et al. (2007).

Remembering that the whole sub-halo flux reads $\phi_{\rm cl}^{\rm tot} \propto (N_{\rm cl} \langle \xi \rangle_M) \times (\langle \tilde{\mathcal{G}} \rangle_V)$, it makes sense to gather the impact of the various ingredients into two main physical classes.

Mass-related effects ($N_{\rm cl} \langle \xi \rangle_M$): these are encoded in the mean value and the variance of ξ, as defined in Eqs. (62) and (65). The relevant parameters to discuss (see Table 2) are the minimal mass $M_{\rm min}$ of sub-halos, the logarithmic slope of the mass distribution $\alpha_{\rm m}$, the mass-concentration model and the inner profile.

Space-related effects ($\langle \tilde{\mathcal{G}} \rangle_V$): these are encoded in the mean value and the variance of $\tilde{\mathcal{G}}$, as defined in Eqs. (61) and (64), which depend on both the propagation model (through the propagator and the propagation parameters) and the spatial distribution of sub-halos, besides of course the antimatter species.

More details on this classification can be found in the appendix (see Appendix B). We first discuss the mass-related effects. We then focus on each antimatter species, for which we explain space-related effects, before describing the whole consequences of clumpiness on fluxes and boost factors. When discussing positrons, we will comment on the so-called HEAT excess.

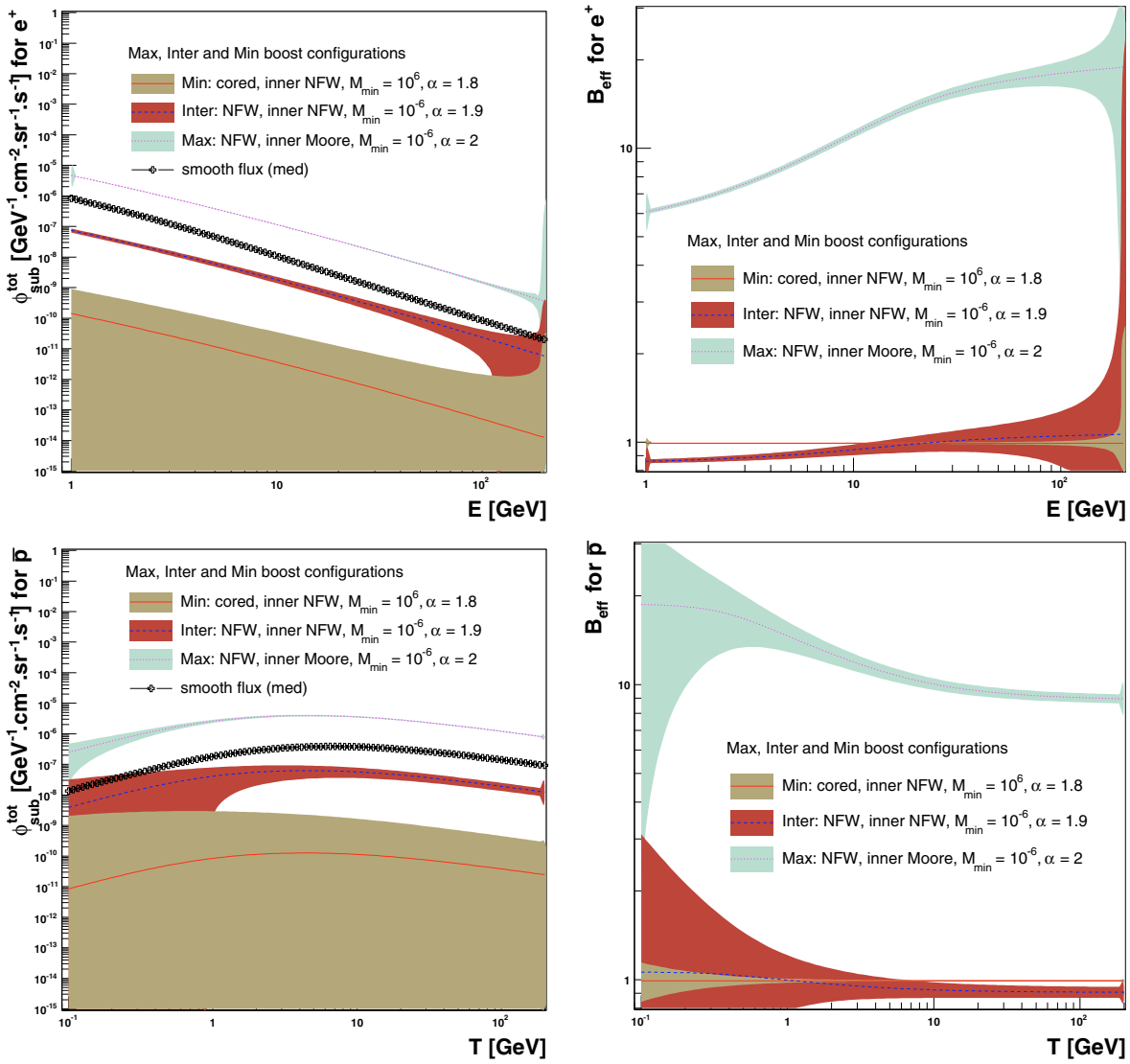

Fig. 6. Extreme cases for the DM configurations: sub-halo antimatter fluxes associated with the maximal, intermediate and minimal DM configurations (medium set of propagation parameters). *Left/right*: fluxes/boosts and corresponding $1-\sigma$ contours. *Top/bottom*: positrons/anti-protons. See the details in the text.

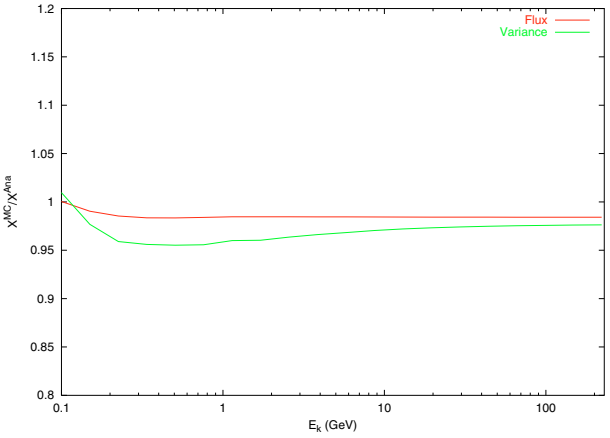

Fig. 7. Ratio of MC over semi-analytic results for the anti-proton flux and associated variance.

6.1. Mass-related effects

Once the space distribution of sub-halos and the propagation model are fixed, the propagator mean value $\langle\tilde{\mathcal{G}}\rangle_V$ of the sub-halo flux Eq. (60) is fully determined, as well as its statistical fluctuation σ_G. Hence, provided the WIMP model is also fixed, the only differences from one sub-halo configuration to another will be the averaged total amount of antimatter yielded by clumps, given by the integrated clump luminosity $L_{\rm cl} \equiv N_{\rm cl} \times \langle\xi\rangle_M$, and its associated fluctuations. Such a quantity depends on two parameters only: $M_{\rm min}$ and $\alpha_{\rm m}$ (plus the concentration-mass relation, plus the choice of the inner sub-halo profile). A decrease of $M_{\rm min}$ enhances the total number of clumps in the Galaxy, and an increase of $\alpha_{\rm m}$ raises the relative density of light compared to heavy objects (and the total luminosity accordingly because the clump number density is normalised with respect to the heaviest clumps, as given in Eq. (17)). More precisely, we find the luminosity to approximately scale with $M_{\rm min}$only logarithmically (see the details in Appendix B.1) like:

$$L_{\rm cl} \propto M_{\rm ref}^{\alpha_{\rm m}-1} \times \ln\left(M_{\rm max}/M_{\rm min}\right). \quad (79)$$

Therefore, we do not expect a large variation when spanning $(\alpha_{\rm m}, M_{\rm min})$ from the minimal $(1.8 \times 10^6\ M_\odot)$ to the maximal $(2 \times 10^{-6}\ M_\odot)$ parameter sets. Actually, we find the total luminosity to drop by a factor of ~40 only, while running the number

of clumps over 13 orders of magnitude in the meantime (the above approximate expression sightly over-estimates the difference, leading to a factor of ∼150). For completeness, an additional factor of 10 appears if one also considers inner Moore profiles for clumps (see Sect. 3.3.1), whereas a factor of 1/10 results from using an ENS01 mass-concentration relation.

Regarding the pure mass-related relative fluctuations, given by $N_{\rm cl}{}^{-1/2}(\sigma_\xi/\langle\xi\rangle)$ (see Eq. (63)), we would naively expect them to significantly deplete when decreasing $M_{\rm min}$, which enhances the total number of clumps. Furthermore, since the relative luminosity of light clumps is raised by increasing $\alpha_{\rm m}$, the relative variance should be significantly reduced accordingly. Nevertheless, interestingly, we find the mass-related relative fluctuations to roughly scale like $(\ln(M_{\rm max}/M_{\rm min}))^{-1}$, and to vary only in the range 0.1−10% when spanning over $(\alpha_{\rm m}, M_{\rm min})$ from minimal to maximal parameter sets (see above). The physical interpretation is the following: as $M_{\rm min}$ goes up, the number of clumps decreases accordingly, but in the meantime, the intrinsic clump luminosity ($\propto\xi$), which is fixed by the mass, fluctuates much less from clump to clump; there is a trade-off between shrinking the statistical sample and reducing the phase space, so that the relative mass-related variance remains almost constant. Taking a Moore inner profile does not affect the relative mass-related variance, while adopting the ENS01 mass-concentration relation increases it by a few (see the third line panels of Fig. 8).

As a consequence, the global flux relative variance given in Eqs. (63) and (66), should vary over two orders of magnitude at most, once the GCR propagation is fixed and at a given energy. Indeed, as mass-related uncertainties are almost always greater than space-related ones (see Appendix B.1), the dominant contribution is the space-mass crossing term $N_{\rm cl}{}^{-1/2}(\sigma_\xi/\langle\xi\rangle)(\sigma_{\tilde{\mathcal{G}}}/\langle\tilde{\mathcal{G}}\rangle)$, so that the global relative variance encompasses values in the range $(0.1-10\%)\times(\sigma_{\tilde{\mathcal{G}}}/\langle\tilde{\mathcal{G}}\rangle)$ when varying $\alpha_{\rm m}$ and $M_{\rm min}$ from extreme configurations.

From the previous statements together with the luminosity profiles already discussed and shown in Fig. 5, scanning over the most likely mass-related parameters is unlikely to make the sub-halo contribution dominate over the smooth flux, except for extreme configurations combining the B01 concentration model, Moore inner profiles, large $\alpha_{\rm m}$ and very small $M_{\rm min}$.

6.2. Positrons

6.2.1. Space-related effects for positrons

The space-related effects for positrons come through the averaging of the propagator $\langle\tilde{\mathcal{G}}^{\,e^+}\rangle_V$ over the sub-halo spatial distribution. We summarise here a more detailed discussion that will be found in the appendix (see Appendix B.2). The relevant scale is the propagation scale $\lambda_{\rm D}$ that depends on both diffusion and energy loss processes for positrons. $\lambda_{\rm D}$ is obviously larger for larger diffusion coefficients, and smaller when the detected energy gets closer to the injected energy. Since it is of the order of kpc, we can safely focus on local quantities. Actually, $\langle\tilde{\mathcal{G}}^{\,e^+}\rangle_V$ encodes an effective detection volume bound by $\lambda_{\rm D}$ and weighted by the clump spatial probability function $\mathrm{d}\mathcal{P}/\mathrm{d}V(r)$ in the solar neighbourhood. In the limit of infinite 3D diffusion, and when the propagation length is small enough, we find in Appendix B.2 that $\langle\tilde{\mathcal{G}}^{\,e^+}\rangle \simeq (\tau_E/\epsilon^2)\times\mathrm{d}\mathcal{P}(R_\odot)/\mathrm{d}V$. Hence, the averaged propagator increases linearly with the local value of the clump spatial probability function. As $\mathrm{d}\mathcal{P}/\mathrm{d}V(R_\odot)\langle\rho_\odot/M_{\rm vir}^{\rm h}\rangle$ for the reference case (clumps are spatially distributed according to a cored isothermal profile), we see that given mass-related parameters, a configuration in which the clumps track the smooth profile will give a higher flux.

Regarding the pure space-related relative variance for a single object $\sigma_{\tilde{\mathcal{G}}}/\langle\tilde{\mathcal{G}}\rangle$, we find it to scale like $(\lambda_{\rm D}^3\times\mathrm{d}\mathcal{P}(R_\odot)/\mathrm{d}V)^{-1/2}$, thus, decreasing when the effective detection volume or the clump local spatial probability increase (detected energies much lower than injected ones). When taking the whole contribution, an additional factor of $N_{\rm cl}{}^{-1/2}$ reduces the global variance, and the picture becomes very simple: the relative space-related variance scales like $N_{\rm obs}^{-1/2}$, one over the square root of the number of clumps contributing to the signal at the Earth. It is maximal at high energy for positrons.

To summarise, the space-related contribution for positrons increases with the diffusion coefficient, and with the clump local space probability function. The relative space-related variance decreases when the propagation length raises (at low energy for positrons), because a larger number of sub-halos can contribute to the signal at the Earth.

6.2.2. Overall effect on the positron flux: boost factor estimate

Taking this fiducial injection model, we assess the different effects and draw four typical plots, which will compose four specific panels in the next figures, from left to right: positron flux, relative flux variance, boost factor, relative boost variance (as functions of the positron detected energy).

Figure 8 illustrates the mass-like effects, whereas Fig. 9 show the space-like ones.

– Mass-related effects

In the first line of Fig. 8, we vary the minimal mass of the sub-halos, in other words the cut-off of the mass distribution. We actually compare three configurations by taking $M_{\rm min} = 10^{-6}$, 1 and $10^6\ M_\odot$, the remaining parameters being those of the reference configuration given in Sect. 3.1. The top left panel shows the whole contribution of sub-halos to the positron flux with the associated $1-\sigma$ contour, as well as the smooth contribution. We see that varying the minimal mass mainly influences the variance, while the mean values predicted for the flux remain of the same order of magnitude (only a factor of ∼5 in flux between $M_{\rm min} = 10^{-6}$ and $10^6\ M_\odot$). The flux ratios of the three configurations are plotted in the second panel of the first line, taking the reference $\phi_{-6} = \phi(M_{\rm min} = 10^{-6}\ M_\odot)$. This is due to the fact that the product $N_{\rm cl}\times\langle\xi\rangle$ is almost independent of the minimal mass in this case. Should $\alpha_{\rm m}$ have taken a value different than 1.9, the mean contribution of clumps would have a much stronger dependence on $M_{\rm min}$. Nevertheless, the relative flux variance is different between the three configurations, as also shown in the bottom left panel. Actually, this comes from the total number of sub-halos, which is strongly depleted when $M_{\rm min}$ is increased ($\propto {M_{\rm min}}^{1-\alpha_{\rm m}}$). Therefore, the statistical flux variance, which scales like $1/\sqrt{N_{\rm cl}}$, is increased accordingly. Another effect comes from the energy loss of positrons. While the detected energy gets closer to the injected energy, the diffusion volume decreases, as explained in Sect. 6.2.1, and the number of clumps effectively contributing damps in the same way. Hence, the relative variance is enhanced when getting closer to the injected energy. However, the whole sub-halo contribution is finally far below the smooth flux, by about two orders of magnitude. This translates to an effective boost of $B_{\rm eff}(E_{\rm d}) \simeq (1-f_\odot)^2 \sim 1$, with a very small variance, because it is also diluted by the smooth component.

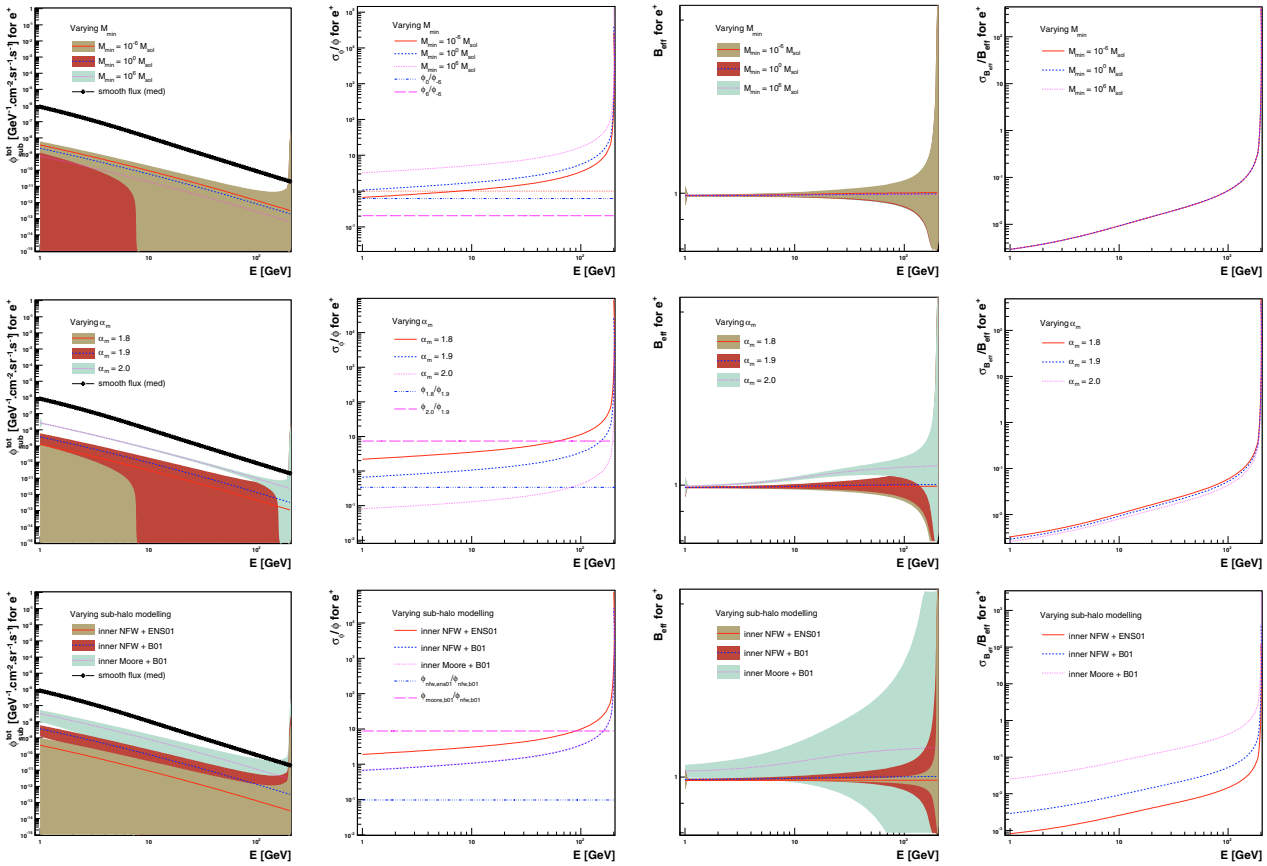

Fig. 8. Mass-related effects on the positron flux (*first column*) with a focus on the corresponding relative uncertainty (*second column*), for positron lines of 200 GeV injected at sources, with a rate corresponding to standard values of WIMP annihilation, and the associated boost factor with its relative variance (third and fourth columns). The plain contours account for one standard deviation. *First row*: effect of changing the minimal mass of sub-halos, $M_{\rm min} = 10^{-6}$, 1 and 10^{-6} $M_\odot$. *Second row*: effect of changing the logarithmic slope $\alpha_{\rm m}$ of the sub-halo mass function, with $\alpha_{\rm m} = 1.8$, 1.9 and 2.0. *Third row*: effect of changing the sub-halo inner properties; the inner profile is taken to be either NFW or Moore, and the concentration model varies from B01 to ENS01.

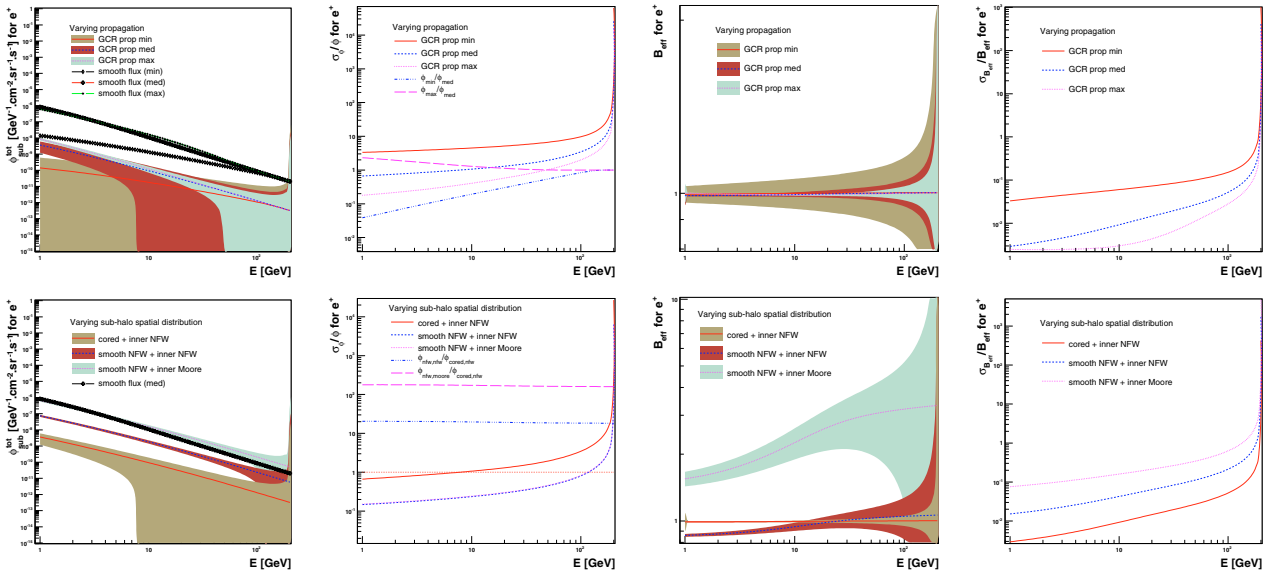

Fig. 9. Space-related effects on positrons, with the same panel organisation as in Fig. 8. *First row*: effects of varying the GCR propagation modelling, by using the three propagation sets of parameters of Table 4. *Second row*: effect of varying the space distribution of sub-halos, going from the cored isothermal space distribution to a case in which sub-halos track the smooth NFW component (for completeness, we also take an example where we also modify the inner sub-halo profile by taking a Moore instead of an NFW).

In the second line panels of Fig. 8, α_m is varied, giving three different mass configurations: 1.8, 1.9 and 2.0. As expected, the flux due to sub-halos is affected, and predictions slightly spread within one order of magnitude (a factor of ∼30 between 1.8 and 2.0). The relative flux variance is lower for large values of α_m, as expected, because this increases the total number of sub-halos, more precisely the lighter ones. Nevertheless, varying α_m within the reference configuration is not enough for sub-halos to strongly dominate over the smooth contribution: the averaged boost factors associated with the three examples lie around unity, even when getting closer to the injected energy (the maximum value is 1.08 for $\alpha_m = 2.0$), with small statistical uncertainties.

The third line of Fig. 8 shows the consequences of varying the mass-concentration relation and the inner sub-halo profile. The reference model, which is inner NFW + B01, is compared with NFW+ENS01 (less concentrated sub-halos) and with Moore+B01 (more cuspy sub-halos). As expected, the flux obtained with the ENS01 concentration model is far below the reference one, by a factor of ∼20, whereas the Moore sub-halos gives ten times more signal (this can also be seen from Fig. 3). These ratios are constant with the detected energy, as they are characterised by the ratios of $\langle\xi\rangle$'s. Again, we see that the expected boost factor is again negligible in all cases, around unity (∼1.13 for the best case, i.e. Moore inner profile + B01). Nevertheless, the increase of the variance associated with the latter happens at lower energies than previously, because the probability for a single clump to contribute more than the smooth component becomes sizable at farther distances.

– Space-related effects

The first line panels of Fig. 9 illustrate how GCR propagation can strongly influence the predictions by using the three models of Table 4 with the reference DM configuration. Differences grow when the detected energy is far below the injected one. This is mainly due to the change in the thickness of the diffusive slab. At energies close to the injected energy, the volume probed is very small, so propagation is not sensitive to the slab boundaries anymore. We see that for positrons, there is no huge differences between the maximal and medium propagation models, while the minimal one strongly depletes the positron flux at low energies. Indeed, the characteristic propagation length for positrons (a few kpc) is almost always contained in the maximal and medium slabs, whereas it is not the case for the minimal one. Anyhow, even the maximal propagation set is not enough to boost the sub-halo positron flux above the smooth contribution. Indeed, the values obtained (see the left panels) stack to unity, again with a small statistical uncertainty.

Finally, the second line panels of Fig. 9 show the effect of changing the spatial distribution of clumps, from the reference cored isothermal to a situation in which they track the smooth NFW profile. For completeness, we do the exercise for both inner NFW and Moore profiles. In the left panels, we see that the sub-halo flux is enhanced when they track the smooth profile, of about one order of magnitude in this case. The effect is obviously stronger when an inner Moore density is taken, for which another order of magnitude arises. Nevertheless, the boost factors do not obey the same hierarchy. This is due to the way the smooth component is normalised when clumps are added. Indeed, we chose to readjust the smooth density by a factor $(1 - f_\odot)$, where the fraction density $f_\odot$ is defined in Eq. (22), in order to get a constant local density $\rho_\odot$. When clumps track the smooth component, their number density is enhanced in the local neighbourhood, so that $f_\odot$ is enhanced accordingly. As the boost factor remains around $(1 - f_\odot)^2$ (the sub-halo contribution is negligible), except when considering inner Moore profiles, the case for which clumps track the smooth component is worse. However, taking an inner Moore profile for clumps gives a higher flux than the smooth alone, and the mean boost factor can reach an asymptotic value of ∼2−3.

In summary, we have shown, by extensively playing with the maximum number of available parameters, that sizable boost factors to the positron flux are unlikely to arise from clumpiness. There could be situations in which a single sub-halo would be close enough to the Earth to dominate over the smooth component, but within the most reasonable modellings, the probability for this to happen is vanishingly small. Nevertheless, in order to provide more optimistic scenarios, even if less realistic according to the standard values of the parameters, a model characterised by $10^{-6}\ M_\odot$ sub-halos with inner Moore profiles, with concentrations described by the B01 relation, spatially tracking the smooth DM density, would yield a mean boost factor whose asymptotic value would be around 3 for a logarithmic slope $\alpha_m = 1.9$ (see lower panels of Fig. 8). Taking $\alpha_m = 2$ leads to a boost of ∼20 (see Fig. 6). This is the most optimistic estimate that we can provide so far, but also the most unrealistic. Note finally that although the primary fluxes may vary by 2 orders of magnitude due to uncertainties in the propagation parameters (see Table 4 and upper panels of Fig. 9), the resulting average boost factors are unaffected because they are defined as flux ratios; the variance is nevertheless larger when the GCR horizon is reduced (*min* configuration).

6.2.3. Comments on the positron excess

The HEAT experiment results for the 1994 flight hinted at the possibility of an excess of positrons near 8 GeV (Barwick et al. 1997), which could not be explained by a purely secondary production mechanism (Coutu et al. 1999). Baltz & Edsjö (1999) then found that neutralino annihilation could account for the missing flux providing that boost factors are larger than six; at that time, these authors estimate realistic boost factors to fall in the range $B_{\rm eff} \lesssim 100-1000$. Note that such high boost factors would be ruled out in the present study. However, later on, combining both 1994 and 1995 HEAT balloon flights, DuVernois et al. (2001) concluded that the positrons flux was consistent with a secondary origin. Results from the MASS91 balloon-borne magnetic spectrometer above 7 GeV (Grimani et al. 2002) do not provide a definitive answer either. As emphasised by these authors, very high energy ∼100 GeV measurements are probably necessary to positively conclude for standard or exotic mechanisms. Finally, from the most recent data coming from the HEAT 2000 flight, Beatty et al. (2004) cautiously conclude that a primary contribution above a few GeV can still not be ruled out.

Given these observations, several subsequent studies have focused on finding a good DM candidate to explain this possible excess. We do not wish to comment here on the best candidate, but rather survey the boost factors used in the studies. For example, for SUSY candidates, boost factors of 2.7 and 3.9 were used in Kane et al. (2002b), values in the range 30−100 in Baltz et al. (2002), from *small* to *large* boost factors in Kane et al. (2002a), in the range 1−5 in Hisano et al. (2006), and around 100 in Cumberbatch & Silk (2007). Mambrini et al. (2006) favoured boosts of 5−10 to accommodate the expected measurements of PAMELA, for SUSY models with non-universal scalar and gaugino masses. For KK DM, Hooper & Kribs (2004) found a

range of 10−30. The boost factor used to fit the data depends of course on the WIMP candidate considered and its mass.

It appears that most of the models found so far to match the positron data require mild to significant boost factors. Such boost factors are disfavoured by our results if the clump parameters fall in the large ranges taken in this study. A high energy feature in the positrons data could still be an important clue to DM indirect detection, and it would be interesting in forthcoming studies to scan, e.g. the SUSY parameter space looking for models matching the data without boost factors. According to Asano et al. (2007), the little Higgs model provides good options for detectability by the AMS-02 experiment, but could be short for PAMELA. In addition, it is worth noting that if some χ^2-like searches for clump signatures are performed in the coming positron data, it will be very important to take the energy dependence of any boost factor into account, as soon as it is invoked.

To conclude, although having no boost factors may be less interesting for SUSY theories to explain the data, any result that will be obtained when comparing to forthcoming data, if an excess is confirmed, will be more robust if no boost factor (an additional unknown parameter till now) is invoked. We recall that the two main uncertainties for WIMP annihilation induced antimatter signals are the propagation parameters in the Galaxy (a factor $\lesssim$100) and the local DM density (a factor $\lesssim$2, that shifts to 4 in terms of annihilation rate).

6.3. Anti-protons

First of all, it is worth quoting that contrary to positrons, for which an excess is still not understood, anti-proton present measurements are now well accounted for by purely *standard* secondary production (e.g. Donato et al. 2001). This means that there is no need of DM, and obviously of any clump to fit the data: the present data has to be consider as an upper limit for the DM contribution. Things could change with the future results of PAMELA and AMS-02 at higher energies.

The flux enhancement for anti-protons has features different from positrons, as already stressed by Bringmann & Salati (2007) and Brun et al. (2007). This is mainly due to propagation, which is quite different from the positron case. Indeed, anti-protons do not lose energy, and can experience spallation processes and wind convection along their travel to the Earth, which occurs to be dominant at low energy. Nevertheless, as for positrons, the same classes of physical effects can be discussed.

Regarding the space-related effects, the comments are the same as for positrons but with a reversal energy point of view (see Appendix B.3). The relative variance is then maximal at low anti-proton energy. Note, however, that the three sets of propagation parameters give separate absolute fluxes (decreasingly according to *max*, *med* and *min*), whereas *max* and *med* configurations give about the same fluxes for positrons.

6.3.1. Overall effect on the anti-proton flux: boost factor estimate

We now discuss the origin of systematic differences when varying the DM configuration as well as the propagation modelling. Figure 10 illustrates effects that are of mass type, while Fig. 11 shows the space-related ones. They are presented the same way as for positrons.

For the mass-type category, the comments are exactly the same as those for positrons, and are already discussed in Sect. 6.2.2.

Regarding space-related consequences, the picture is the reversal from that of positrons, and the conclusion are the same as for positron, given the energy axis is read inversely.

In summary, the maximum boost factor occurs at low antiproton energies when clumps are spatially distributed according to the smooth profile, and when they have an inner Moore profile. But even in this (disfavoured) configuration, the asymptotic mean value of the enhancement factor is $\lesssim$3.

7. Summary and conclusions

Clumpiness is a robust prediction of hierarchical structure formation, where the bottom-up growth of structures is a consequence of the ΛCDM cosmology. Many issues remain about clumps, beside their survival, such as their number density, their mass and spatial distribution, as well as their intrinsic properties. In recent years, high resolution N-body simulations succeeded in tracing their gross features, although we are still far from a definite answer for several key parameters. Indeed, whereas numerical experiments now converge to a level better than 10% over wide dynamic ranges (Heitmann et al. 2007), the inclusion of baryons in hydrodynamical simulations, which could strongly modify the inner properties of sub-halos, remains a very difficult task.

The impact of the DM inhomogeneities on DM annihilation in the Galaxy was first underlined in Silk & Stebbins (1993). With the achievement of cosmological N-body simulations in the last decade, and due to their positive results on clumpiness, many papers have subsequently focused on the consequences for the phenomenology of SUSY indirect detection in several channels, involving γ-rays and antimatter GCRs (e.g. Bergström et al. 1999). The effects for γ-rays have been extensively studied, whereas diffusion processes make the study much more difficult for antimatter GCRs. Berezinsky et al. (2003) carried out a detailed study of boost factors for γ-ray signal (so the conclusions also hold for neutrinos), and concluded to a factor of 2 to 5 for different density profiles in a clump. However, whether or not primary antimatter fluxes may be boosted by clumpiness is an important issue for the interpretation of forthcoming data, especially for positrons (see the discussion below), and for putting more robust constraints on new physics.

In this paper, we have inspected the boost factors for antimatter GCRs as deeply as possible and the results are mostly independent from any WIMP model, in the context of cosmological substructures. To this aim, we have followed the semi-analytical method proposed in Lavalle et al. (2007), already used by Bringmann & Salati (2007) and Brun et al. (2007) to compute the boost factors for positrons and anti-protons, but in a scenario in which DM inhomogeneities are due to the presence of intermediate mass black holes. We have also cross-checked our results with a more time-consuming MC simulation.

A full DM model was defined with (i) the host halo smooth DM profile, (ii) inner properties, minimal mass, space and mass distributions of sub-halos, and (iii) the mass-concentration relation. The reference set was chosen accordingly, with (i) NFW (kept fixed throughout the paper, see Table 1), (ii) inner-NFW + 10^{-6} $M_\odot$ + cored isothermal + α_m = 1.9, and (iii) B01 concentration. We then extensively spanned over some extreme values of each parameter. We normalised all configurations so that the average local DM density was kept constant $\rho_{tot}(R_\odot) = \rho_\odot = 0.3$ GeV cm^{-3}. For completeness, we also considered three sets

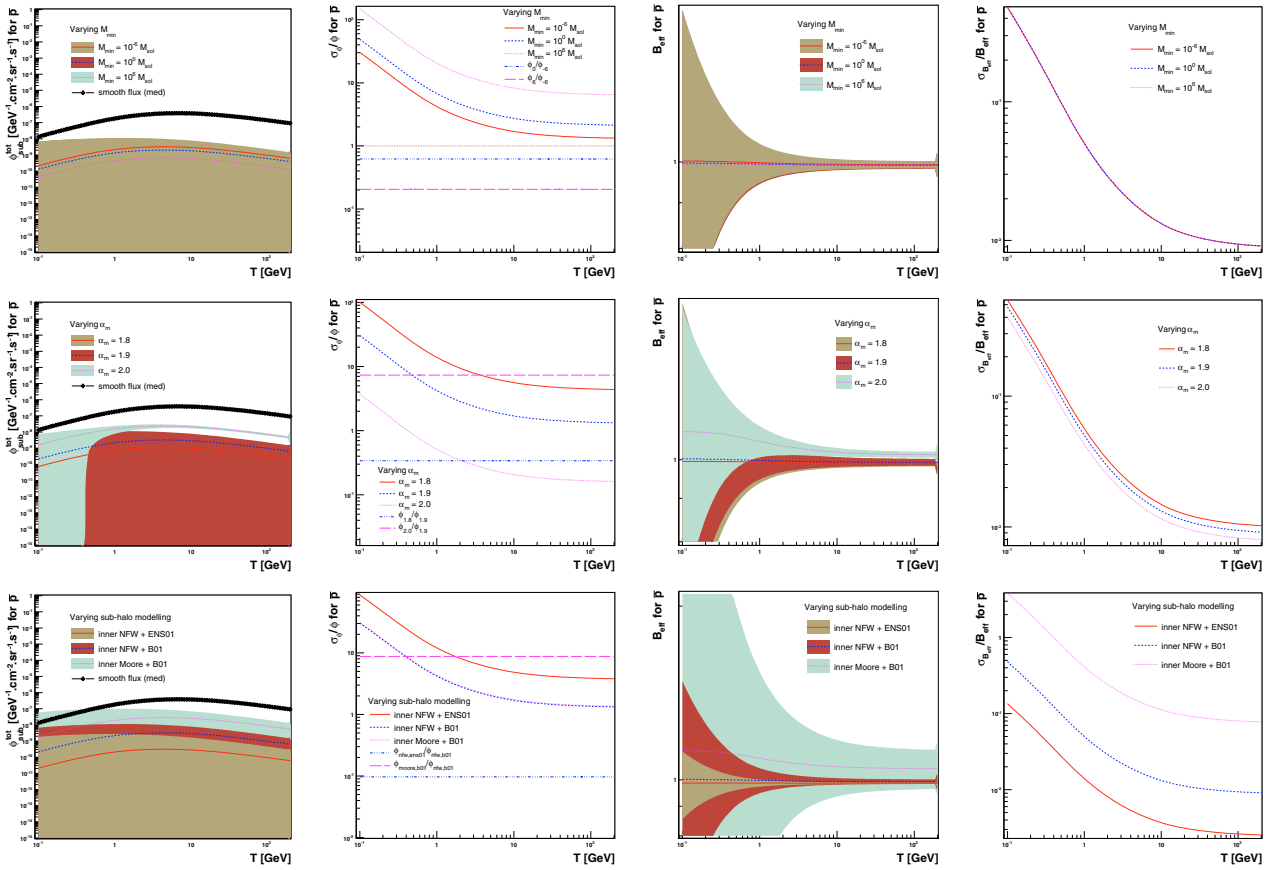

Fig. 10. Mass-related effects for anti-protons; a toy flat spectrum is injected at the sources, at a rate corresponding to standard values of WIMP annihilation – same panel organisation as for positrons (see Fig. 8). *First row*: varying $M_{\rm min}$. *Second row*: varying $\alpha_{\rm m}$. *Third row*: varying the sub-halo inner properties.

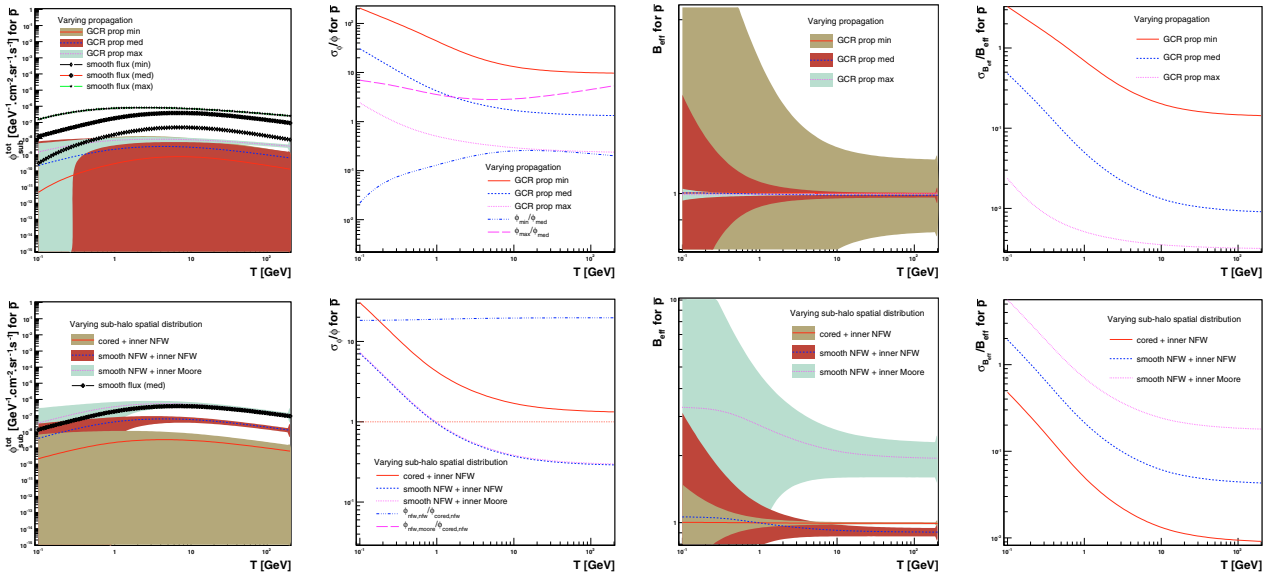

Fig. 11. Same than Fig. 9, but focusing on space-related effects for anti-protons. *First row*: varying the propagation modelling. *Second row*: varying the space distribution (and the sub-halo inner profile).

of GCR propagation modelling, mainly characterised by the size of the diffusive halo, and by the amplitudes of diffusion and convection processes; all of them decrease from *max* to *min* settings (*med* being the reference).

We found our results to depend on two main classes of effects, namely mass- and space-related. The mass-type effects characterise the full amount of antimatter produced in clumps through WIMP annihilations, given by the product $N_{\rm cl}\langle\xi\rangle_M$ (see Sect. 6.1), and its variance; they depend on the number of clumps (fixed by $M_{\rm min}$ at a given $\alpha_{\rm m}$), their inner profiles (NFW or Moore) and mass distribution ($\alpha_{\rm m}$). The space-related effects describe the average probability for the produced antimatter to

reach the Earth, and is determined by $\langle\tilde{\mathcal{G}}\rangle$, and the associated variance; they therefore encode the whole spatial information, i.e. the propagation averaged on the clump space distribution, as well as the energy dependency. Our results are the following, some trends being consistent with some found in previous studies:

- larger $\alpha_{\rm m}$ values lead to larger luminosity of clumps (hereafter $\mathcal{L}_{\rm cl} \propto N_{\rm cl}\langle\xi\rangle_M$), because $N_{\rm cl}$ increases faster than $\langle\xi\rangle_M$ decreases;
- smaller $M_{\rm min}$ values lead to larger $\mathcal{L}_{\rm cl}$ if $\alpha_{\rm m} \geq 1.9$, and is otherwise insensitive to $M_{\rm min}$ (massive clumps are more luminous);
- the luminosity of clumps with an inner Moore profile is 10 times that obtained for an NFW profile (which can be analytically handled); hence, the whole clumpy flux can be evaluated from a NFW profile and rescaled to any profile very easily, being for instance 10 times larger for a Moore profile; this is independent of the concentration relation assumed and the species considered;
- the maximum flux is obtained for a B01 $c_{\rm vir} - M_{\rm vir}$ relation, and is lower for the ENS01 case (respectively a factor of ∼3 and ∼30 lower – mass dependent – for $M_{\rm cl} = 10^{10}\ M_\odot$ and $M_{\rm cl} = 10^{-6}\ M_\odot$);
- spanning extreme ranges of parameters leads to the same conclusion that no sizable enhancement is expected from clumpiness in average, asymptotic values of $B_{\rm eff}$ varying from $(1 - f_\odot)^2 \sim 1$ to ∼2.5;
- boost factors for GCRs depend on energy, which characterises the size of the effective volume of sensitivity that can be probed around the Earth;
- the relative statistical uncertainties on the whole sub-halo fluxes and on the corresponding boost factors are dominated by mass-related effects – linked to the internal properties of clumps and to their mass distribution – as soon as small clump masses are considered ($\lesssim 1\ M_\odot$), and are hugely enhanced due to the mixing with the (weaker) space-related ones – linked to the spatial distribution of clumps and to propagation – especially when the GCR propagation scale gets slender and slender, i.e. for low energy anti-protons, and detected (high) energies close to the injected one for positrons (while the absolute fluxes do depend strongly on propagation);
- statistical uncertainties are small at low energies for positrons and at high energies for anti-protons (when the propagation scale is larger).

As a first and mere conclusion concerning the whole sub-halo flux, the combination of smooth-like space distribution, small $M_{\rm min}$, large $\alpha_{\rm m}$, large concentrations, and very cuspy inner profiles will obviously lead to the largest mean flux (in the statistical sense of averaging over many DM outcomes for a given configuration). The maximum set of parameters that we considered for the sub-halos was defined by a spatial smooth-like NFW distribution, $M_{\rm min} = 10^{-6}\ M_\odot$, $\alpha_{\rm m} = 2$, a Moore inner profile ($\propto r^{-1.5}$), and the B01 concentration model. This led to asymptotic values of boost factors around 20 with small statistical errors (see Fig. 6). Conversely, a cored isothermal spatial distribution, large $M_{\rm min}$, small $\alpha_{\rm m}$, small concentrations (here ENS01) and mildly cuspy (e.g. NFW) inner profiles will lead to the smallest mean flux. We remind the reader that a very simple and straightforward way to estimate whether or not sub-halos may enhance the DM contribution to the antimatter fluxes is to verify whether the condition given by Eq. (69) is fulfilled.

Furthermore, note that the only relevant parameters for estimating the variance on the sub-halo flux are the minimal mass of clumps, their mass distribution and their local number density, beside the propagation length of the GCR species that defines an effective detection volume.

These results are in agreement with those of Hooper et al. (2004), who concluded, though mostly qualitatively, that it is very unlikely that significant boost factors occur for positrons. Our results, however, are more quantitative and detailed, apply to both anti-protons and positrons for any set of propagation parameters, and encompass the single configuration (NFW-ENS01) used in the above paper for clumps. This is also consistent with the results of Berezinsky et al. (2003) for γ-rays, where slightly larger boost factors were found: such a difference is expected because, as already underlined, γ-rays are integrated along the line of sight (we remind that the luminosity of clumps dominates over the smooth distribution one beyond a few tens of kpc from the Galactic centre), instead of integrated inside a more *local* volume like for GCRs.

It is interesting to ask the dependence of our calculation on the mass resolution achieved so far in N-body simulations, which we have referred to in defining our parameter sets. Indeed, the N-body numerical results are only valid at the spatial scale associated with the test particle mass, so that the Vlasov limit may not be reached at the smallest scales considered here (see discussion in Sect. 2). Therefore, extrapolations of the physical properties of sub-halos down to $10^{-6}\ M_\odot$ should always be taken cautiously, even if some numerical studies were able to survey such small systems at high redshifts (Diemand et al. 2005a). Besides, even if DM sub-halos of $10^{-6}\ M_\odot$ wander in the Galaxy, we can actually not know anything about their characteristics. Nevertheless, theoretical arguments based on the (inflation-motivated) scale invariance of the DM power spectrum down to the free streaming scale set by particle physics, the theoretical understanding of the DM mass function, the current knowledge, would it be far from complete, of hierarchical structure formation, and some numerical studies on the survival of very small sub-halos, somehow guarantee that our choice of parameter ranges is rather reasonable and sufficiently large to encompass a wide field of possibilities. Therefore, while this strongly asks for more detailed studies of the smallest DM structures, our results should also be taken as general statements that describe the effect of each considered parameter on boost factor predictions.

One could recover a sizable (energy dependent) boost factor by considering either a sub-halo which would be very massive ($\gtrsim 10^7\ M_\odot$) as well as very close to the Earth ($\lesssim$1 kpc, see e.g. Sect. 6.2.1), or very cuspy inner profiles combined with a significant local abundance of sub-halos. The latter case would correspond to a clump configuration given by a smooth-tracking spatial distribution, $M_{\rm min} \lesssim 10^{-6}\ M_\odot$, $\alpha_{\rm m} \gtrsim 2$, concentration ≳B01, and $r^{-\beta}$ inner profiles with $\beta \gtrsim 1.5$. Such a situation is very improbable given the current theoretical results of gravitational collapse or mass function studies, and also considering the most likely configurations of clumpiness found among N-body results. Thus, it may not be taken as a natural prediction of structure formation. Regarding the former case, we stress that the statistical probability to find such a massive object in the solar neighbourhood is vanishingly small (such masses are now well resolved in numerical simulations, and are not expected to be numerous). Moreover, some observational constraints might exist on the presence of such a massive and close object. Anyway, the calculation of fluxes originating from a single nearby source is straightforward, and one can very easily model its required

features. The price to pay would be to invoke some kind of Galactic *lottery* in order to explain *why* a single clump would wander *here* and *now*.

Acknowledgements. We warmly thank C. Tao and all the organisers of the 2nd Sino-French Workshop on the Dark Universe, during which this work has been initiated. We are grateful to J. Diemand, P. Salati and R. Taillet for enlightening exchanges and comments, and to V. Eke for providing us with his concentration code. J.L. and D.M. acknowledge the support from the French GDR-SUSY, as well as the incentive of its current headmaster J. Orloff. D.M. thanks all people at IHEP for warm hospitality during his stay. X.-J.B. is supported by the NSF of China under the grant Nos. 10575111, 10773011 and also in part by the Chinese Academy of Sciences under the grant No. KJCX3-SYW-N2.

References

Aceves, H., & Velázquez, H. 2006, Rev. Mex. Astron. Astrofis., 42, 41
Aharonian, F., Akhperjanian, A. G., Bazer-Bachi, A. R., et al. 2006, Phys. Rev. Lett., 97, 221102
Ahn, K., & Shapiro, P. R. 2005, MNRAS, 363, 1092
Allgood, B., Flores, R. A., Primack, J. R., et al. 2006, MNRAS, 367, 1781
Angus, G. W., & McGaugh, S. S. 2007, [arXiv:0704.0381]
Angus, G. W., & Zhao, H. 2007, MNRAS, 375, 1146
Angus, G. W., Famaey, B., & Zhao, H. S. 2006, MNRAS, 371, 138
Angus, G. W., Shan, H. Y., Zhao, H. S., & Famaey, B. 2007, ApJ, 654, L13
Asano, M., Matsumoto, S., Okada, N., & Okada, Y. 2007, Phys. Rev. D, 75, 063506
Athanassoula, E. 2007, MNRAS, 339
Baer, H., Krupovnickas, T., Profumo, S., & Ullio, P. 2005, J. High Energy Phys., 10, 20
Baltz, E. A., & Edsjö, J. 1999, Phys. Rev. D, 59, 023511
Baltz, E. A., Edsjö, J., Freese, K., & Gondolo, P. 2002, Phys. Rev. D, 65, 063511
Barrau, A., Boudoul, G., Donato, F., et al. 2002, A&A, 388, 676
Barrau, A., Salati, P., Servant, G., et al. 2005, Phys. Rev. D, 72, 063507
Barwick, S. W., Beatty, J. J., Bhattacharyya, A., et al. 1997, ApJ, 482, L191
Battaglia, G., Helmi, A., Morrison, H., et al. 2005, MNRAS, 364, 433
Battaglia, G., Helmi, A., Morrison, H., et al. 2006, MNRAS, 370, 1055
Battiston, R. 2007, Nuclear Physics B Proceedings Supplements, 166, 19
Beatty, J. J., Bhattacharyya, A., Bower, C., et al. 2004, Phys. Rev. Lett., 93, 241102
Bélanger, G., Boudjema, F., Kraml, S., Pukhov, A., & Semenov, A. 2006, Phys. Rev. D, 73, 115007
Berentzen, I., & Shlosman, I. 2006, ApJ, 648, 807
Berentzen, I., Shlosman, I., & Jogee, S. 2006, ApJ, 637, 582
Berezinskii, V. S., Bulanov, S. V., Dogiel, V. A., & Ptuskin, V. S. 1990, Astrophysics of cosmic rays, Amsterdam, North-Holland, ed. V. L. Ginzburg
Berezinsky, V. S., Gurevich, A. V., & Zybin, K. P. 1992, Phys. Lett. B, 294, 221
Berezinsky, V., Dokuchaev, V., & Eroshenko, Y. 2003, Phys. Rev. D, 68, 103003
Berezinsky, V., Dokuchaev, V., & Eroshenko, Y. 2006, Phys. Rev. D, 73, 063504
Bergström, L. 2000, Rep. Prog. Phys., 63, 793
Bergström, L., Ullio, P., & Buckley, J. H. 1998, Astropart. Phys., 9, 137
Bergström, L., Edsjö, J., Gondolo, P., & Ullio, P. 1999, Phys. Rev. D, 59, 043506
Bertone, G., & Merritt, D. 2005, Modern Phys. Lett. A, 20, 1021
Bertone, G., Hooper, D., & Silk, J. 2005a, Phys. Rep., 405, 279
Bertone, G., Zentner, A. R., & Silk, J. 2005b, Phys. Rev. D, 72, 103517
Bertschinger, E. 2006, Phys. Rev. D, 74, 063509
Bett, P., Eke, V., Frenk, C. S., et al. 2007, MNRAS, 376, 215
Bi, X.-J. 2006, Nucl. Phys. B, 741, 83
Bi, X.-J., Zhang, J., Yuan, Q., Zhang, J.-L., & Zhao, H. 2006, [arXiv:astro-ph/0611783]
Bi, X.-J., Guo, Y.-Q., Hu, H.-B., & Zhang, X. 2007, Nucl. Phys. B, 775, 143
Boylan-Kolchin, M., & Ma, C.-P. 2004, MNRAS, 349, 1117
Bradač, M., Clowe, D., Gonzalez, A. H., et al. 2006, ApJ, 652, 937
Bringmann, T., & Hofmann, S. 2007, J. Cosmol. Astro-Part. Phys., 4, 16
Bringmann, T., & Salati, P. 2007, Phys. Rev. D, 75, 083006
Brun, P., Bertone, G., Lavalle, J., Salati, P., & Taillet, R. 2007, Phys. Rev. D, 76, 083506
Bullock, J. S., Kolatt, T. S., Sigad, Y., et al. 2001, MNRAS, 321, 559
Buote, D. A., Gastaldello, F., Humphrey, P. J., et al. 2007, ApJ, 664, 123
Capuzzo-Dolcetta, R., Leccese, L., Merritt, D., & Vicari, A. 2006, ArXiv Astrophysics e-prints
Carr, J., Lamanna, G., & Lavalle, J. 2006, Rep. Prog. Phys., 69, 2475
Casolino, M., Picozza, P., Altamura, F., et al. 2007, [arXiv:0708.1808]
Clowe, D., Gonzalez, A., & Markevitch, M. 2004, ApJ, 604, 596
Clowe, D., Bradač, M., Gonzalez, A. H., et al. 2006, ApJ, 648, L109
Colafrancesco, S., Profumo, S., & Ullio, P. 2006, A&A, 455, 21
Colín, P., Valenzuela, O., & Klypin, A. 2006, ApJ, 644, 687
Comerford, J. M., & Natarajan, P. 2007, MNRAS, 379, 190
Coutu, S., Barwick, S. W., Beatty, J. J., et al. 1999, Astropart. Phys., 11, 429
Cowsik, R., Ratnam, C., Bhattacharjee, P., & Majumdar, S. 2007, New Astron., 12, 507
Cumberbatch, D., & Silk, J. 2007, MNRAS, 374, 455
De Lucia, G., Kauffmann, G., Springel, V., et al. 2004, MNRAS, 348, 333
Debattista, V. P., Moore, B., Quinn, T., et al. 2007, [arXiv:0707.0737]
Dehnen, W., & Binney, J. 1998, MNRAS, 294, 429
Dehnen, W., McLaughlin, D. E., & Sachania, J. 2006, MNRAS, 369, 1688
Diemand, J., Moore, B., & Stadel, J. 2004a, MNRAS, 353, 624
Diemand, J., Moore, B., & Stadel, J. 2004b, MNRAS, 352, 535
Diemand, J., Moore, B., & Stadel, J. 2005a, Nature, 433, 389
Diemand, J., Zemp, M., Moore, B., Stadel, J., & Carollo, C. M. 2005b, MNRAS, 364, 665
Diemand, J., Kuhlen, M., & Madau, P. 2006, ApJ, 649, 1
Diemand, J., Kuhlen, M., & Madau, P. 2007a, ApJ, 657, 262
Diemand, J., Kuhlen, M., & Madau, P. 2007b, ApJ, 667, 859
Djouadi, A., Drees, M., & Kneur, J.-L. 2006, J. High Energy Phys., 33, 0603
Dolag, K., Bartelmann, M., Perrotta, F., et al. 2004, A&A, 416, 853
Donato, F., Maurin, D., Salati, P., et al. 2001, ApJ, 563, 172
Donato, F., Maurin, D., & Taillet, R. 2002, A&A, 381, 539
Donato, F., Fornengo, N., Maurin, D., Salati, P., & Taillet, R. 2004, Phys. Rev. D, 69, 063501
DuVernois, M. A., Barwick, S. W., Beatty, J. J., et al. 2001, ApJ, 559, 296
Eke, V. R., Navarro, J. F., & Steinmetz, M. 2001, ApJ, 554, 114
Ellis, J., Olive, K. A., Santoso, Y., & Spanos, V. C. 2003, Phys. Lett. B, 565, 176
Famaey, B., Angus, G. W., Gentile, G., & Zhao, H. S. 2007, [arXiv:0706.1279]
Fedeli, C., Bartelmann, M., Meneghetti, M., & Moscardini, L. 2007, A&A, 473, 715
Gao, L., & White, S. D. M. 2006, MNRAS, 373, 65
Gao, L., & White, S. D. M. 2007, MNRAS, 377, L5
Gao, L., White, S. D. M., Jenkins, A., Stoehr, F., & Springel, V. 2004, MNRAS, 355, 819
Ghigna, S., Moore, B., Governato, F., et al. 2000, ApJ, 544, 616
Gill, S. P. D., Knebe, A., & Gibson, B. K. 2004, MNRAS, 351, 399
Gnedin, O. Y., & Primack, J. R. 2004, Phys. Rev. Lett., 93, 061302
Gnedin, O. Y., Kravtsov, A. V., Klypin, A. A., & Nagai, D. 2004, ApJ, 616, 16
Goerdt, T., Gnedin, O. Y., Moore, B., Diemand, J., & Stadel, J. 2007, MNRAS, 375, 191
Graham, A. W., Merritt, D., Moore, B., Diemand, J., & Terzić, B. 2006, AJ, 132, 2701
Green, A. M., & Goodwin, S. P. 2007, MNRAS, 375, 1111
Green, A. M., Hofmann, S., & Schwarz, D. J. 2004, MNRAS, 353, L23
Green, A. M., Hofmann, S., & Schwarz, D. J. 2005, J. Cosmol. Astro-Part. Phys., 8, 3
Grimani, C., Stephens, S. A., Cafagna, F. S., et al. 2002, A&A, 392, 287
Gustafsson, M., Fairbairn, M., & Sommer-Larsen, J. 2006, Phys. Rev. D, 74, 123522
Hahn, O., Carollo, C. M., Porciani, C., & Dekel, A. 2007a, [arXiv:0704.2595]
Hahn, O., Porciani, C., Carollo, C. M., & Dekel, A. 2007b, MNRAS, 375, 489
Hayashi, E., Navarro, J. F., Taylor, J. E., Stadel, J., & Quinn, T. 2003, ApJ, 584, 541
Hayashi, E., Navarro, J. F., & Springel, V. 2007, MNRAS, 377, 50
Heitmann, K., Lukic, Z., Fasel, P., et al. 2007, [arXiv:0706.1270]
Helmi, A. 2004a, MNRAS, 351, 643
Helmi, A. 2004b, ApJ, 610, L97
Hisano, J., Matsumoto, S., Saito, O., & Senami, M. 2006, Phys. Rev. D, 73, 055004
Hofmann, S., Schwarz, D. J., & Stöcker, H. 2001, Phys. Rev. D, 64, 083507
Hooper, D., & Kribs, G. D. 2004, Phys. Rev. D, 70, 115004
Hooper, D., Taylor, J. E., & Silk, J. 2004, Phys. Rev. D, 69, 103509
Jee, M. J., Ford, H. C., Illingworth, G. D., et al. 2007, ApJ, 661, 728
Jing, Y. P., Suto, Y., & Mo, H. J. 2007, ApJ, 657, 664
Johnston, K. V., Law, D. R., & Majewski, S. R. 2005, ApJ, 619, 800
Joyce, M., & Marcos, B. 2007, Phys. Rev. D, 75, 063516
Jungman, G., Kamionkowski, M., & Griest, K. 1996, Phys. Rep., 267, 195
Kane, G. L., Wang, L.-T., & Wang, T. T. 2002a, Phys. Lett. B, 536, 263
Kane, G. L., Wang, L.-T., & Wells, J. D. 2002b, Phys. Rev. D, 65, 057701
Kazantzidis, S., Kravtsov, A. V., Zentner, A. R., et al. 2004a, ApJ, 611, L73
Kazantzidis, S., Mayer, L., Mastropietro, C., et al. 2004b, ApJ, 608, 663
Kazantzidis, S., Zentner, A. R., & Kravtsov, A. V. 2006, ApJ, 641, 647
Klypin, A., Kravtsov, A. V., Valenzuela, O., & Prada, F. 1999, ApJ, 522, 82
Koushiappas, S. M., Zentner, A. R., & Walker, T. P. 2004, Phys. Rev. D, 69, 043501
Kravtsov, A. V., Gnedin, O. Y., & Klypin, A. A. 2004, ApJ, 609, 482
Kuhlen, M., Diemand, J., & Madau, P. 2007, [arXiv:0705.2037]

Kuhlen, M., Strigari, L. E., Zentner, A. R., Bullock, J. S., & Primack, J. R. 2005, MNRAS, 357, 387
Lavalle, J., Pochon, J., Salati, P., & Taillet, R. 2007, A&A, 462, 827
Lee, J., & Kang, X. 2006, ApJ, 637, 561
Lesgourgues, J. 2004, ArXiv e-prints [arXiv:astro-ph/0409426]
Libeskind, N. I., Frenk, C. S., Cole, S., et al. 2005, MNRAS, 363, 146
Lionetto, A. M., Morselli, A., & Zdravkovic, V. 2005, J. Cosmology Astro-Part. Phys., 9, 10
Loeb, A., & Zaldarriaga, M. 2005, Phys. Rev. D, 71, 103520
Macciò, A. V., Moore, B., Stadel, J., & Diemand, J. 2006, MNRAS, 366, 1529
Macciò, A. V., Dutton, A. A., van den Bosch, F. C., et al. 2007a, MNRAS, 378, 55
Macciò, A. V., Sideris, I., Miranda, M., Moore, B., & Jesseit, R. 2007b, [arXiv:0704.3078]
Mambrini, Y., Muñoz, C., & Nezri, E. 2006, J. Cosmol. Astro-Part. Phys., 12, 3
Mashchenko, S., Couchman, H. M. P., & Wadsley, J. 2006, Nature, 442, 539
Maulbetsch, C., Avila-Reese, V., Colín, P., et al. 2007, ApJ, 654, 53
Maurin, D., & Taillet, R. 2003, A&A, 404, 949
Maurin, D., Donato, F., Taillet, R., & Salati, P. 2001, ApJ, 555, 585
Maurin, D., Taillet, R., & Donato, F. 2002, A&A, 394, 1039
Maurin, D., Taillet, R., Donato, F., et al. 2004, Research Signposts, Recent Research Developments in Astronomy and Astrophys., 2, 193 [arXiv:astro-ph/021211]
Maurin, D., Taillet, R., & Combet, C. 2006a,[arXiv:astro-ph/0609522]
Maurin, D., Taillet, R., & Combet, C. 2006b, [arXiv:astro-ph/0612714]
McMillan, P. J., & Dehnen, W. 2005, MNRAS, 363, 1205
McMillan, P. J., Athanassoula, E., & Dehnen, W. 2007, MNRAS, 376, 1261
Merritt, D. 2004, Phys. Rev. Lett., 92, 201304
Merritt, D., Graham, A. W., Moore, B., Diemand, J., & Terzić, B. 2006, AJ, 132, 2685
Metz, M., Kroupa, P., & Jerjen, H. 2007, MNRAS, 374, 1125
Moore, B., Governato, F., Quinn, T., Stadel, J., & Lake, G. 1998, ApJ, 499, L5
Moore, B., Ghigna, S., Governato, F., et al. 1999, ApJ, 524, L19
Moore, B., Kazantzidis, S., Diemand, J., & Stadel, J. 2004, MNRAS, 354, 522
Moskalenko, I. V., & Strong, A. W. 1998, ApJ, 493, 694
Muñoz, C. 2004, Int. J. Mod. Phys. A, 19, 3093
Nagai, D., & Kravtsov, A. V. 2005, ApJ, 618, 557
Navarro, J. F., Frenk, C. S., & White, S. D. M. 1997, ApJ, 490, 493
Navarro, J. F., Hayashi, E., Power, C., et al. 2004, MNRAS, 349, 1039
Neto, A. F., Gao, L., Bett, P., et al. 2007, [arXiv:0706.2919]
Novak, G. S., Cox, T. J., Primack, J. R., Jonsson, P., & Dekel, A. 2006, ApJ, 646, L9
Picozza, P., Galper, A. M., Castellini, G., et al. 2006, [arXiv:astro-ph/0608697]
Pieri, L., Bertone, G., & Branchini, E. 2007, [arXiv:0706.2101]
Profumo, S., Sigurdson, K., & Kamionkowski, M. 2006, Phys. Rev. Lett., 97, 031301
Ragone-Figueroa, C., & Plionis, M. 2007, MNRAS, 377, 1785
Reed, D., Governato, F., Quinn, T., et al. 2005, MNRAS, 359, 1537
Ricotti, M., Pontzen, A., & Viel, M. 2007, ApJ, 663, L53
Romano-Díaz, E., Hoffman, Y., Heller, C., et al. 2007, ApJ, 657, 56
Ružička, A., Palouš, J., & Theis, C. 2007, A&A, 461, 155
Sellwood, J. A. 2006, [arXiv:astro-ph/0610468]
Shaw, L. D., Weller, J., Ostriker, J. P., & Bode, P. 2007, ApJ, 659, 1082
Sheth, R. K., & Tormen, G. 2004, MNRAS, 350, 1385
Silk, J., & Stebbins, A. 1993, ApJ, 411, 439
Simon, J. D., Bolatto, A. D., Leroy, A., Blitz, L., & Gates, E. L. 2005, ApJ, 621, 757
Springel, V., White, S. D. M., Tormen, G., & Kauffmann, G. 2001, MNRAS, 328, 726
Stoehr, F. 2006, MNRAS, 365, 147
Taillet, R., & Maurin, D. 2003, A&A, 402, 971
Tormen, G., Diaferio, A., & Syer, D. 1998, MNRAS, 299, 728
Tytler, D., O'Meara, J. M., Suzuki, N., & Lubin, D. 2000, Phys. Scr. T, 85, 12
Ullio, P., Bergström, L., Edsjö, J., & Lacey, C. 2002, Phys. Rev. D, 66, 123502
Valluri, M., Vass, I. M., Kazantzidis, S., Kravtsov, A. V., & Bohn, C. L. 2007, ApJ, 658, 731
van den Bosch, F. C., Tormen, G., & Giocoli, C. 2005, MNRAS, 359, 1029
Wechsler, R. H., Bullock, J. S., Primack, J. R., Kravtsov, A. V., & Dekel, A. 2002, ApJ, 568, 52
Wechsler, R. H., Zentner, A. R., Bullock, J. S., Kravtsov, A. V., & Allgood, B. 2006, ApJ, 652, 71
Weinberg, D. H., Colombi, S., Davé, R., & Katz, N. 2006, [arXiv:astro-ph/0604393]
Yao, W.-M., et al. 2006, J. Phys. G Nucl. Phys., 33, 1
Yuan, Q., & Bi, X.-J. 2007, JCAP, 0705, 001
Zentner, A. R., & Bullock, J. S. 2003, ApJ, 598, 49
Zentner, A. R., Kravtsov, A. V., Gnedin, O. Y., & Klypin, A. A. 2005, ApJ, 629, 219
Zhao, H. 1996, MNRAS, 278, 488
Zhao, H., Hooper, D., Angus, G. W., Taylor, J. E., & Silk, J. 2007, ApJ, 654, 697

Appendix A: Effective propagation volumes and the threshold mass M_{th}

On the one hand, the spatial distribution and the number of clumps in each mass decade is known. On the other hand, the propagation properties define *effective* volumes $V_{\rm eff}$ (Taillet & Maurin 2003; Maurin & Taillet 2003), which enclose and preselect the sources contributing to the flux. This is all we need for a quick estimate of the variance on the fluxes (for the clumps in that given mass range), hence the estimate of the threshold mass $M_{\rm th}$. Effective volumes $V_{\rm eff}$ are reminded in Appendix A.1 and $M_{\rm th}$ is given in Appendix A.2. In Appendix A.3, we show that $M_{\rm th}$ can be set to a higher value than that derived from the effective volumes.

The method is general, and is discussed below for $\alpha_{\rm m} = 1.9$ (Sect. 2.3.1, Eq. (14)) and the cored distribution of clumps (Sect. 2.3.2, Eq. (16)).

A.1. Effective volumes V_{eff}

All DM sources beyond the boundary $z = L$ (size of the diffusive halo of the Galaxy) can be safely discarded (Barrau et al. 2002). Furthermore, in a diffusive process, a source located at a radial distance r gives a negligible contribution if $\eta \equiv r/L$ is larger than a few (Taillet & Maurin 2003; Maurin & Taillet 2003). These two boundaries generate a cylinder $V_{\rm eff} = \pi\eta^2 L^2 \times 2L$; sources out of it may be considered to add negligible contribution to the total flux[12].

In addition to the parameter L, effective volumes may be further decreased depending on the value of the galactic convecting wind $V_{\rm c}$: the effective halo size $L^* = 2K(E)/V_{\rm c}$ plays a similar role as L (exponential cut-off of the contributions, Taillet & Maurin 2003). At low energy, $L \lesssim L$, decreasing $V_{\rm eff}$. This set the effective volume for $\overline{\rm p}$,

$$V_{\rm eff}^{\bar{\rm p}} = 2\pi\eta^2 \{\min(L, L^*)\}^3. \quad (A.1)$$

Because of energy losses, the typical distance travelled by positrons is $r_* = \sqrt{4K(E)\tau_{\rm loss}}$ (e.g. Maurin & Taillet 2003; see Brun et al. 2007; and Appendix B.2 for a more precise description). If $r_* \gg L$, we recover $V_{\rm eff}^{\bar{\rm p}}$, but if $r_* \lesssim L$, the effective volume for positrons is

$$V_{\rm eff}^{\rm e^+} = \frac{4}{3}\pi\eta^3 r_*^3. \quad (A.2)$$

Note that the above volumes are in practise distorted in various directions (also because of the intrinsic spatial distribution of DM sources), but they suffice for a qualitative estimate.

A.2. Threshold mass M_{th} for the three propagation sets

In Eqs. (A.1) and (A.2), we set $\eta = 10$. We remind that this parameter sets the distance beyond which sources can be discarded. Taking a high value for η gives a conservative estimate of $M_{\rm th}$. The effective volumes, which do depend on energy, completely determine the number of clumps $N_{\rm eff}$ contributing to the flux. As fluctuations in $N_{\rm eff}$ generate fluctuations in the signal, the mass threshold $M_{\rm th}$ is obtained demanding that $N_{\rm eff}[M_{\rm th} - 10M_{\rm th}] \gtrsim 10$. We recall that for antimatter primaries, the most relevant contribution comes from the local neighbourhood, so that the local number density of sub-halos $\mathrm{d}\mathcal{P}(R_\odot)/\mathrm{d}V$ can be used in the next approximations.

[12] An analysis of these effective volumes has been presented and discussed in great details in Maurin & Taillet (2003), for both $\overline{\rm p}$ and $\rm e^+$.

Table A.1. Threshold mass (as defined in the text) in units of $10^5\ M_\odot$ for $\overline{\rm p}$ and $\rm e^+$ at various energies for the three representative sets of propagation parameters (see Table 4 in Sect. 4.3).

E_k	0.5 GeV	1 GeV	10 GeV	100 GeV
$M_{\rm th}(\times 10^5\ M_\odot)$	$\bar{\rm p}$ |$\rm e^+$	$\bar{\rm p}$ |$\rm e^+$	$\bar{\rm p}$ |$\rm e^+$	$\bar{\rm p}$ |$\rm e^+$
max	340./37.	340./21.	340./3.3	340./0.51
med	0.32/1.6	1.2/1.2	6.4/0.42	6.4/0.15
min	0.0007/0.08	0.003/0.06	0.1/0.04	0.1/0.02

Anti-protons: the effective number of clumps is given by

$$N_{\rm eff}^{\bar{\rm p}}[M - 10M] \approx N_{\rm tot}[M - 10M] \times \frac{\mathrm{d}\mathcal{P}}{\mathrm{d}V}(R_\odot) \times V_{\rm eff} \approx 10^5 \left(\frac{M}{M_\odot}\right)^{-0.9} \times \left\{\frac{\min(L, L^*)}{1\ \mathrm{kpc}}\right\}^3,$$

leading to

$$M_{\rm th}^{\bar{\rm p}} \approx 10^4\ M_\odot \times \left\{\frac{\min(L, L^*)}{1\ \mathrm{kpc}}\right\}^3. \quad (A.3)$$

For example, for the reference halo size $L = 4$ kpc and no galactic wind, we get the energy independent result $M_{\rm th}^{\bar{\rm p}} \sim 6.4 \times 10^5\ M_\odot$.

Positrons: using $\tau_{\rm loss} = 300\ \mathrm{Myr} \times 1\ \mathrm{GeV}/E$, and plugging the diffusion coefficient $K(E) \approx K_0 E^\delta$ in r_*, we get, at high energy,

$$N_{\rm eff}^{\rm e^+}[M - 10M] \approx 10^9 \left(\frac{M}{M_\odot}\right)^{-0.9} \left(\frac{K_0 \times E^{\delta-1}}{1\ \mathrm{kpc^2\ Myr^{-1}}}\right)^{3/2}$$

and

$$M_{\rm th}^{\rm e^+} \approx 10^8\ M_\odot \times \left(\frac{K_0 \times E^{\delta-1}}{1\ \mathrm{kpc^2\ Myr^{-1}}}\right)^{3/2}. \quad (A.4)$$

For example, for the best propagation parameters set (Table 4), i.e. $\delta = 0.7$ and $K_0 = 0.0112$, we get at $E = 10$ GeV, $M_{\rm th}^{\rm e^+} \sim 5 \times 10^4\ M_\odot$.

Comparison: for the three sets of propagation parameters (as reminded in Table 4 of Sect. 4.3) and for various energies, Table A.1 gathers the threshold mass for $\overline{\rm p}$ and $\rm e^+$, calculated from Eqs. (A.3) and (A.4). For anti-protons, we repeat that the leading parameter is L, except at low energy when the Galactic wind blows particles efficiently out of the diffusive volume. If the halo size L is large (max set, i.e. $L = 15$ kpc), the variance associated with the flux of a clump mass range is sizable only for masses above $\gtrsim 3 \times 10^7\ M_\odot$, independent of the energy. A small halo size (min set, i.e. $L = 1$ kpc) is associated with a strong wind, for which the threshold mass decreases down to $\sim 10^2\ M_\odot$ at 0.5 GeV (unmodulated). For positrons, the leading parameter is the value of the diffusion coefficient, hence K_0 and δ. As for anti-protons, this is the min propagation set that leads to the smaller threshold mass. The range spanned by the various configurations is, however, tighter than that for anti-protons. The smaller values are observed at high energy (strong energy losses). At low energy and for the min set of parameters, as emphasised above, taking into account the wind would give extremely small $M_{\rm th}$ as for anti-protons.

From these numbers, we may already predict that propagation parameters corresponding to small $V_{\rm eff}$ will lead to smaller

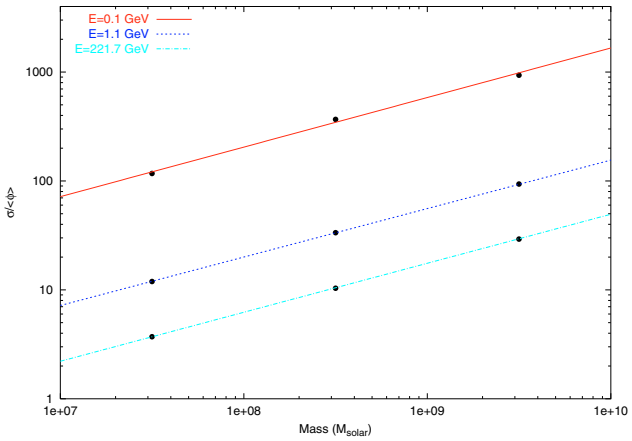

Fig. A.1. Relative error $\sigma/\langle\phi\rangle$ as a function of mass for several energies. The three lines are fitting results using function AM^{β}, with $\beta = 0.455$, 0.445 and 0.45 from the top to bottom, respectively. The quantity $10^{(2i+1)/2}$ is used to represent the mass bin M_i.

fluxes (Barrau et al. 2002, 2005; Donato et al. 2004; Maurin et al. 2006b), but also a larger associated variance than the configurations with large $V_{\rm eff}$.

A.3. Choosing a higher M_{th} for the MC simulation

In principle, in the MC realisations (Sect. 5.3), all sub-halos with a mass larger than $M_{\rm th}$ need to be generated. We just provided an *absolute* criterion in Appendix A.2. Using a *relative* criterion, a higher $M_{\rm th}$ (useful for reducing the computational time) can be found.

The mean flux from clumps in the mass range $[M, M + {\rm d}M]$ is given by the number of clumps $N(M)$ in the diffusive volume, and the variance of the signal is just proportional to $\sqrt{N}$, so that the variance-flux-ratio is (see also Lavalle et al. 2007)

$$\frac{\sigma_\phi}{\langle\phi\rangle}(M) \propto \frac{1}{\sqrt{N(M)}}\,. \tag{A.5}$$

Using the relation $N(M) \propto M^{1-\alpha_{\rm m}}$ of Eq. (14), we get

$$\frac{\sigma_\phi}{\langle\phi\rangle}(M) \propto M^{(\alpha_{\rm m}-1)/2}, \tag{A.6}$$

thus recovering the results of Lavalle et al. (2007), who used sub-halos of equal masses and properties. As discussed in Sect. 3.3, for $\alpha_{\rm m} = 1.9$, the luminosity is roughly constant per logarithmic mass bin, so that considering the sub-halo mass range $M_i \equiv [10^i - 10^{i+1}]\ M_\odot$, we get

$$\sigma_\phi(M_i) \propto M_i^{0.45}. \tag{A.7}$$

This equation states that the clumps maximally contributing to the variance are the heaviest ones, and only these need to be taken into account. If we adopt $M_{\rm th} = 10^7\ M_\odot$, the neglected part will contribute only 0.1% to the total variance.

As an illustration, Eq. (A.6) is shown to be in full agreement with the result of the MC simulation in Fig. A.1 (for anti-protons and $\alpha_{\rm m} = 1.9$). The latter graphs are independent of the intrinsic profile of the clumps and of the propagation parameters. In Sect. 5.3, we take advantage of this higher value to speed up the MC calculations.

Appendix B: More details on mass- and space-related effects on fluxes and boosts

We recall that the total contribution of sub-halos to the antimatter flux has a mean value given by:

$$\phi_{\rm cl}^{\rm tot} = \frac{v}{4\pi} S \times N_{\rm cl} \times \langle\xi\rangle_M \times \langle\tilde{\mathcal{G}}\rangle_V, \tag{B.1}$$

which can be expressed as the product of two main terms. The first one is the integrated luminosity of clumps:

$$L_{\rm cl} = N_{\rm cl} \times \langle\xi\rangle_M, \tag{B.2}$$

which is purely mass-related in the sense that it depends only on the mass distribution and internal features of sub-halos. The relevant parameters are $M_{\rm min}$, $\alpha_{\rm m}$, the mass-concentration relation and the inner sub-halo profile. The second is merely the propagation term $\langle\tilde{\mathcal{G}}\rangle_V$ averaged over the spatial distribution of sub-halos, which is then of purely space type.

B.1. Mass-related effects

A simple analysis of the behaviour $L_{\rm cl}$ is helpful, and gives already interesting insights on the final results. In the limit for which $M_{\rm min} \ll M_{\rm max}$ and $\alpha_{\rm m} \sim 2$, we find that the total number of clumps $N_{\rm cl} \propto M_{\rm ref}^{\alpha_{\rm m}-1} {M_{\rm min}}^{1-\alpha_{\rm m}}$ (see Eq. (18)), and that the mean value $\langle\xi\rangle_M \propto {M_{\rm min}}^{\alpha_{\rm m}-1} \times \ln(M_{\rm max}/M_{\rm min}) \sim {M_{\rm min}}^{\alpha_{\rm m}-1}$ (assuming $\xi \propto M_{\rm cl}$), at variance of small factors. This means that $L_{\rm cl} \propto M_{\rm ref}^{\alpha_{\rm m}-1} \times \ln(M_{\rm max}/M_{\rm min})$ increases with $\alpha_{\rm m}$, and slightly (logarithmically) depends on $M_{\rm min}$. Actually, we find that spanning $(\alpha_{\rm m}, M_{\rm min})$ respectively from $(2{\times}10^{-6}\ M_\odot)$ to $(1.8{\times}10^6\ M_\odot)$ makes a decrease of only ~40 in the integrated luminosity (the above approximation gives ~150, but we recall that the actual dependence of ξ in $M_{\rm cl}$ is not merely linear). Some numerical values are given in Table B.1.

The pure mass-induced relative fluctuations of the sub-halo flux are given by $\sigma_\xi/(\sqrt{N_{\rm cl}}\langle\xi\rangle_M)$ (see Eq. (63)). As $\sigma_\xi \propto {M_{\rm min}}^{(\alpha_{\rm m}-1)/2}$ from the same arguments as above, those relative uncertainties approximately scale like $(\ln(M_{\rm max}/M_{\rm min}))^{-1}$, and are thus expected to only slightly (logarithmically) decrease when $M_{\rm min}$ increases. They are actually found to lie in the range 10–0.1% for $(\alpha_{\rm m}, M_{\rm min})$ going respectively from $(2\times10^{-6}\ M_\odot)$ to $(1.8{\times}10^6\ M_\odot)$ (see Table B.1). This may appear surprising because we would naively expect the relative variance to scale like ${N_{\rm cl}}^{-1/2} \propto {M_{\rm min}}^{(\alpha_{\rm m}-1)/2}$, and then to depend much more strongly on $M_{\rm min}$. To summarise, the dropping of the total number of clumps, which reduces the statistical sample, is compensated by smaller fluctuations around the mean luminosity $\langle\xi\rangle$ from clump to clump (the range $M_{\rm min}{-}M_{\rm max}$ gets thinner), so that the mass-induced relative uncertainties remain roughly constant.

B.2. Space-related effects for positrons

The space-related effects for positrons are characterised by the mean value and the variance of $\tilde{\mathcal{G}}$ over the spatial sub-halo distribution. For positrons, the relevant scale is the energy loss scale, which sets the characteristic propagation length, as stressed in Lavalle et al. (2007). This propagation length is given by the following equation:

$$\lambda_{\rm D} \equiv \sqrt{4K_0\tau_E \left(\frac{\epsilon^{\delta-1} - \epsilon_S^{\delta-1}}{1-\delta}\right)}, \tag{B.3}$$

Table B.1. Total number of clumps $N_{\rm cl}$, mean effective annihilation volume $\langle\xi\rangle_M$ and its relative variance $\sigma_\xi/\langle\xi\rangle_M$, and product $N_{\rm cl}\times f\langle\xi\rangle_M$ (proportional to the total number of primary GCRs produced in clumps) for different mass models. We choose three different mass ranges varying the minimal mass from 10^{-6} to 10^6 $M_\odot$, and for different logarithmic slopes $\alpha_{\rm m}=\{1.8|1.9|2.0\}$ of the mass distribution.

$M_{\rm min}$ ($M_\odot$)	$N_{\rm cl}$	$\langle\xi\rangle_M$ (kpc^3)	$\sigma_\xi/\langle\xi\rangle_M$	$N_{\rm cl}\times\langle\xi\rangle_M$ (kpc^3)
10^{-6}	$(1.6\|4.1\|1.0)\times10^{13\|14\|16}$	$(85\|10\|3)\times10^{-11}$	$(2.1\|3.2\|1.9)\times10^5$	$(1.4\|4.1\|30.0)\times10^4$
1	$(2.6\|1.6\|1.0)\times10^{8\|9\|10}$	$(49\|16\|7)\times10^{-6}$	$(9.1\|10.1\|7.7)\times10^2$	$(1.3\|2.5\|7.4)\times10^4$
10^6	$(4.1\|6.4\|10.1)\times10^3$	$(1.8\|1.3\|1.0)$	$6.0\|6.0\|5.7$	$(7.5\|8.3\|9.9)\times10^3$

Table B.2. Mean value and variance of $\tilde{\mathcal{G}}$ (single clump) for positrons (left-hand side) and anti-protons (right hand side), each line accounting for each set of propagation parameters of Table 4. The results for positrons correspond to particles injected at 200 GeV in sources, and detected at 10|150 GeV. For anti-protons, a flat spectrum $dN/dT=1$ GeV^{-1} is injected at sources and detected kinetic energies of 10|150 GeV are also considered. For both positrons and anti-protons, the DM configuration is the reference one, except for *Med**, for which we take a space distribution of sub-halos that tracks the smooth NFW component.

Propagation	$\langle\tilde{\mathcal{G}}^{\rm e^+}\rangle$ (s kpc^{-3} GeV^{-1})	$\sigma_{\tilde{\mathcal{G}}^{\rm e^+}}/\langle\tilde{\mathcal{G}}^{\rm e^+}\rangle$	$\langle\tilde{\mathcal{G}}^{\bar{\rm p}}\rangle$ (s kpc^{-3} GeV^{-1})	$\sigma_{\tilde{\mathcal{G}}^{\bar{\rm p}}}/\langle\tilde{\mathcal{G}}^{\bar{\rm p}}\rangle$
Min	$5.462\times10^6\|1.723\times10^5$	287.1|1089	$2.335\times10^8\|4.850\times10^7$	829.2|622.2
Med	$2.840\times10^7\|1.744\times10^5$	67.95|446.6	$9.220\times10^8\|2.320\times10^8$	106.2|84.6
Max	$3.666\times10^7\|1.742\times10^5$	25.84|267.3	$2.652\times10^9\|1.157\times10^9$	18.42|15.22
Med*	$5.589\times10^8\|3.191\times10^6$	15.02|104.3	$1.801\times10^{10}\|4.561\times10^9$	23.34|18.53

where K_0 and δ are the normalisation and the logarithmic slope of the diffusion coefficient, respectively, and $\epsilon\equiv(E/\{E_0=1\ \text{GeV}\})$. If we take the medium propagation parameters of Table 4, and a typical timescale for energy loss of $\tau_E\approx10^{16}$ s, then for a 200 GeV injected energy, we find a propagation length $\lambda_{\rm D}\simeq6.9\ {\rm kpc}\times\sqrt{\epsilon^{-0.3}-0.2}$, which ranges from 0.4 kpc at a detected energy E_d of 190 GeV to 5.7 kpc at 1 GeV. This shows that for positrons, the main contributions to the flux are likely to come from regions close to the solar neighbourhood. From Eq. (B.3), we also see that a larger diffusion coefficient or/and a lower detected energy will allow the integration of contributions over a larger volume (the former case is, however, generally associated with a smaller diffusion slab model, which erases those extra contributions).

Assuming now that all relevant contributions are those inside a volume $V_{\rm D}$ around the Earth bounded by $\lambda_{\rm D}\lesssim L$ (L is half the vertical extension of the diffusive halo), and that the propagation is roughly constant over this small volume, we can simplify the propagator $\tilde{\mathcal{G}}^{\rm e^+}$ in the limit of infinite 3D diffusion:

$$\tilde{\mathcal{G}}^{\rm e^+}\simeq\frac{\tau_E}{E_0\epsilon^2}\times\frac{\theta(\lambda_{\rm D}-|\boldsymbol{r}-\boldsymbol{r}_\odot|)}{(\pi\lambda_{\rm D}^2)^{3/2}}\,. \tag{B.4}$$

Assuming also that the spatial distribution of clumps does not vary that much within $V_{\rm D}$, thus given by $d\mathcal{P}(R_\odot)/dV$, we get:

$$\langle\tilde{\mathcal{G}}^{\rm e^+}\rangle_V=\int_V{\rm d}^3\boldsymbol{x}\ \tilde{\mathcal{G}}^{\rm e^+}\frac{{\rm d}\mathcal{P}}{{\rm d}V}(\boldsymbol{x})\simeq\frac{\tau_E}{E_0\epsilon^2}\times\frac{{\rm d}\mathcal{P}}{{\rm d}V}(R_\odot). \tag{B.5}$$

The interpretation is trivial, as well as the consequences for the boost estimate. Besides, the relative variance straightforwardly reads:

$$\frac{\sigma_{\tilde{\mathcal{G}}^{\rm e^+}}}{\langle\tilde{\mathcal{G}}^{\rm e^+}\rangle}\propto\left(V_{\rm D}^2\times\frac{{\rm d}\mathcal{P}}{{\rm d}V}(R_\odot)\right)^{-1/2}. \tag{B.6}$$

This means that the relative variance decreases when the spatial probability function of clumps raises and when the effective detection volume increases, which is physically obvious but better quantified with the previous equations. If we argue in terms of local number density of clumps, this only says that the global space-related variance scales like $N_{\rm obs}^{-1/2}$, where $N_{\rm obs}$ is the number of clumps inside $V_{\rm D}$.

A more quantitative information is given in Table B.2. In this table, we calculate the mean value and the variance of $\tilde{\mathcal{G}}^{\rm e^+}$ as defined by Eqs. (61) and (64), respectively, for the three propagation models detailed in Table 4. We consider the injection of 200 GeV positrons in sources, ($Q(E_S)=\delta(E_S-200\ \text{GeV})$), and compute the propagator averaged on the spatial distribution of sub-halos together with the associated statistical variance. We show the results obtained for detected energies of 150 and 10 GeV, which correspond to diffusion lengths $\lambda_{\rm D}$ of $\sim$0.9 and 3.8 kpc, respectively. Such quantities are parts of the flux probability function related to a single clump, but encoding only the spatial and propagation information.

We see from this table the expected behaviour when varying the propagation model: at a given detected energy, $\langle\tilde{\mathcal{G}}^{\rm e^+}\rangle$ increases from the minimal to the maximal propagation configuration, and also increases when the positron is detected at a lower energy (its mean free path is somehow longer). There is a factor of $\sim$20 between the minimum (*min* model, high E_d) and maximum values (*max* model, low E_d). The space-associated contribution to the relative variance affecting the single clump flux is also given in Table B.2, and is in the range 10−1000. It has to be compared with the relative mass-induced variance of Table B.1, i.e. that on ξ. We see that while the relative variance on $\tilde{\mathcal{G}}^{\rm e^+}$ is large, the one affecting ξ almost always dominates, unless the minimal mass of clumps is $\gtrsim10^6$ $M_\odot$. Thus, though propagation uncertainties are important, the mass-induced effects are likely to outclass the systematic uncertainties over a large energy range. Nevertheless, they re-enter the game as soon as the propagation scale gets very short (detected energies very close to the injected energy). As the crossing space-mass term dominates the global relative variance, we can determine the systematic errors affecting the global flux predictions, taking the previous ranges obtained for mass-like contributions. For the average clumpy contribution to the flux, we get $\sim40\times20$, which are three orders of magnitude. For the associated relative variance, we find ranges 0.1−10% (clump mass and number) and 10−1000

(space-induced), which yield a total of four orders of magnitude. This provides the systematic uncertainties on the flux and its variance. Nevertheless, such uncertainties are diluted for the boost factor estimate, as only a small part of the parameter space gives a sub-halo contribution greater than that of the smooth.

B.3. Space-related effects for anti-protons

The same reasoning used for positrons can apply to anti-protons, that is the use of the propagation effective volume. Therefore, complementary to the following discussion, we refer the reader to the arguments and conclusion of the previous paragraph.

The typical diffusion length for anti-protons depends mainly on the convective wind, and can be expressed as:

$$\Lambda_{\rm D} \equiv \frac{K(E)}{V_{\rm conv}}, \tag{B.7}$$

where $K(E)$ is the diffusion coefficient at energy E and $V_{\rm conv}$ is the velocity of convection. This is quite different to that used for positrons in the sense that this length is much lower at low energy. With the medium set of propagation parameters, we get $\Lambda_{\rm D} \simeq 1.4{-}86$ kpc for kinetic energies of $0.1{-}10$ GeV, respectively. However, the vertical boundary L of the diffusive halo limits that range to a few times L, so that the actual characteristic propagation length for anti-protons is usually comparable with the size of the slab. Anyhow, this means that above a few GeV, anti-protons can almost probe the entire diffusive slab, as they can originate from far away regions. Hence, the picture for anti-protons is the reversal of that for positrons. Besides, the characteristic diffusion length is larger for anti-protons than for positrons, so that the arguments using local quantities are less relevant here, unless for asymptotic values of the boost factor (which occur at low energy for anti-protons, see Eq. (68)).

Numerical values for the mean value and variance of $\tilde{\mathcal{G}}^{\bar{\rm p}}$ are given in Table B.2, where we have taken a flat injection spectrum for anti-protons, $\mathrm{d}N/\mathrm{d}T = 1$ GeV^{-1}, and we have considered two detected kinetic energies of 10 and 150 GeV (no energy losses for anti-protons). We recover the same range for systematic uncertainties as for positrons (see Appendix B.2).